

**Direction-Dependent Communication Mechanisms in
Individual-Based Models of Collective Behaviour**

by
Cole Zmurchok

A thesis submitted in partial fulfillment of the requirements for the degree of
Master of Science
in
Applied Mathematics

Department of Mathematical and Statistical Sciences
University of Alberta

© Cole Zmurchok, 2014

Abstract

In this thesis, we study direction-dependent communication mechanisms in individual-based models (IBMs) of collective behaviour. Previously, direction-dependent communication mechanisms were incorporated into a non-local hyperbolic PDE model for collective behaviour. The PDE model exhibits numerous spatial patterns observed in nature by considering a variety of communication mechanisms. Like the PDE model, the IBM is formulated in terms of three social interaction forces: repulsion, alignment, and attraction, and the IBM includes information regarding conspecifics' direction of travel. We find that the IBM produces a variety of spatial patterns such as stationary groups, traveling groups, zigzagging aggregations, feathers, and ripple-like patterns, matching the rich behaviour of the PDE model. We also investigate the effect of incorporating density-dependent speed. We find that if individuals slow and speed in response to conspecifics, group splitting and group merging patterns arise. While the PDE model allows for the effect of direction-dependent communication mechanisms on collective behaviour to be seen at the population density level, the IBM model reveals how individuals move within these spatial patterns. To complete the study of direction-dependent communication mechanisms, 2-particle models are proposed as a framework for understanding how individuals respond to their neighbours. The foundation for this work is the anti-symmetric exclusion process that describes the movement of two particles on an infinite one-dimensional lattice when the particles exclude each other from space yet have an anti-symmetric movement bias. We incorporate non-local repulsion and attraction interactions in the anti-symmetric exclusion process, and study this model by developing a master equation. Stochastic simulations reveal that non-local repulsion and attraction interactions result in group behaviour, with a finite mean separation distance. We also consider alignment interactions by considering the position and direction of travel

of the particles, and develop a master equation for this process. Moving groups result from the inclusion of alignment interactions. We find that the 2-particle model framework reveals inter-individual behaviour that is characteristic of group patterns and provides a foundation for analytical work. Studying direction-dependent communication with these three perspectives (PDE, IBM, and 2-particle model) reinforces the important role that direction-dependent communication mechanisms have in producing the complex spatial patterns in nature.

Preface

A manuscript containing versions of Chapter 1, Chapter 3, and Chapter 4 is in preparation for publication.

Acknowledgements

This work would not have been possible without the friendship, support, and guidance of those closest to me.

Firstly, I would like to thank Dr. Gerda de Vries for being an exemplary mentor, an inspiring leader, and for her dedication to the highest standards. Secondly, I would like to thank Raluca Eftimie, Radek Erban, and Jan Haskovec for their questions and thoughts during the early stages of this work. I would also like to extend my gratitude to Mark Lewis, Brendan Pass, and Jonathan Potts for their helpful discussions and directed ideas. I also would like to acknowledge Rita Wong for starting down this path of research and sparking my interest in modelling collective behaviour. Many thanks to my fellow Math Biology Journal Club-ers for their support and pointed questions. I am grateful to have received support from a University of Alberta Queen Elizabeth II Scholarship. Moreover, I would like to thank my friends and family for all the wonderful distractions they provided over long weekends, lunch hours, and late evenings. Finally, I would like to thank Annie Hervieux for her continuous love and support.

Table of Contents

1	Introduction	1
1.1	Overview	1
1.2	Eulerian Models	2
1.3	Lagrangian Models	5
1.4	Animal Communication Mechanisms	7
1.5	Thesis Outline	7
2	The Eftimie Model	10
2.1	Introduction	10
2.2	Model Development	10
2.2.1	Adaptation of Existing PDE Model	11
2.2.2	Derivation from Correlated Random Walk	15
2.3	Key Results	20
2.4	Discussion	23
3	IBM with Communication Mechanisms	24
3.1	Introduction	24
3.2	Model Development	25
3.2.1	Social Interaction Forces and Communication Mechanisms	26
3.3	Numerical Simulations	30
3.4	Social Interaction Kernels	37
3.5	Discussion	39
4	Density-Dependent Speed	42
4.1	Introduction	42
4.2	Density-Dependent Speed in the PDE model	43
4.3	Density-Dependent Speed in the IBM	50
4.4	Density-Dependent Speed and Exponential Kernels	55
4.5	Discussion	61
5	2-Particle Model with Communication Mechanisms	68
5.1	Introduction	68
5.2	Anti-symmetric Exclusion Process	69

5.3	Anti-symmetric Exclusion Process with Social Interactions	74
5.4	Incorporating Directionality	86
5.5	2-particle Eftimie Model	94
5.6	Discussion	102
6	Discussion	105
	Bibliography	109

List of Tables

2.1	Summary of direction-dependent interactions with conspecifics.	15
2.2	The social interaction forces in the PDE model.	17
2.3	Patterns produced by the PDE model.	22
3.1	The social interaction forces depend directly on the direction-dependent communication mechanism prescribed by each submodel.	29
3.2	Example parameter values and submodels that produce complex spatial patterns.	31
3.3	Patterns produced by the IBM.	36
4.1	Sample parameter values for patterns produced by the PDE model with density-dependent speed.	44
4.2	Parameter values for patterns when $q_r > q_a$ (PDE model).	48
4.3	Parameter values for patterns when $q_a > q_r$ (PDE model).	50
4.4	Example parameter values for patterns produced by the IBM model with density-dependent speed.	54
4.5	Parameter values for patterns when $q_a < q_r$ (IBM model).	59
4.6	Parameter values for patterns when $q_a > q_r$ (IBM model).	59
5.1	Mean separation and diffusion coefficients for 10000 samples with different $p(d)$	82
5.2	Mean separation and diffusion coefficients for 10000 samples with different $p(d)$ with range $[0.25, 0.75]$	84
5.3	Mean separation and diffusion coefficients for 10000 samples with different $p(d)$ and alignment.	91
5.4	Example parameters and patterns for investigation using the 2-particle Eftimie model.	99
5.5	Mean separation distance and diffusion coefficients for patterns produced by the IBM.	99

List of Figures

1.1	Cartoon depiction of the social interaction zones.	3
2.1	Cartoon depiction of the three social interaction zones surrounding an individual at location x	12
2.2	The social interaction kernels, $K_j(s)$, $j = r, al, a$	13
2.3	Cartoon depiction of the direction-dependent communication mechanisms in submodels M1 through M5.	16
2.4	The movement of right- and left-moving individuals.	19
2.5	Examples of patterns produced by the PDE model.	21
3.1	The direction-dependent communication mechanism in submodel M1.	27
3.2	Examples of patterns obtained by the IBM with various communication mechanisms.	32
3.3	Density plots of patterns obtained by the IBM with various communication mechanisms.	33
3.4	Semi-zigzag pulse produced by submodel M4.	34
3.5	Zigzag pulses with different turning rates.	37
3.6	The revised repulsion social interaction kernel, $\tilde{K}_r(s)$	38
3.7	Stationary pulse formed using the revised repulsion kernel, $\tilde{K}_r(s)$	39
4.1	Examples of patterns produced by the PDE model with density-dependent speed.	45
4.2	Social interaction kernels in the PDE model with density-dependent speed.	47
4.3	Patterns formed in the PDE model when repulsion is stronger than attraction, $q_r > q_a$	49
4.4	Patterns formed in the PDE model when attraction is stronger than repulsion, $q_r < q_a$	51
4.5	Examples of patterns obtained by the IBM with various communication mechanisms and density-dependent speed.	56
4.6	Density plots of examples of patterns obtained by the IBM with various communication mechanisms and density-dependent speed.	57
4.7	Splitting and merging behaviour in the IBM with density-dependent speed.	58
4.8	Patterns formed in the IBM model when repulsion is stronger than attraction.	62

4.9	Estimated probability density corresponding to the trajectories shown in Figure 4.8	63
4.10	Patterns formed in the IBM model when attraction is stronger than repulsion.	64
4.11	Estimated probability density corresponding to the trajectories shown in Figure 4.10.	65
5.1	Cartoon depiction of the one-dimensional anti-symmetric exclusion process. .	70
5.2	Cartoon depiction of particle movement in the anti-symmetric exclusion process.	71
5.3	Cartoon depiction of the one-dimensional anti-symmetric exclusion process with social interactions.	75
5.4	Example interaction functions, $p(d)$	77
5.5	Sample trajectories of the 2-particle model with social interactions.	80
5.6	Statistics for 10000 samples with the Heaviside $p(d)$, (5.11).	81
5.7	Statistics for 10000 samples with the piecewise linear $p(d)$, (5.12).	81
5.8	Statistics for 10000 samples with the saturating $p(d)$, (5.13).	82
5.9	Sample interaction functions, $p(d)$, with range $[0.25, 0.75]$	84
5.10	Statistics for 10000 samples with the modified Heaviside $p(d)$ with range $[0.25, 0.75]$	85
5.11	Statistics for 10000 samples with the modified piecewise linear $p(d)$ with range $[0.25, 0.75]$	85
5.12	Statistics for 10000 samples with the modified saturating $p(d)$ with range $[0.25, 0.75]$	86
5.13	Relationship between mean separation distance and D_M	87
5.14	Example trajectories of the 2-particle model with alignment	90
5.15	Statistics for 10000 samples with the Heaviside $p(d)$ and alignment interactions.	92
5.16	Statistics for 10000 samples with the piecewise linear $p(d)$ and alignment interactions.	92
5.17	Statistics for 10000 samples with the saturating $p(d)$ and alignment interactions.	93
5.18	Mean separation distance and diffusion coefficient for different interaction zone sizes.	94
5.19	Mean separation distance, $d(t)$, for patterns produced by the IBM.	100
5.20	MSD for patterns produced by the IBM.	101

Chapter 1

Introduction

1.1 Overview

Flocks of birds, schools of fish, and insect swarms provide examples of animals exhibiting collective behaviour. These groups of animals form complex spatial patterns as individuals coordinate their movements in efforts to search for a mate, forage for sustenance, or to evade predation. It is scientifically important to understand the underlying decisions and rules that lead groups of individuals to form complex spatial patterns as it is often necessary to understand how to develop controls to these behaviours. For instance, understanding animal behaviour is useful in efforts to develop effective fishing strategies [32], to predict and prevent insect outbreaks [37], or to manage the movements of collections of robots. For example, in [27], a group of robots is able to perform collective tasks without centralized control or explicit instructions, demonstrating that an understanding of collective behaviour has application to robotics and autonomous systems.

In this thesis, we only focus on groups of individuals that are self-organized. We do not include external factors such as environmental conditions or spatial structures that lead to group formation, but instead on those complex spatial patterns that result from interactions between conspecifics. Within this context, there are two general methodologies for studying collective behaviour. On the one hand, continuum models track the dynamics of the density of individuals throughout time and space. On the other hand, an individual-based approach can be taken, where a set of rules guides the decision-making and subsequent movement of members of the population in question. A variety of analytical methods exist for continuum models, and the study of these types of models is quite active [11]. Individual-based models (IBMs) rely on computer simulations and qualitative results; however, a few quantitative

methods are beginning to become prevalent such as coarse-grained analysis [25, 26].

Mathematical models of collective behaviour seek to understand the basic interactions between individuals that lead to pattern formation. By incorporating different assumptions regarding an individual's movement and interactions with conspecifics into models, links between mechanism and emergent phenomena can be created. Eftimie *et al.* [10, 12, 14] incorporated direction-dependent animal communication mechanisms into a partial differential equation (PDE) model of collective behaviour, resulting in a wide variety of spatial patterns, including some novel patterns. These spatial patterns are visible at the level of the population density, and it is unknown exactly how individuals in a population respond to conspecifics. The main purpose of this thesis is to understand direction-dependent communication from the perspective of an individual in a population by studying an individual-based model (IBM) with direction-dependent communication mechanisms.

To provide background, some continuum models are reviewed in Section 1.2 and some individual-based models are reviewed in Section 1.3. Animal communication mechanisms are discussed in Section 1.4, and an outline of this thesis is presented in Section 1.5.

1.2 Eulerian Models

In this section, we briefly review selected Eulerian models of collective behaviour. These models describe the dynamics of the population density of individuals, typically using partial differential equations (PDEs). The interactions between individuals in these models is often restricted to attractive and repulsive interactions alone, or to alignment interactions alone. Attractive interactions refer to the impetus for individuals separated by large distances to move together; repulsive interactions refer to individuals to avoid collision with neighbours in their immediate vicinity; and alignment interactions refer to the tendency to align in the same direction of travel as neighbours at intermediate distances. These interactions are viewed as intervals surrounding a reference individual in one-dimension, as circles in two-dimensions, and as spheres in three-dimensions. A cartoon of the interaction zones and their relation to the reference individual is presented in Figure 1.1. Moreover, these interactions can be local, where very close neighbours are important, or these interactions can be nonlocal, where distant individuals are prioritized. Typically, these models are adapted from other models, derived using correlated random walk methods, or by using Fick's law [10]. The advantage of using partial differential equation models in the study of collective behaviour is the well-developed study of these equations and their solutions. The biggest disadvantage,

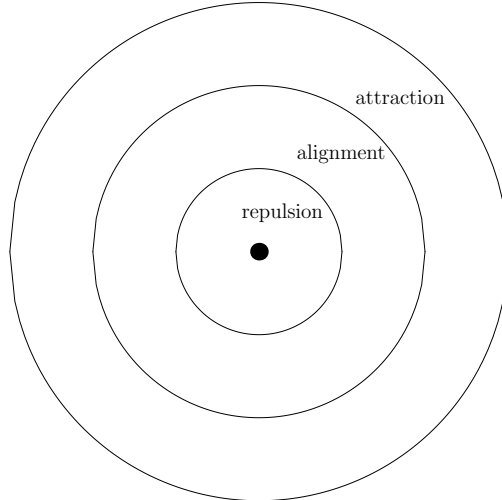


Figure 1.1: Cartoon depiction of the social interaction zones. Repulsion acts on short distances from the target individual, alignment acts on intermediate distances from the target individual, and attraction acts on large distances from the target individual.

however, is that many of the PDE models are only biologically realistic for large numbers of individuals.

Eulerian models of collective behaviour fall into two types: parabolic and hyperbolic models. The type depends on the partial differential equation used to describe the dynamics of the population. In the remainder of this section, we will review the complex spatial patterns produced by parabolic and hyperbolic PDE models for collective behaviour.

The use of *parabolic* PDE in models of collective behaviour is widespread [10,11]; however, these models unrealistically imply infinite propagation speed of population density. Parabolic models are well-suited to measure the population as a whole using mean square displacement and mean population drift [11]. Typically, these equations take the form

$$\frac{\partial u(x, t)}{\partial t} = \nabla \cdot (D \nabla u) - \nabla \cdot (V u) + G(u), \quad (1.1)$$

where $u(x, t)$ is the population density at x at time t , D is the diffusion coefficient, V is the advection coefficient, and $G(u)$ is an optionally included reaction term (modelling population dynamics). Biological aggregations have well defined boundaries, with the population density falling to zero outside of the group. When biologically realistic models with local interactions failed to exhibit travelling pulses, the research direction changed to focus on non-local interactions. To incorporate non-local interactions, Mogilner and Edelstein-Keshet use an integro-differential equation model to incorporate non-local attraction and

repulsion to investigate the formation of traveling bands of individuals [30]. They consider a one-dimensional equation of the form

$$\frac{\partial u(x, t)}{\partial t} = \frac{\partial}{\partial x} \left(D \frac{\partial u}{\partial x} - V(u)u \right), \quad (1.2)$$

where $V(u)$ is a non-local density-dependent velocity of the form

$$V(u) = K * u = \int_{\Omega} K(x - x')u(x', t)dx'. \quad (1.3)$$

In this case, K is a kernel associating an interaction strength per unit of density. Interaction kernels are common in models of collective behaviour and will be discussed in this thesis. Mogilner and Edelstein-Keshet find traveling pulses, provided that diffusion is also density-dependent. Other parabolic models give rise to rippling patterns [23] as well as stationary pulses [39].

Although the choice of *hyperbolic* models also requires a large population of individuals, the advantage is finite propagation speeds and the ability to incorporate data from individual-tracking experiments [11]. The general equation for hyperbolic models is

$$\frac{\partial u}{\partial t} + \frac{\partial H(u)}{\partial x} = f(u), \quad (1.4)$$

where $u(x, t)$ is the population density, $H(u)$ is a function describing the advective movement, and $f(u)$ is a reaction term modelling the population dynamics. Typically, however, one considers right- and left-moving population densities, and derives a PDE via Goldstein-Kac theory for correlated random walks in one-dimension [18, 24]. This leads to the following hyperbolic equations for the right- (u^+) and left-moving (u^-) population densities:

$$\begin{aligned} \frac{\partial u^+}{\partial t} + \gamma \frac{\partial u^+}{\partial x} &= -\lambda^+ u^+ + \lambda^- u^-, \\ \frac{\partial u^-}{\partial t} - \gamma \frac{\partial u^-}{\partial x} &= \lambda^+ u^+ - \lambda^- u^-, \end{aligned} \quad (1.5)$$

where λ^{\pm} are turning rates, and γ is the constant movement speed.

Lutscher and Stevens [28] use this type of model to describe the formation and movement of colonies of *Myxobacteria*. In their model, the turning rates are allowed to depend pointwise on the population density, that is, the interactions are local. This model reproduces the rippling behaviour found in *Myxobacteria* colonies. Pfister [33] considers non-local align-

ment interactions into a model for *Myxobacteria* colonies, producing stationary and moving swarms. Overall, these models, however apt at explaining a particular behaviour observed in nature, are unable to account for the wide variety of complex spatial patterns found. Eftimie *et al.* [10, 12, 14] address this issue and suggest that animal communication mechanisms are an important ingredient. We will review the work of Eftimie *et al.* in Chapter 2, as it forms the foundation for the work in this thesis.

1.3 Lagrangian Models

In this section, we briefly review selected Lagrangian models of collective behaviour. In these models, a set of decision rules govern the movement of individuals, and the resulting group-level behaviour is studied. Typically, these individual-based models (IBMs) rely on three types of social interactions: repulsion from nearby neighbours, alignment with neighbours at intermediate distances, and attraction to distant neighbours. These zones surround each individual in the population, as sketched in Figure 1.1. The social interactions are dependent on presence or absence of conspecifics in these zones. Typically these social interactions are considered to additively affect the movement of neighbours; however, they may also be considered in a hierarchical decision making process.

To observe the effect of the social interactions on the group-level pattern formation, IBMs use simulations to investigate the structure of the group in response to changes in the social interactions. An early model of collective behaviour is the three-dimensional model for schooling fish proposed by Huth and Wissel [22]. Huth and Wissel assume that individuals move in response to repulsion, attraction, and those conspecifics with parallel orientation, with these effects averaged over a minimum number of neighbours. This model verified the use of repulsion, alignment, and attraction interactions by comparing the model results with experimental data. Simple patterns, such as a highly polarized school, a loosely polarized school, and the merging behaviour of two small schools, result from the model. This polarized behaviour is lost in the absence of attractive and alignment interactions.

In [7], Couzin *et al.* present a three-dimensional model of collective behaviour, and show that group-level behavioural transitions are related to minor changes in individual-level interactions. The model produces four collective behaviours: swarm, torus, dynamic parallel group, and highly parallel group. The collective behaviour of the group depends on the size of the zone of alignment and the zone of attraction, that is, the distance over which alignment and attraction forces are considered, respectively. Small changes in individual

responses, for example, changing the size of the zone of repulsion, influences a large change in group properties. Moreover, the patterns produced by the group depend on the previous arrangement of the individuals. These results suggest that the magnitudes of the social interaction forces strongly influence the group behaviour.

The model proposed by Gueron *et al.* [20] is a two-dimensional stochastic model based on a hierarchical set of decisions made by individuals. Surrounding an individual are several interaction zones of variable size and the presence or absence of conspecifics in these zones govern an individuals' behaviour. Most models of collective behaviour assume that individuals move with constant speed; however, this assumption is not biologically realistic. Gueron *et al.* include a density-dependent speeding and slowing mechanism, leading to group splitting. When leading individuals in the model reduce speed in response to conspecifics behind, group cohesion is maintained, provided the speed of the leaders is not too large. The balance between speeding and slowing in response to conspecifics is responsible for the cohesion or fragmentation of the groups in this stochastic model.

As these examples show, individual-based models of collective behaviour produce a wide variety of spatial patterns. More contemporary approaches also successfully model collective behaviour. For instance, Hildenbrandt *et al.* [21] incorporate additional information from the specific species' biology to accurately model large flocks of starlings. Aside from the three social interaction zones, Hildenbrandt *et al.* include flight mechanics, movement toward a roosting area, and restrict the number of conspecifics that an individual can interact with. As a result of the incorporation of these added ingredients, the model is complicated, but simulated flocks are almost indistinguishable from video of real flocks.

Instead of complicated social interactions, the Cucker-Smale model [9] uses a simple weighted velocity-averaging process to show the emergence of flocking behaviour in contrast to the usual three-zone framework. Cucker-Smale models are often adapted to incorporate other mechanisms, for example to examine the effect of noisy communication [4, 8]. Other models seek to understand collective behaviour in groups with leaders or in other environments (see [42] for an extended review of individual-based models).

In general, some complex spatial patterns form in these models, but the models do not suggest mechanisms for the formation of the multitude of spatial patterns observed in nature. Following the idea of Eftimie *et al.* that animal communication mechanisms are an important ingredient, we include direction-dependent communication mechanisms in an one-dimensional IBM of collective behaviour in Chapter 3, revealing that all of the complex spatial patterns formed by the PDE model are also produced by the IBM.

1.4 Animal Communication Mechanisms

Eftimie *et al.* [10, 12, 14] were the first to suggest animal communication mechanisms as an important ingredient in models of collective behaviour. Eftimie *et al.* superimpose mechanisms that describe not only how much information an individual receives, but also the manner in which that information is received. The three social interaction forces incorporate this additional directional information. This addition complicates the model, but is biologically well motivated as it is known that individuals tend to respond to signals from their conspecifics by changing their behaviour [29]. Many examples of communication can be found in biological systems. The movement of Mormon crickets, for example, is influenced by the signals perceived from conspecifics moving in the same direction as the target individual [38]. In some species of fish, neighbours directly ahead are used to guide movements in place of fish directly adjacent [31], and some species of birds use directional sound signals to coordinate movements where the signal receiver must be faced by the signal emitter [40]. These examples illustrate the importance of incorporating direction-dependent communication mechanisms in animal groups, and we consequently focus on direction-dependent communication mechanisms in this thesis.

1.5 Thesis Outline

The outline of this thesis is the following. In Chapter 2, we review the PDE model of Eftimie *et al.* [10, 12, 14] with direction-dependent communication mechanisms. This non-local hyperbolic PDE model is one-dimensional and describes the dynamics of the densities of the left- and right-moving populations. We review the development of the PDE model from an existing PDE model, and its derivation from a correlated random walk. The correlated random walk links individual-level behaviour to the PDE model, and we focus on how the social interaction forces are modelled in terms of the location and direction of travel of conspecifics.

Given the rich pattern formation behaviour of the PDE model with communication mechanism, a question that arises immediately is whether the complex spatial patterns formed are unique to hyperbolic models. Can an individual-based model reproduce the same patterns?

The goal of Chapter 3 is to understand better how individuals respond to direction-dependent communication mechanisms. We hypothesize that an individual-based model with direction-dependent communication mechanisms will enrich pattern formation and match the rich behaviour of the Eftimie PDE model. We develop a new one-dimensional IBM using the

social interactions and communication mechanisms described in the random walk derivation of the PDE model. Numerical simulations of the IBM with a variety of parameters and communication mechanisms reveals that the IBM matches the rich behaviour of the PDE model. The inherent stochasticity in the IBM adds biological realism to the model, and most importantly the IBM reveals the behaviour of individuals interacting with direction-dependent communication mechanisms.

An assumption of the IBM is that individuals move with a constant speed and only change direction in response to communication from distance neighbours. This assumption is not biologically realistic, and the incorporation of density-dependent movement speed is the subject of Chapter 4. Density-dependent speed has been introduced previously to the PDE model in [10,17], and we briefly review this work in Chapter 4. As a result of including density-dependent movement speeds, splitting and merging patterns are observed. We hypothesize that incorporating density-dependent speed to the new IBM with communication mechanisms will also lead to splitting and merging behaviour. Numerical simulations of the IBM with density-dependent speed reveal a qualitative match to the patterns produced by the PDE model.

To better understand the response of individuals to communication mechanisms, 2-particle models are discussed in Chapter 5. A focus on group-level pattern formation does not reveal how each individual in the group responds to other individuals, motivating the use studying the interaction of just two individuals. 2-particle models have previously been used to study particle interactions on a one-dimensional lattice, and in these cases, the process is solved analytically. We begin by studying the solution to the one-dimensional anti-symmetric exclusion process given by Potts *et al.* [34], as this process provides the foundation for incorporating social interactions. Attractive and repulsive interactions alter the behaviour of the anti-symmetric exclusion process by forming stationary groups, and alignment interactions allow for the formation of moving groups. We also state master equations for these processes. Finally, considering fully direction-dependent communication mechanisms as in the PDE or IBM results in a complicated master equation yet stochastic simulations reveals a connection group-level pattern characteristics and individual-to-individual interactions. The 2-particle model framework is a foundation for further analytical work in the study of communication mechanisms.

Finally, in Chapter 6, we conclude with a discussion of these results, and present directions for future work on this subject. Overall, this thesis highlights the importance of direction-dependent communication mechanisms in the formation of complex spatial patterns

in models of collective behaviour.

Chapter 2

The Eftimie Model

2.1 Introduction

In this chapter, a one-dimensional PDE model for animal collective behaviour with direction-dependent communication mechanisms is reviewed. Direction-dependent communication mechanisms were first incorporated into a model of collective behaviour by Eftimie *et al.* in two papers [12,14], and in Eftimie's doctoral thesis [10]. This addition modifies the assumption that social interactions depend only on the distance between conspecifics to include a dependence on the direction that conspecifics travel. Direction-dependent mechanisms are considered to be facilitated by animal communication, and this addition was hypothesized to account for the variety of complex spatial patterns observed in nature.

In Section 2.2, we briefly review the development of the PDE model and how direction-dependent communication mechanisms are incorporated. In Section 2.2.2, we review the development of the PDE model from a correlated random walk, providing insight into the guiding mechanisms for the IBM presented in Chapter 3. The key results of [10,12,14] are summarized in Section 2.3 to offer a comparison to the new IBM developed in Chapter 3. In Section 2.4, we conclude with a discussion.

2.2 Model Development

The PDE model with direction-dependent communication mechanisms is derived under the assumption that animals move as a result of their own volition and that movement is influenced by interactions with conspecifics. The novelty of the PDE model is the combination of the modelling approach where individuals turn randomly and the approach where indi-

viduals turn in response to conspecifics. The response to conspecifics is assumed to result from animal communication. Communication signals not only include information about the distance between conspecifics but also the direction of travel. These direction-dependent communication mechanisms are translated into 5 submodels, each capturing a hypothetical communication scheme. These submodels distinguish the communication mechanisms, consequently defining the rates at which individuals change direction. In this section, two derivations of the PDE model will be reviewed. The first derivation adapts an existing model to include direction-dependent communication mechanisms, and the second derivation arrives at the PDE model by considering direction-dependent communication mechanisms in a correlated random walk.

2.2.1 Adaptation of Existing PDE Model

A population of right- and left-moving individuals is considered on a one-dimensional domain. The evolution of the density of right-moving ($u^+(x, t)$) and left-moving ($u^-(x, t)$) individuals is governed by the hyperbolic equations:

$$\begin{aligned} u^+(x, t)_t + (\gamma u^+(x, t))_x &= -\lambda^+ u^+(x, t) + \lambda^- u^-(x, t), \\ u^-(x, t)_t - (\gamma u^-(x, t))_x &= +\lambda^+ u^+(x, t) - \lambda^- u^-(x, t), \\ u^\pm(x, 0) &= u_0^\pm(x). \end{aligned} \tag{2.1}$$

The turning rates, λ^+ and λ^- , describe the rate at which right-moving individuals turn left, and left-moving individuals turn right, respectively. These turning rates are assumed to depend on the density of conspecifics and communication mechanisms. Individuals are assumed to move with constant speed γ in their direction of travel. Boundary conditions are periodic throughout the analysis and simulation of the PDE model. This PDE model was first used to describe alignment behaviours in *Mycobacteria* colonies, but the turning rates depended only on alignment interactions [33]. Here, the turning rates depend on repulsive, alignment, and attractive interactions as prescribed by the directional communication mechanism. That is, the turning rates are

$$\lambda^\pm = \lambda_1 + \lambda_2 f(y_r^\pm - y_a^\pm + y_{al}^\pm), \tag{2.2}$$

where the constants λ_1 and λ_2 describe a base-line turning rate and the bias turning rate, respectively, the turning function f is a dimensionless, bounded, and increasing function, and

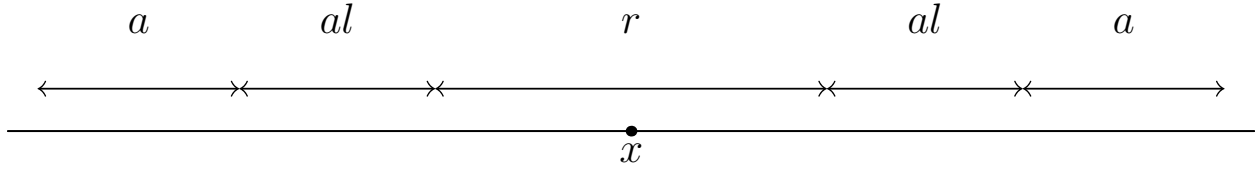


Figure 2.1: Cartoon depiction of the three social interaction zones surrounding an individual at location x . Repulsion (r) acts over short distances from the reference individual at x , alignment (al) over intermediate distances, and attraction (a) over longer distances.

$y_r^\pm, y_{al}^\pm, y_a^\pm$ are functionals of the density of individuals in the surrounding zones of repulsion (r), alignment (al) and attraction (a). The social interaction zones surround an individual, as depicted in Figure 2.1. Repulsion acts on short distances, alignment on intermediate distances, and attraction over large distances to be biologically accurate. Right- and left-moving individuals may have different social interaction forces due to asymmetry in the communication mechanism, requiring the need to distinguish $y_{r,al,a}^+$ from $y_{r,al,a}^-$ in some cases. Here, f is chosen to be a logistic function,

$$f(x) = \frac{1}{1 + e^{-2(x-y_0)}} = \frac{1}{2} + \frac{\tanh(x - y_0)}{2}, \quad (2.3)$$

with $y_0 = 2$, chosen so that in the absence of social interactions, movement is dominated by random turning.

To understand the turning rates and social interactions,(2.2), consider a right-moving individual at location x at time t . For example, suppose that there are a large number of conspecifics in this individual's zone of repulsion immediately ahead of it and only a few conspecifics in the zone of repulsion behind this individual. In this case, the individual should change direction to avoid the large group of individuals ahead of it. Correspondingly, the repulsive social interaction force, y_r^+ , should be large. This large social interaction force contributes additively to λ^+ , the turning rate, via the turning function $f(x)$ in (2.3). Similarly, if there are many conspecifics in the target individual's zone of attraction ahead and few conspecifics behind, the individual is not motivated to change direction, but rather to continue ahead and join the larger group. Hence, the attractive social interaction force, y_a^+ , should also be large, as this will decrease the turning rate λ^+ via the turning function $f(x)$ and the negative sign in front of y_a^+ in (2.2).

To weight the influence of individuals in each of the social interaction zones, Gaussian

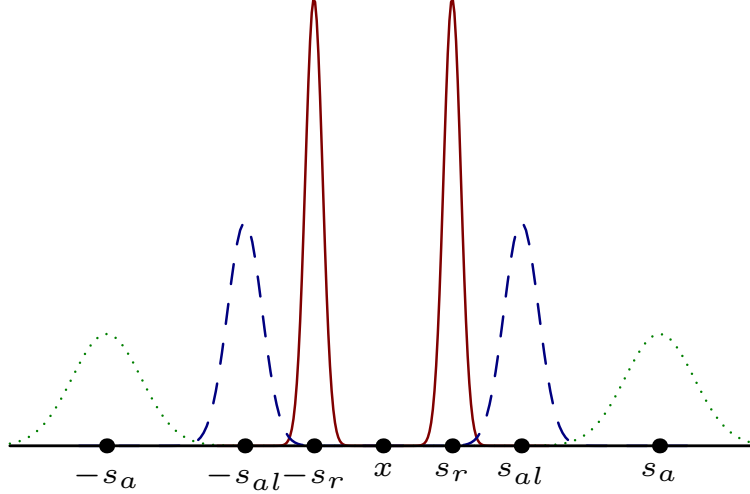


Figure 2.2: The social interaction kernels, $K_j(s)$, $j = r, al, a$. The repulsion kernel (red, solid) weights conspecifics close the target individual, the alignment kernel acts on intermediate distances (blue, dashed), and the attraction kernel acts over large distances (green, dotted).

kernels are chosen:

$$K_j(s) = \frac{1}{\sqrt{2\pi m_j^2}} \exp\left(-\frac{(s - s_j)^2}{2m_j^2}\right), \quad (2.4)$$

$j = r, al, a$. Here, s_j describes the centre of the Gaussian kernel and m_j describes the width ($j = r, al, a$). The parameters s_j and m_j are chosen to arrange the social interaction zones in a biologically meaningful way, namely, with repulsion acting on short distances, alignment on intermediate distances, and attraction on larger distances. In practice, these kernels are truncated to have compact support. The social interaction kernels are sketched in Figure 2.2.

Direction-dependent communication mechanisms are prescribed via 5 hypothetical submodels. For instance, in submodel M1, the reference individual uses information about all conspecifics regardless of their direction of travel for repulsive and attractive signals, but only information from those neighbours who are moving toward the reference individual. The 5 hypothetical submodels are easily described pictorially, as shown in Figure 2.3. The social interaction forces reflect these communication mechanisms by considering the appropriate density of right- or left-moving (or both) individuals. The social interaction forces dictated

by submodel M1 are:

$$y_{r,a}^{\pm} = q_{r,a} \int_0^{\infty} K_{r,a}(s) (u(x \pm s) - u(x \mp s)) ds, \quad (2.5)$$

$$y_{al}^{\pm} = q_{al} \int_0^{\infty} K_{al}(s) (u^{\mp}(x \pm s) - u^{\pm}(x \mp s)) ds. \quad (2.6)$$

The parameters q_j , $j = r, al, a$ are the magnitude of the social interaction forces, and $u(x, t) = u^+(x, t) + u^-(x, t)$ is the total density. The repulsive and alignment forces compare the strength of the forces ahead and behind the reference individual, whereas the alignment forces compare the strength of forces exerted by right- or left-moving individuals. This matches with the biological interpretation of these social forces as it is biologically relevant for an individual be repelled by nearby individuals or to be attracted to distant individuals, regardless of their direction of travel. On the other hand, alignment is to adjust one's direction to match that of neighbours at an intermediate distance. Direction-dependent communication mechanisms are not limited to submodel M1, and 4 other hypothetical submodels are considered. These five submodels capture various information receiving mechanisms, and exemplify how different environmental or biological constraints may be incorporated into this model. The submodels are defined as follows:

- M1: the repulsion and attraction social interaction forces depend on information from all individuals in the repulsion and attraction zones, respectively; however, the alignment social interaction force only depends on individuals heading towards the reference individual (as above);
- M2: all three social interactions depend on all individuals, regardless of their direction of travel within the social interaction zones;
- M3: all three social interaction forces depend only on the information received from individuals ahead of the reference individual;
- M4: all three social interaction forces depend on the information from the zones ahead and behind, but only from those neighbours who are moving toward the reference individual;
- M5: all three social interaction forces depend only on the information from individuals ahead and moving toward the reference individual.

Submodel	Repulsion	Alignment	Attraction
M1	all	toward	all
M2	all	all	all
M3	all ahead	all ahead	all ahead
M4	toward	toward	toward
M5	ahead & toward	ahead & toward	ahead & toward

Table 2.1: Summary of direction-dependent interactions with conspecifics. Each communication mechanism is described as a submodel (M1-M5). The submodel indicate which individuals contribute to the social interaction forces based upon their direction of movement and location relative to the target individual. In the table, “all” refers to all neighbours, “all ahead” refers to all neighbours ahead, “toward” refers to all neighbours moving toward the target individual, and “ahead & toward” refers to all neighbours ahead of the target individual that are moving toward the target individual.

A summary of the direction-dependent interactions is presented in Table 2.1, and the social interaction forces for the 5 submodels are listed in Table 2.2. The 5 submodels are easily understood graphically, and cartoons are presented in Figure 2.3.

2.2.2 Derivation from Correlated Random Walk

The PDE model, (2.1), can be derived from a correlated random walk, as in Section 2.4 of [10]. This derivation provides insight into the direction-dependent mechanisms that lead to group pattern formation, and forms the basis for the new individual-based model developed in Chapter 3.

To describe the correlated random walk, one-dimensional space is discretized into intervals of length Δx , and time is discretized into intervals of length Δt . Let $p^+(x, t)$ denote the probability of finding a right-moving individual in the interval $[x - \frac{\Delta x}{2}, x + \frac{\Delta x}{2})$ at time t and $p^-(x, t)$ denote the probability of finding a left-moving individual in the interval $[x - \frac{\Delta x}{2}, x + \frac{\Delta x}{2})$ at time t . A right-moving individual can be at x at time $t + \Delta t$ if either the individual was left-moving at $x + \Delta x$ at time t and turns in response to distant neighbours at $x \pm k\Delta x$, $k \in \mathbb{N}$, describing the social interaction zones, or if the individual was right-moving at $x - \Delta x$ at time t and does not change direction, as illustrated in Figure 2.4. That is,

$$p^+(x, t + \Delta t) = p^+(x - \Delta x, t)(1 - \lambda^+ \Delta t) + p^-(x + \Delta x, t)\lambda^- \Delta t. \quad (2.7)$$

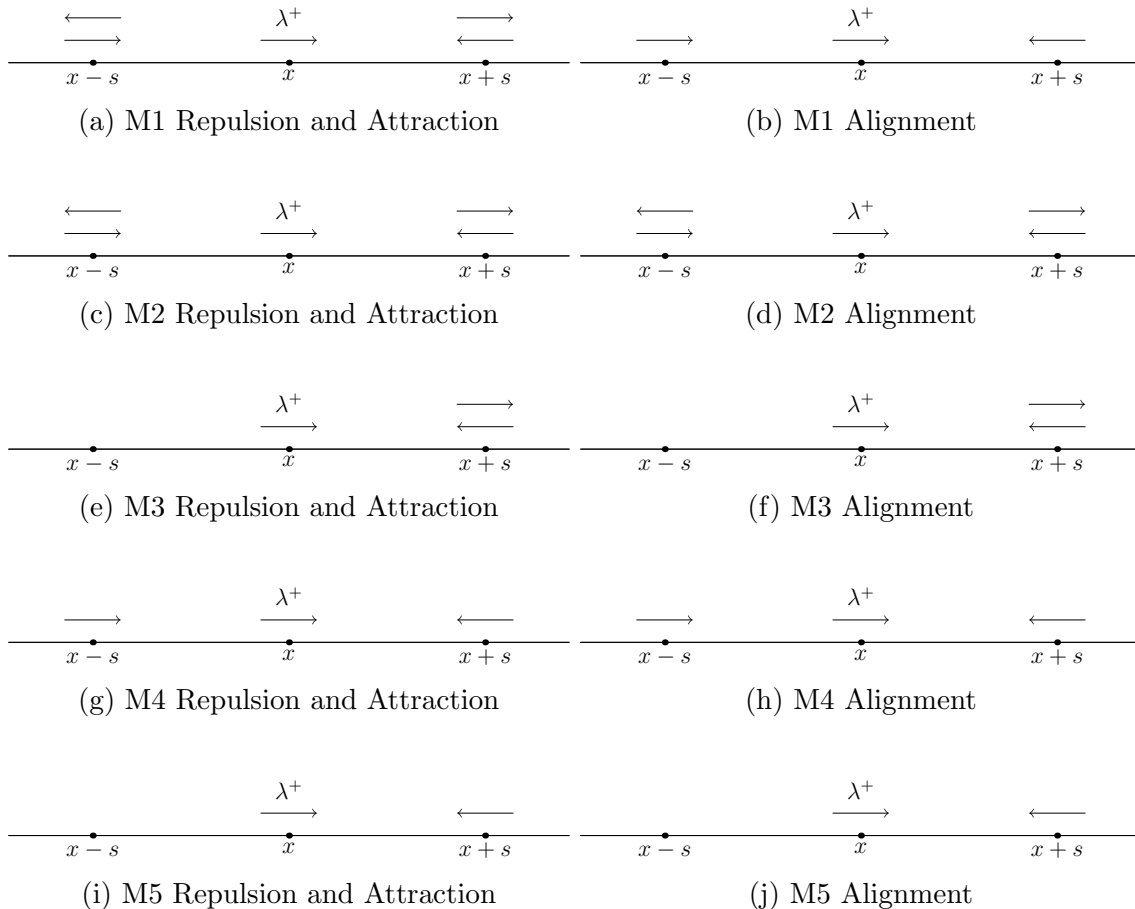


Figure 2.3: Cartoon depiction of the direction-dependent communication mechanisms in submodels M1 through M5. A right-moving reference individual at x receives signals from distant individuals, to the right at $x+s$, and from the left at $x-s$. Arrows at $x+s$ and $x-s$ indicate whether the reference individual will receive stimuli from distant right-moving (right arrow) and distant left-moving (left arrow) neighbours. For example, the direction-dependent communication mechanism in submodel M3 ((e) and (f)) uses information from both left- and right-moving neighbours ahead of the reference individual for repulsion, attraction, and alignment.

Submodel	Repulsion & Attraction interaction force Alignment interaction force
M1	$y_{r,a}^{\pm} = q_{r,a} \int_0^{\infty} K_{r,a}(s) (u(x \pm s) - u(x \mp s)) ds$ $y_{al}^{\pm} = q_{al} \int_0^{\infty} K_{al}(s) (u^{\mp}(x \pm s) - u^{\pm}(x \mp s)) ds$
M2	$y_{r,a}^{\pm} = q_{r,a} \int_0^{\infty} K_{r,a}(s) (u(x \pm s) - u(x \mp s)) ds$ $y_{al}^{\pm} = q_{al} \int_0^{\infty} K_{al}(s) (u^{\mp}(x \pm s) + u^{\mp}(x \mp s) - u^{\pm}(x \pm s) - u^{\pm}(x \mp s)) ds$
M3	$y_{r,a}^{\pm} = q_{r,a} \int_0^{\infty} K_{r,a}(s) (u(x \mp s)) ds$ $y_{al}^{\pm} = q_{al} \int_0^{\infty} K_{al}(s) (u^{\mp}(x \pm s) - u^{\pm}(x \pm s)) ds$
M4	$y_{r,a}^{\pm} = q_{r,a} \int_0^{\infty} K_{r,a}(s) (u^{\mp}(x \pm s) - u^{\pm}(x \mp s)) ds$ $y_{al}^{\pm} = q_{al} \int_0^{\infty} K_{al}(s) (u^{\mp}(x \pm s) - u^{\pm}(x \mp s)) ds$
M5	$y_{r,a}^{\pm} = q_{r,a} \int_0^{\infty} K_{r,a}(s) (u^{\mp}(x \pm s)) ds$ $y_{al}^{\pm} = q_{al} \int_0^{\infty} K_{al}(s) (u^{\mp}(x \pm s)) ds$

Table 2.2: The social interaction forces in the PDE model. These forces depend directly on the direction-dependent communication mechanism prescribed by each submodel. The repulsive and alignment forces compare the strength of the forces ahead and behind the reference individual; whereas, the alignment forces compare the strength of forces exerted by right- or left-moving individuals. $u = u^+ + u^-$ is the total density of individuals, q_j , $j = r, al, a$, are the magnitudes of the social interaction forces, and K_j , $j = r, al, a$, are Gaussian kernels described in Equation 2.4.

Similarly, the probability of finding a left-moving individual at x at time $t + \Delta t$ is

$$p^-(x, t + \Delta t) = p^-(x + \Delta x, t)(1 - \lambda^- \Delta t) + p^+(x - \Delta x, t)\lambda^+ \Delta t. \quad (2.8)$$

Here, λ^\pm are the turning rates, and so $\lambda^\pm \Delta t$ is the probability that an individual changes direction. A Taylor expansion of (2.7) and (2.8) about (x, t) gives

$$p^+(x, t) + \Delta t p_t^+(x, t) = [p^+(x, t) - \Delta x p_x^+(x, t)] (1 - \lambda^+ \Delta t) + [p^-(x, t) + \Delta x p_x^-(x, t)] \lambda^- \Delta t + O(\Delta x^2, \Delta t^2) \quad (2.9)$$

$$p^-(x, t) + \Delta t p_t^-(x, t) = [p^-(x, t) + \Delta x p_x^-(x, t)] (1 - \lambda^- \Delta t) + [p^+(x, t) + \Delta x p_x^+(x, t)] \lambda^+ \Delta t + O(\Delta x^2, \Delta t^2), \quad (2.10)$$

where the subscripts denote partial derivatives, for example, $p_x^+(x, t) = \frac{\partial p^+}{\partial x}(x, t)$. Omitting the function arguments and neglecting higher order terms, we find,

$$\begin{aligned} p_t^+ + \frac{\Delta x}{\Delta t} p_x^+ &= -\lambda^+ p^+ + \lambda^- p^- + \Delta x \lambda^+ p_x^+ + \Delta x \lambda^- p_x^-, \\ p_t^- - \frac{\Delta x}{\Delta t} p_x^- &= \lambda^+ p^+ - \lambda^- p^- - \Delta x \lambda^+ p_x^+ - \Delta x \lambda^- p_x^-. \end{aligned} \quad (2.11)$$

Taking the limit as $\Delta x \rightarrow 0$, $\Delta t \rightarrow 0$, with $\frac{\Delta x}{\Delta t} = \gamma$ results in the PDE model:

$$\begin{aligned} u^+(x, t)_t + (\gamma u^+(x, t))_x &= -\lambda^+ u^+(x, t) + \lambda^- u^-(x, t), \\ u^-(x, t)_t - (\gamma u^-(x, t))_x &= +\lambda^+ u^+(x, t) - \lambda^- u^-(x, t), \end{aligned} \quad (2.12)$$

where u^\pm are interpreted as probability density functions.

Typically, the turning rates λ^\pm are only random, that is, individuals change direction according to Poisson processes with rates λ^\pm ; however, to incorporate direction-dependent mechanisms, a nonlocal response is added to the turning rates. This leads to the definition of the turning probability

$$\lambda^\pm = \frac{\lambda_1}{2} + \frac{\lambda_2}{2} F^\pm, \quad (2.13)$$

where λ_1 and λ_2 describe a base-line and bias turning probabilities, and F is a increasing, uniformly continuous, function of distant conspecifics, with $0 < \lambda_1, \lambda_2, F < 1$. In order to calculate the function F , a Poisson point assumption needs to be imposed [10,19]. Formally, a group of individuals are Poisson points if

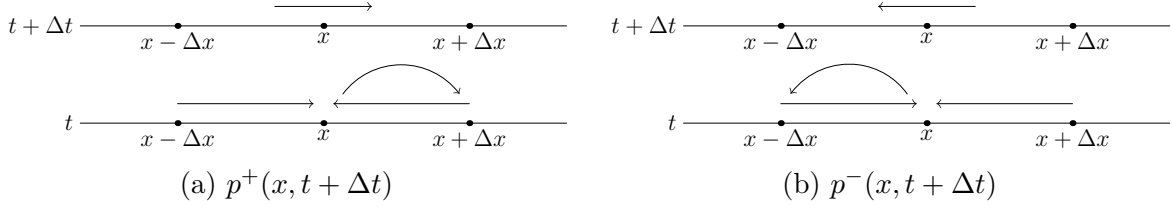


Figure 2.4: The movement of right- and left-moving individuals. A right-moving individual at x at time $t + \Delta t$, (a), was either right-moving at $x - \Delta x$ at time t and did not change direction or was left-moving at $x + \Delta x$ at time t and changes direction. Similarly, a left-moving individual at x at time $t + \Delta t$, (b), was either left-moving at $x + \Delta x$ at time t and does not change direction or was right-moving at $x - \Delta x$ at time t and changes direction. These jumps and direction changes describe the correlated random walk that lead to the hyperbolic PDE model (2.1).

1. the probability of ν individuals being present in a sample from an interval $[a, b]$ depends only on ν, a, b ,
2. the probabilities of n samples from n distinct intervals are independent, and
3. there is a zero probability that a sample on a finite interval is infinite.

Here, 1 and 2 are not explicitly satisfied, as one of the fundamental assumptions of the movement model is that a large number of individuals in an interval may be correlated with a change of individuals in a neighbouring interval. The Poisson point assumption is therefore necessary to calculate the expected number of individuals at distant spatial locations from the reference individual. That is, if the reference individual is at x , the expected number of individuals at $x + k\Delta x$, $k \in \mathbb{Z}$, is $Np^\pm(x + k\Delta x, t)$, where N is the total population size. Without the Poisson point assumption, this expected number of individuals is conditional upon the location and direction of other individuals. Hence, the probability of turning in response to distant neighbours, assuming the communication mechanism in submodel M1, is

$$\lambda^\pm = \frac{\lambda_1}{2} + \frac{\lambda_2}{2} F \left(\pm N \sum_{j=-\infty}^{\infty} K_r(j\Delta x) (p(x + j\Delta x, t) - p(x - j\Delta x, t)) \mp N \sum_{j=-\infty}^{\infty} K_a(j\Delta x) (p(x + j\Delta x, t) - p(x - j\Delta x, t)) \pm N \sum_{j=-\infty}^{\infty} K_{ai}(j\Delta x) (p^-(x + j\Delta x, t) - p^+(x - j\Delta x, t)) \right), \quad (2.14)$$

where $p = p^+ + p^-$. Since F is uniformly continuous, we find the turning rate as given by equation (2.2) as the same limit from (2.12) is taken.

2.3 Key Results

In [10], the numerical method used to study the PDE model, (2.1), is described. These details are omitted here, and this section focus on the complex spatial patterns formed by varying communication mechanisms and by exploring parameter space. An analysis of the PDE model reveals that the stability of the steady states depend on the magnitude of the interaction parameters (q_r, q_{al}, q_a) and the magnitude of the turning rates (λ_1, λ_2) . Unsurprisingly, these are the parameters that can be used to characterize animal groups during movement and different behaviours. The goal of parameter exploration in [10] was not to find all the patterns, but rather to demonstrate the variety of complex spatial patterns that result from varying direction-dependent communication mechanisms. Example patterns are shown in Figure 2.5 (from [10]). Not only does the PDE model reproduces classic patterns such as stationary pulses, ripples, and traveling trains, but also produces novel patterns, namely, zigzag pulses, semi-zigzag pulses, breathers, traveling breathers, and feathers. Stationary pulses (Figure 2.5 (1) and (2)) are aggregations that remain at a spatial location. Ripples (Figure 2.5 (3)) form when a right-moving aggregation and left-moving aggregation pass through each other. Feathers form when individuals are lost from the boundary of stationary pulses (Figure 2.5 (4)). Traveling pulses and traveling trains are aggregations that move across the domain. Traveling pulses are characterized by a large aggregation moving (Figure 2.5 (5)), whereas traveling trains consist of many small groups, like train cars, that travel in unison (Figure 2.5 (6)). Zigzag pulses (Figure 2.5 (7)) are pulses that travel across the domain while occasionally changing direction. Breathers and traveling breathers (Figure 2.5 (8) and (9)) are groupings that expand and contract throughout time, and are either stationary or traveling. A portion of parameter space was also explored in each submodel. Three cases were considered:

Case (a): attraction and repulsion only,

Case (b): alignment only,

Case (c): all three social interaction forces.

For details, refer to Section 3.3, as the same parameter space is sampled when simulating the IBM, or refer to [10]. Table 2.3 summarizes the results of this parameter exploration.

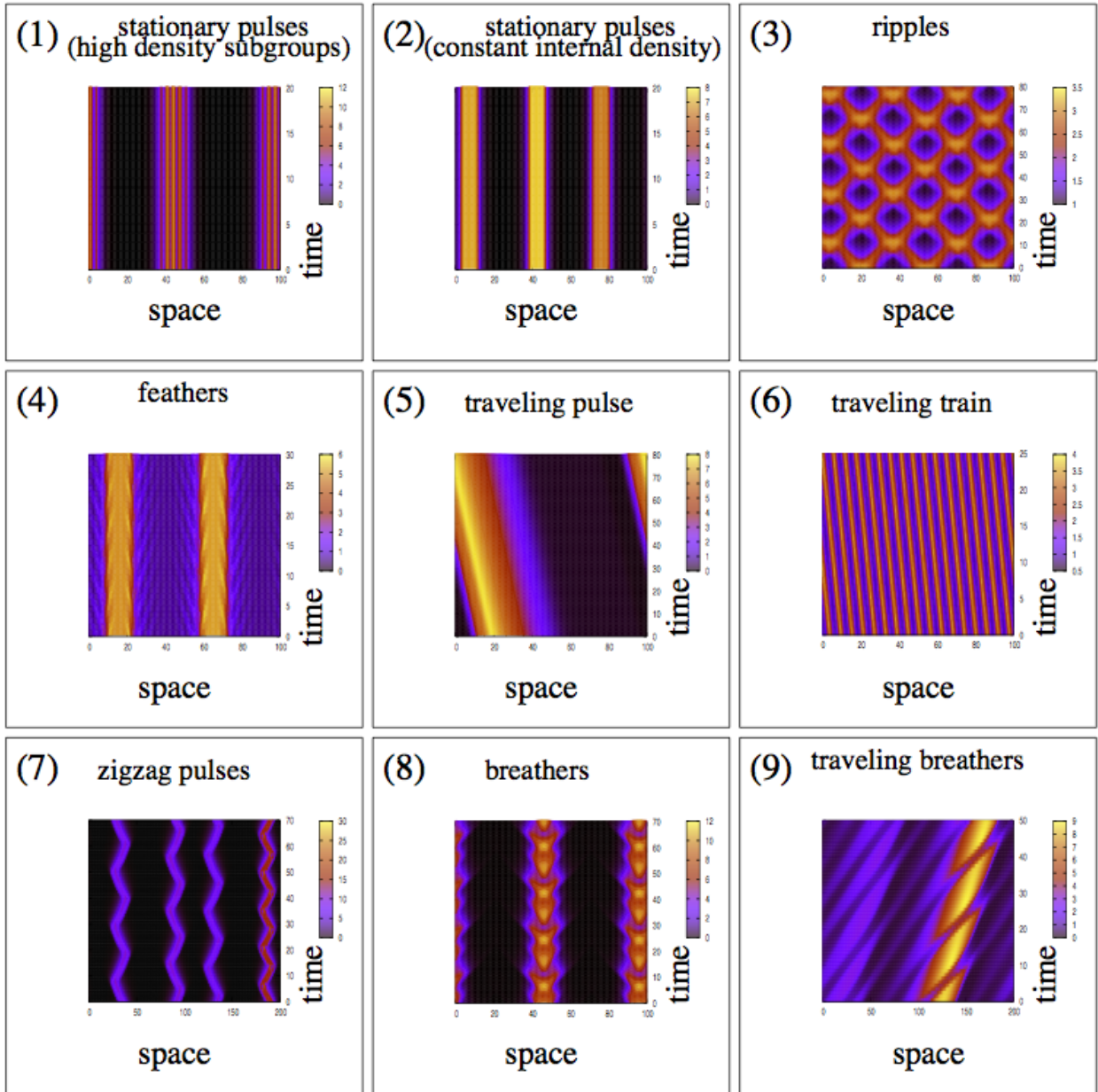


Figure 2.5: Examples of patterns produced by the PDE model. Figure from [10]. Boundary conditions are periodic, and parameters listed in Table 3.2.

Model	Stationary Pulse	Ripples	Feathers	Traveling pulse	Traveling train	Zigzag pulse	Breathers	Traveling breathers	Semi-zigzag pulse
M1	(a),(b),(c)	-	-	(c)	(b)	-	-	-	(b)
M2	(a),(c)	-	-	(b),(c)	(b),(c)	(c)	-	-	-
M3	-	-	(a),(c)	(c)	(b)	-	-	-	-
M4	(a),(b),(c)	-	-	(c)	(b)	(a),(c)	(a)	(a),(c)	(b)
M5	(b)	(a),(c)	-	-	-	-	-	-	-

Table 2.3: Patterns produced by the PDE model for submodels M1 through M5. (a),(b), and (c) indicate that the corresponding pattern was produced by parameters from the corresponding parameter regime. Dashes indicate that the parameter was not observed for any of the parameter regimes.

2.4 Discussion

This chapter briefly reviewed a one-dimensional PDE model for animal collective behaviour with direction-dependent communication mechanisms developed by Eftimie *et al.* This model is the first to incorporate direction-dependent communication mechanisms, and consequently, the model behaviour is greatly enriched. The PDE model was formulated in two ways, firstly, by adapting the turning rates in an existing hyperbolic PDE model for *Myxobacteria* colonies, and secondly, from a correlated random walk with nonlocal communication mechanisms. The correlated random walk derivation provides a foundation for the individual-based model with direction-dependent communication mechanisms, as discussed in Chapter 3.

The inclusion of direction-dependent communication mechanisms to the PDE model enriches the model behaviour. To incorporate nonlocal communication mechanisms, a Poisson point assumption was necessary. The validity of including this Poisson point assumption can be asserted if the movement of individuals is sufficiently random. In this case, the assumption can be validated if a stochastic IBM can match the model behaviour. Another question that arises immediately is whether the complex spatial patterns formed are unique to hyperbolic models [11]. Will an individual-based model with direction-dependent communication mechanisms produce the same patterns? This is the subject of Chapter 3.

Chapter 3

IBM with Communication Mechanisms

3.1 Introduction

In this chapter, an individual-based model with direction-dependent communication mechanisms is formulated to match the behaviour of the PDE model in Chapter 2. Here, it is hypothesized that an individual-based model (IBM) with direction-dependent communication mechanisms will enrich pattern formation, and thus suggest the importance of communication mechanisms as a factor in complex group formations.

The mechanisms behind the IBM follow from the correlated random walk that results in the PDE model, as described in Section 2.2.2. This random walk describes the movement of right- and left-moving individuals, and how individuals change direction due to the social interaction forces. However, the random walk was concerned with the time evolution of the probability of finding a right- or left-moving individual at x at time t , that is, $p^\pm(x, t)$. In place of describing the probability of finding an individual at x at time t or the population density, $u(x, t)$, the IBM is strictly Lagrangian, and tracks the position and velocity of an individual over time.

In Section 3.2, we describe the development of the IBM, specifically how the population of right- and left-moving individuals move and change direction. The social interaction forces and communication mechanisms are described in detail. In Section 3.3, we present numerical simulations of the IBM and the formation of complex spatial patterns. Finally, in Section 3.5, we discuss how communication mechanisms enrich pattern formation in this IBM.

3.2 Model Development

Individual interactions with conspecifics are described through three social interaction forces: repulsion, alignment, and attraction. Repulsion describes the tendency for individuals at close distances to avoid each other, alignment describes the tendency for individuals to align with individuals at intermediate distances, and attraction describes the tendency for individuals to be attracted toward distant individuals. In one-dimension, the social interaction forces manifest as intervals surrounding a target individual at location x as in Figure 2.1. Conspecifics in these intervals exert a social force and affect the movement of the target individual. For example, if many conspecifics are found in the zone of attraction of an individual, that individual will move towards the individuals in the zone of attraction.

An individual-based model, consisting on N individuals moving in one dimensional space, can be used to describe this social interaction mechanism. Following the development of the model in [12–14, 41], but using a Lagrangian approach, we track the position and the direction of individuals moving on a line throughout time. Individual i has position $x_i(t)$ and direction $v_i(t)$ at time t , with $x_i(t) \in \mathbb{R}$ and $v_i(t) = \pm 1$. An individual with $v_i(t) = 1$ (-1) is considered to be right- (left-) moving, and individuals change direction in response to conspecifics in their interaction zones. The social interaction forces felt by individual i are denoted by $y_{j,i}^\pm$, where the \pm sign indicates whether an individual is right-moving (+) or left-moving (-), and $j = r, al, a$ denotes repulsion (r), alignment (al), or attraction (a). A right- or left-moving individual i changes direction with rate λ_i^+ or λ_i^- , respectively, dependent on the social interaction forces:

$$\lambda_i^\pm = \lambda_1 + \lambda_2 f(y_{r,i}^\pm - y_{a,i}^\pm + y_{al,i}^\pm), \quad (3.1)$$

where the constants λ_1 and λ_2 describe a base-line turning rate and the bias turning rate, respectively, and the turning function f is some dimensionless, bounded, and increasing function. Here, f is chosen to be a logistic function,

$$f(x) = \frac{1}{1 + e^{-2(x-y_0)}} = \frac{1}{2} + \frac{\tanh(x - y_0)}{2}, \quad (3.2)$$

with $y_0 = 2$, chosen so that in the absence of social interactions, movement is dominated by random turning. Moreover, the repulsion and attraction social interaction forces enter the turning function with the opposite sign as these two interactions have opposite biological effects. Hence, the movement of individuals is influenced by both the base-line turning rate

as well as the bias turning rate, which depends on the social interaction forces.

In each time step, individuals first receive stimuli based on the social interaction forces and calculate their turning rate. They then update their position by moving in their direction of travel with constant speed γ . Lastly, individuals change direction if their probability of turning, $\lambda_i^\pm \Delta t$, is sufficiently large. That is, the change of direction of an individual is a Bernoulli random variable with probability of success $\lambda_i^\pm \Delta t$. That is,

$$x_i(t + \Delta t) = x_i(t) + \gamma v_i(t) \Delta t, \quad (3.3)$$

$$v_i(t + \Delta t) = \begin{cases} -v_i(t), & \text{if } \lambda_i^\pm \Delta t \geq X, \\ v_i(t), & \text{otherwise.} \end{cases} \quad (3.4)$$

To complete the model development, the social interaction forces and direction-dependent communication mechanisms need to be described. In Section 3.2.1, we describe how an individual measures the social interaction forces. Direction-dependent communication mechanisms directly influence which signals, and how much of those signals are received by an individual.

3.2.1 Social Interaction Forces and Communication Mechanisms

As in the PDE model, the social interaction forces of repulsion ($y_{r,i}^\pm$) and attraction ($y_{a,i}^\pm$) enter the turning function, (3.2), with opposite signs, as repulsion and attraction have opposite effects. The turning function additively depends on alignment ($y_{al,i}^\pm$). This is to capture the biological mechanisms of avoiding close individuals, aligning with nearby individuals, and moving toward distant individuals.

The formula for $y_{j,i}^\pm$, $j = r, al, a$, not only depends on the weighting of conspecifics in the interaction zones as described above, but also upon how information between individuals in interaction zones is shared. A communication mechanism could, for example, be purely directional, and individuals could only receive information from individuals traveling towards them.

Communication mechanisms describe which signals, and how much of those signals, are received by the target individual. By way of example, one could define a communication mechanism to be that the target individual uses information from all neighbours in the repulsion and attraction zones, but only information from individuals heading toward in the alignment zone, as illustrated in Figure 3.1. A right-moving reference individual i at x_i is surrounded by individuals to the right ($x + s$) and individuals to the left ($x - s$). For

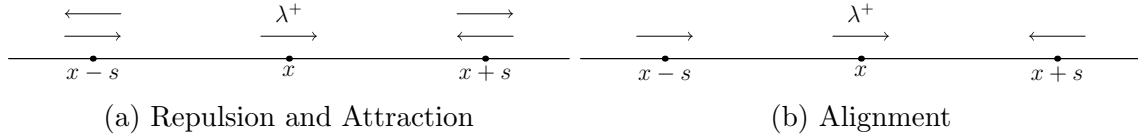


Figure 3.1: The direction-dependent communication mechanism in submodel M1. A right-moving reference individual at x receives signals from distant individuals, to the right at $x + s$ and from the left at $x - s$. For attraction and repulsion (a), this individual uses all information from neighbours regardless of their direction of travel. Arrows pointing left and right indicate this. For alignment (b), the reference individual only uses information from neighbours heading toward it, as indicated by the arrows heading toward the reference individual.

repulsion and attraction, the target individual uses information from all neighbours in these zones as indicated by the right and left moving arrows in Figure 3.1(a). For alignment, the target individual only uses information from individuals moving toward it as indicated by right facing arrow at $x - s$ and by the left facing arrow at $x + s$ in Fig. 3.1(b). In the PDE model, this is called submodel M1, and we will adopt this naming scheme. The communication mechanism in submodel M1 is direction-dependent as information transfer between individuals depends on the direction in which conspecifics are traveling. The social interaction forces for submodel M1 thus need to reflect this direction-dependent communication mechanism.

To incorporate the direction-dependent communication mechanism as described in submodel M1 in the social interaction forces, $y_{j,i}^{\pm}$, $j = r, al, a$, we consider how a reference individual i at x_i receives information from conspecifics in its social interaction zones. For repulsion and attraction, this individual uses information about all neighbours in its repulsion and attraction zones, regardless of the neighbours' direction of travel. For alignment, this individual uses information about only those neighbours who are traveling toward it in the alignment zone. Define q_j , $j = r, al, a$, to be the magnitude of the repulsive, alignment, and attractive force, respectively. Individual i at x_i experiences a *repulsive force*, $y_{r,i}^{\pm}$, given by

$$y_{r,i}^{\pm} = \pm q_r \sum_{j \in Z_{r,i}^R} K_r(|x_i - x_j|) \mp q_r \sum_{j \in Z_{r,i}^L} K_r(|x_i - x_j|), \quad (3.5)$$

where $K_r(s)$ is defined in (2.4) and $Z_{r,i}^{R,L}$ represents individual i 's zone of repulsion, to the right (superscript R) or to the left (superscript L). The $+$ and $-$ superscripts represent the direction of the target individual i , and the \pm and \mp signs are responsible for comparing

the social interaction forces between left (L) and right (R) zones. Similarly, as information is used from all neighbours in the zone of attraction, individual i at x_i then experiences an *attractive force*, $y_{a,i}^\pm$, given by

$$y_{a,i}^\pm = \pm q_a \sum_{j \in Z_{a,i}^R} K_a(|x_i - x_j|) \mp q_a \sum_{j \in Z_{a,i}^L} K_a(|x_i - x_j|), \quad (3.6)$$

where $Z_{a,i}^{R,L}$ represents individual i 's zone of attraction to the right (R) or to the left (L). The repulsive and alignment forces compare the strength of the forces ahead and behind the reference individual, as it is biologically relevant for an individual be repelled by nearby individuals or to be attracted to distant individuals, regardless of their direction of travel. On the other hand, the alignment forces compare the strength of forces exerted by right- or left-moving individuals (subject to the communication mechanism), as the biological meaning of alignment is to adjust one's direction to match that of neighbours at an intermediate distance. Since individual i uses information about only those neighbours who are traveling toward it in the alignment zone, the *alignment force* selects only those individuals who are left-moving ($v_j < 0$) to right (R) of individual i , or those individuals who are right-moving ($v_j > 0$) to the left (L) of individual i . Thus, the alignment force is given by

$$y_{al,i}^\pm = \pm q_{al} \sum_{\substack{j \in Z_{al,i}^R \\ v_j < 0}} K_{al}(|x_i - x_j|) \mp q_{al} \sum_{\substack{j \in Z_{al,i}^L \\ v_j > 0}} K_{al}(|x_i - x_j|), \quad (3.7)$$

where $Z_{al,i}^{R,L}$ represents individual i 's zone of attraction to the right (R) or to the left (L).

Direction-dependent communication mechanisms are not restricted to the mechanism described as submodel M1. In the PDE model, submodel M1 is one of five direction-dependent communication mechanisms considered. This submodel paradigm allows for communication mechanisms to be varied beyond the five mechanisms proposed above and studied via simulations of the IBM. To incorporate a direction-dependent communication mechanism into the IBM, it is only necessary to specify which conspecifics a reference individual will interact with for the repulsive, alignment, and attractive social interaction forces. These interactions for the five submodels studied here are summarized in Table 2.1 and are illustrated in Figure 2.3. The social interaction forces for each submodel are given in Table 3.1.

Submodel	Repulsion & Attraction interaction force Alignment interaction force
M1	$y_{r,a,i}^{\pm} = \pm q_{r,a} \sum_{j \in Z_{r,a,i}^R} K_{r,a}(d_{ij}) \mp q_{r,a} \sum_{j \in Z_{r,a,i}^L} K_{r,a}(d_{ij})$ $y_{al,i}^{\pm} = \pm q_{al} \sum_{\substack{j \in Z_{al,i}^R \\ v_j < 0}} K_{al}(d_{ij}) \mp q_{al} \sum_{\substack{j \in Z_{al,i}^L \\ v_j > 0}} K_{al}(d_{ij})$
M2	$y_{r,a,i}^{\pm} = \pm q_{r,a} \sum_{j \in Z_{r,a,i}^R} K_{r,a}(d_{ij}) \mp q_{r,a} \sum_{j \in Z_{r,a,i}^L} K_{r,a}(d_{ij})$ $y_{al,i}^+ = q_{al} \left(\sum_{\substack{j \in Z_{al,i}^R \\ v_j < 0}} K_{al}(d_{ij}) + \sum_{\substack{j \in Z_{al,i}^L \\ v_j < 0}} K_{al}(d_{ij}) - \sum_{\substack{j \in Z_{al,i}^R \\ v_j > 0}} K_{al}(d_{ij}) - \sum_{\substack{j \in Z_{al,i}^L \\ v_j > 0}} K_{al}(d_{ij}) \right)$ $y_{al,i}^- = q_{al} \left(\sum_{\substack{j \in Z_{al,i}^L \\ v_j > 0}} K_{al}(d_{ij}) + \sum_{\substack{j \in Z_{al,i}^R \\ v_j > 0}} K_{al}(d_{ij}) - \sum_{\substack{j \in Z_{al,i}^L \\ v_j < 0}} K_{al}(d_{ij}) - \sum_{\substack{j \in Z_{al,i}^R \\ v_j < 0}} K_{al}(d_{ij}) \right)$
M3	$y_{r,a,i}^+ = q_{r,a} \sum_{j \in Z_{r,a,i}^R} K_{r,a}(d_{ij})$ $y_{r,a,i}^- = q_{r,a} \sum_{j \in Z_{r,a,i}^L} K_{r,a}(d_{ij})$ $y_{al,i}^+ = q_{al} \sum_{\substack{j \in Z_{al,i}^R \\ v_j < 0}} K_{al}(d_{ij}) - q_{al} \sum_{\substack{j \in Z_{al,i}^L \\ v_j > 0}} K_{al}(d_{ij})$ $y_{al,i}^- = q_{al} \sum_{\substack{j \in Z_{al,i}^L \\ v_j > 0}} K_{al}(d_{ij}) - q_{al} \sum_{\substack{j \in Z_{al,i}^R \\ v_j < 0}} K_{al}(d_{ij})$
M4	$y_{r,a,i}^{\pm} = \pm q_{r,a} \sum_{\substack{j \in Z_{r,a,i}^R \\ v_j < 0}} K_{r,a}(d_{ij}) \mp q_{r,a} \sum_{\substack{j \in Z_{r,a,i}^L \\ v_j > 0}} K_{r,a}(d_{ij})$ $y_{al,i}^{\pm} = \pm q_{al} \sum_{\substack{j \in Z_{al,i}^R \\ v_j < 0}} K_{al}(d_{ij}) \mp q_{al} \sum_{\substack{j \in Z_{al,i}^L \\ v_j > 0}} K_{al}(d_{ij})$
M5	$y_{r,a,i}^+ = q_{r,a} \sum_{\substack{j \in Z_{r,a,i}^R \\ v_j < 0}} K_{r,a}(d_{ij})$ $y_{r,a,i}^- = q_{r,a} \sum_{\substack{j \in Z_{r,a,i}^L \\ v_j > 0}} K_{r,a}(d_{ij})$ $y_{al,i}^+ = q_{al} \sum_{\substack{j \in Z_{al,i}^R \\ v_j < 0}} K_{al}(d_{ij})$ $y_{al,i}^- = q_{al} \sum_{\substack{j \in Z_{al,i}^L \\ v_j > 0}} K_{al}(d_{ij})$

Table 3.1: The social interaction forces depend directly on the direction-dependent communication mechanism prescribed by each submodel. Here, $d_{ij} = |x_i - x_j|$ is the distance between individuals i and j , q_j , $j = r, al, a$, is the magnitude of the interaction force, K_j , $j = r, al, a$, are the social interaction kernels, (2.4), and $Z_{j,i}^{R,L}$, $j = r, al, a$, describe individual i 's zone of repulsion, alignment, or attraction to the right (superscript R) or to the left (superscript L). The direction of individual j , v_j , is necessary to distinguish between right- and left-moving individuals in the social interaction zones. The repulsive and alignment forces compare the strength of the forces ahead and behind the reference individual, as it is biologically relevant for an individual be repelled by nearby individuals or to be attracted to distant individuals, regardless of their direction of travel. On the other hand, the alignment forces compare the strength of forces exerted by right- or left-moving individuals, as the biological meaning of alignment is to adjust one's direction to match that of neighbours at an intermediate distance.

3.3 Numerical Simulations

In this section, we simulate the model using a variety of communication mechanisms and a wide range of parameters. The previous investigation into the behaviour of the PDE model revealed formation of complex spatial patterns as in Chapter 2. Here, we aim to reproduce the complex spatial patterns previously seen in the analogous PDE model.

$N = 500$ individuals are randomly scattered on a domain of length $L = 10$ with periodic boundary conditions. The social interaction kernels are truncated at $2s_j$, $j = r, al, a$, respectively, to avoid infinite interaction ranges. Individuals continue to move with a constant speed $\gamma = 0.1$. To ensure that we can translate between the parameter space in the analogous PDE model, we normalize the social interaction forces by multiplying by $\frac{AL}{N}$, where $A = 2$ is the total population size in the PDE model. This normalization ensures that the magnitudes of the social interaction forces are scaled to match the choices of λ_1 , λ_2 , and the turning function, (3.2). The normalization constant, in effect, scales the social interaction forces by the reciprocal of the density, $\frac{L}{N}$, then by $A = 2$, to match the total population size from [10, 12, 14].

Examples of the complex spatial patterns observed are shown in Figure 3.2. Corresponding density plots are shown in Figure 3.3. The density plots in Figure 3.3 allow the interior structure of the aggregations to be observed and for the patterns to be compared to the PDE model. Stationary pulses consist of an aggregation that does not travel and can have high-density subgroups, or have constant internal density. Figure 3.2(a) and Figure 3.3(a) show stationary pulses with high-density subgroups, and Fig. 3.2(b) and 3.3(b) show stationary pulses with constant internal density. Ripples are formed when left-moving and right-moving groups of individuals intersect but continue moving apart. Figure 3.2(c) and Figure 3.3(c) show the formation of the ripple pattern. Figure 3.2(d) and Figure 3.3(d) show stationary pulses that lose individuals from the edges of the groups, but eventually rejoin a group. This creates a feather-like pattern as individuals move away from the larger stationary pulse. A traveling pulse is a large group of individuals that travels together; whereas, a traveling train consists of multiple small groups of individuals that travel together. An example traveling pulse is shown in Figure 3.2(e) and Figure 3.3(e). Figure 3.2(f) and Figure 3.3(f) reveal multiple small groups moving across the domain in the traveling train pattern. When an group of individuals behaves like a traveling pulse but reverses direction sporadically, a zigzagging pulse is formed, as in Figure 3.2(g) and Figure 3.3(g). Aggregations that expand and contract over time are called breathers. Breathing patterns can be stationary, as in Figure 3.2(h) and Figure 3.3(h), or can travel across the domain, as in Figure 3.2(i) and Figure 3.3(i). Feath-

Pattern	Submodel	λ_1	λ_2	q_r	q_{al}	q_a
Stationary pulse with high density subgroups	M1	0.2	0.9	2.4	0	2
Stationary pulse with constant internal density	M2	0.2	0.9	0.5	0	4
Ripples	M5	0.2	0.9	1.1	2	1.5
Feathers	M3	0.2	0.9	6.4	0	6
Traveling pulse	M1	0.2	0.9	0.5	2	1.6
Traveling train	M3	6.67	30	0	2	6
Zigzag pulse	M2	0.2	0.9	1	2	6
Breathers	M4	0.2	0.9	1	0	2
Traveling breathers	M4	0.2	0.9	4	2	4
Semi-zigzag pulse	M4	0.667	3	0	2.2	0

Table 3.2: Example parameter values and submodels that produce complex spatial patterns. In this study, fixed model parameters are $N = 500$, $L = 10$, $\Delta t = 0.05$ and $\gamma = 0.1$.

ers, zigzag pulses, breathers, and traveling breathers are novel patterns that have not been previously observed in individual-based models of collective behaviour. Another previously unobserved pattern is the semi-zigzag pulse, as shown in Figure 3.4. Semi-zigzag pulses are obtained by movement in one direction alternated by periods of stationary rest.

Simulations of the IBM with the parameter values in Table 3.2 provide specific examples of well-defined patterns that match the PDE model. To ensure the IBM matches the behaviour of the PDE model throughout parameter space, numerical simulations of the IBM were performed using the same parameter spaces described in [10]:

Case (a): Repulsion and attraction only. In this case, the fixed parameters are $q_{al} = 0$, $\gamma = 0.1$, $\lambda_1 = 0.2$, and $\lambda_2 = 0.9$. The magnitude of the repulsive and attractive social interaction forces, q_r and q_a , are varied, with $(q_r, q_a) \in [0.5, 9]$.

Case (b): Alignment only. In this case, the fixed parameters are $q_r = q_a = 0$, $\gamma = 0.1$, and the influence of turning rates is investigated. Set $\lambda_1 = \frac{0.2}{\alpha}$ and $\lambda_2 = \frac{0.9}{\alpha}$. α and q_{al} are varied, with $\alpha \in [0.006, 1]$ and $q_{al} \in [0.5, 10]$.

Case (c): All social interactions. In this case, we fix $\gamma = 0.1$, $\lambda_1 = 0.2$, and $\lambda_2 = 0.9$. The magnitudes of the social interaction forces are varied, with $(q_r, q_{al}, q_a) \in [1, 10]$.

Each of these parameter regimes was investigated using the communication mechanisms described by submodels M1 through M5. Numerical simulations reveal that the patterns formed by the IBM match those patterns formed by the PDE model throughout parameter space, and among submodels. The results of this investigation are described in Table 3.3 by

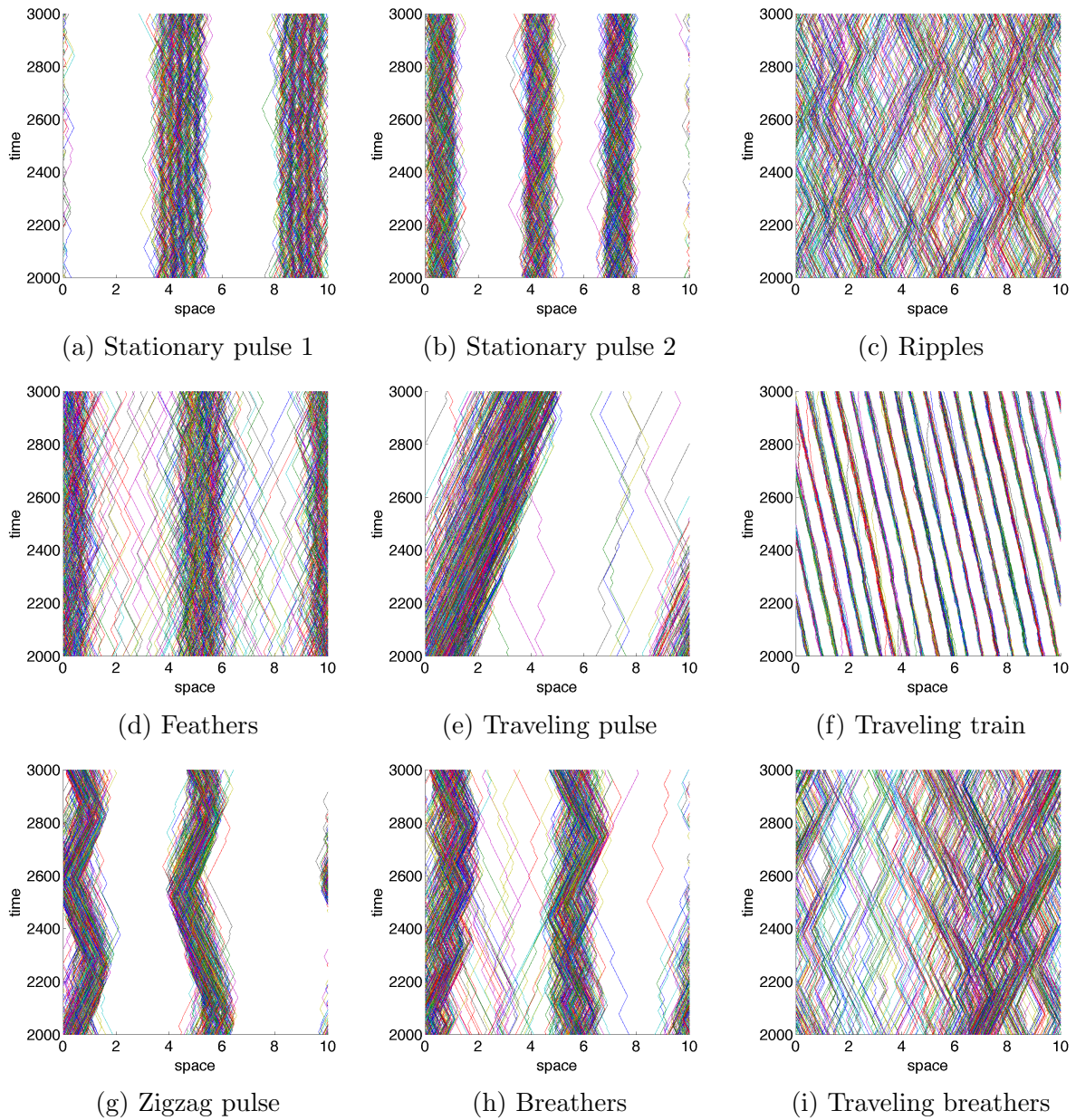


Figure 3.2: Examples of patterns obtained by the IBM with various communication mechanisms. Parameters and communication mechanism (submodel) are described in Table 3.2, and boundary conditions are periodic.

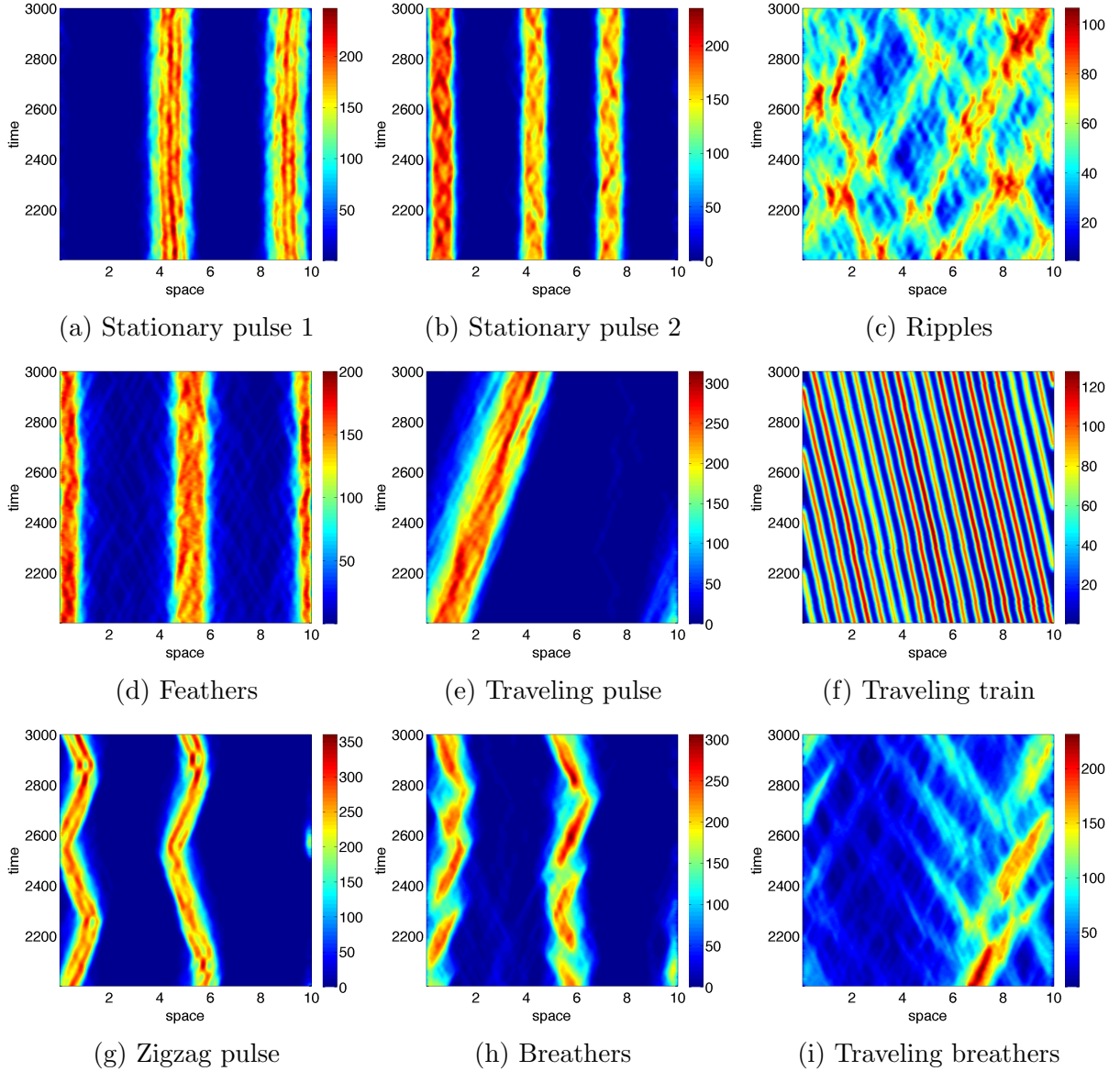


Figure 3.3: Density plots of patterns obtained by the IBM with various communication mechanisms. Subfigures correspond to the patterns shown in Figure 3.2. Parameters and communication mechanism (submodel) are described in Table 3.2.

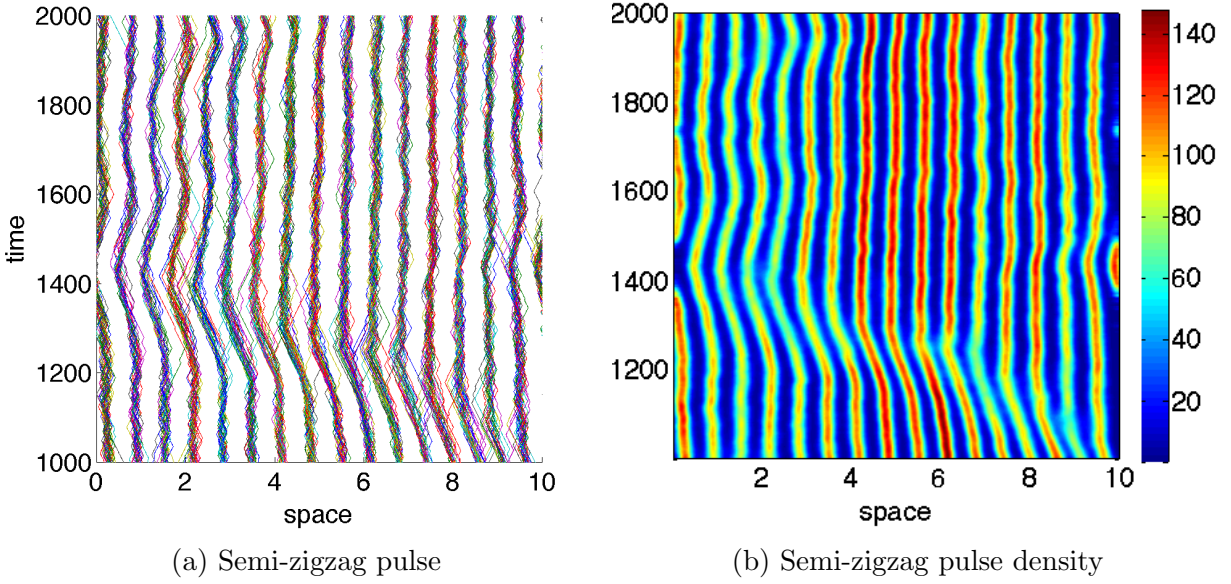


Figure 3.4: Semi-zigzag pulse produced by submodel M4 with alignment only. Semi-zigzag pulses are characterized by alternating periods of stationary rest and travel. Parameters are listed in Table 3.2.

indicating which patterns form as a result of considering a certain submodel and parameter regime (Case (a), (b), or (c)). For example, the communication mechanism described by submodel M1 produces traveling trains using parameters in case (b), traveling pulses using parameters in case (c), stationary pulses can be observed for cases (a), (b), and (c). Dashes indicated that the particular pattern has not been observed for that range of parameters. This investigation reveals the importance of alignment in the formation of moving groups. Traveling groups, such as the traveling pulse and traveling train, require non-zero alignment forces. Traveling breathers can be produced without alignment; however, in this case, attraction and repulsion have the same magnitude. This allows individuals to escape the group and subsequently rejoin, leading to the expansion and contraction of the group.

The parameter investigation reveals that the PDE model and the IBM model generally have the same behaviour. Pattern formation of the PDE model is summarized in Table 2.3 across parameter space and the five submodels. Comparing the patterns formed by the IBM (Table 3.3) with those patterns formed by the PDE model (Table 2.3) demonstrates that the two modelling approaches reveal the same group formation patterns. However, it also reveals the subtle differences between the IBM and the PDE model, namely which submodels and parameter regimes produce patterns. The ripples, breathers, and semi-zigzag pulse patterns

are produced by both the IBM and PDE model using the same communication mechanisms and in the same parameter regimes. Other patterns are, in general, produced in both models using the same parameter regimes and the same communication mechanisms. For example, feathers appear in the PDE model only in submodel M3 with parameters from cases (a) and (c), but they appear in the IBM in submodel M3 with parameters from cases (a) and (c) as well as in submodel M4 with parameters from case (c). These differences likely result from the stochasticity built into the IBM. Stochasticity allows for individuals to escape large aggregations on occasion, and given enough escapees, these individuals may alter the group level patterns.

Stochasticity is built into the IBM in two ways. Firstly, the base-line turning rate, λ_1 , describes how often individuals change direction in the absence of signals from conspecifics. Secondly, at each time step, individuals change direction if their turning probability is greater than a randomly chosen number between 0 and 1, as in (3.3). Case (b) of the parameter investigation investigates the effect of varying the base-line and bias turning rates. This is accomplished by adjusting λ_1 and λ_2 , the base-line and bias turning rates, respectively. Patterns formed in this investigation are mainly stationary aggregations. When λ_1 and λ_2 are increased, the groups become less cohesive and it is qualitatively apparent that individuals are turning more often. Case (b) restricts the investigation to the case where repulsion and attraction signals are not considered, and does not describe how pattern formation is affected by varying the turning rates in the IBM. To investigate the effect of stochasticity, that is, the effect of modifying the turning rates on the pattern formation, simulations were performed with increased or decreased turning rates. Specifically, the turning rate for each individual i , (3.1), was modified to become

$$\lambda_i^\pm = c \left(\lambda_1 + \lambda_2 f \left(y_{r,i}^\pm - y_{a,i}^\pm + y_{al,i}^\pm \right) \right), \quad (3.8)$$

where $c \in \mathbb{R}$ is a constant. Increasing the constant c increases individual i 's turning rate; similarly, decreasing the constant c decreases individual i 's turning rate. Increased turning rates lead to less cohesive aggregations and rougher patterns, as observed in the parameter investigation in case (b). On the other hand, for c approximately equal to 1, pattern formation is largely unaffected. For $c \ll 1$, individuals are not likely to change direction, and will move in their initial direction, $v_i(0)$. The zigzag pattern reveals the sensitivity of pattern formation to the turning rates, as the time between direction reversals increases with the turning rates. For example, Figure 3.5 shows three patterns formed using the same parameters but with increasing c . In Figure 3.5(a), the turning rates are $\lambda_1 = 0.04$ and $\lambda_2 = 0.18$

Model	Stationary Pulse	Ripples	Feathers	Traveling pulse	Traveling train	Zigzag pulse	Breathers	Traveling breathers	Semi-zigzag pulse
M1	(a),(b),(c)	-	-	(c)	(b)	(c)	-	-	(b)
M2	(a),(c)	-	-	(c)	(c)	(c)	-	-	-
M3	-	-	(a),(c)	(b),(c)	(b)	-	-	-	-
M4	(b)	-	(c)	-	(b)	-	(a)	(a)	(b)
M5	(b)	(a),(c)	-	-	-	-	-	-	-

Table 3.3: Patterns produced by the IBM for submodels M1 through M5. (a),(b), and (c) indicate that the corresponding pattern was produced by parameters from the corresponding parameter regime. Dashes indicate that the parameter was not observed for any of the parameter regimes.

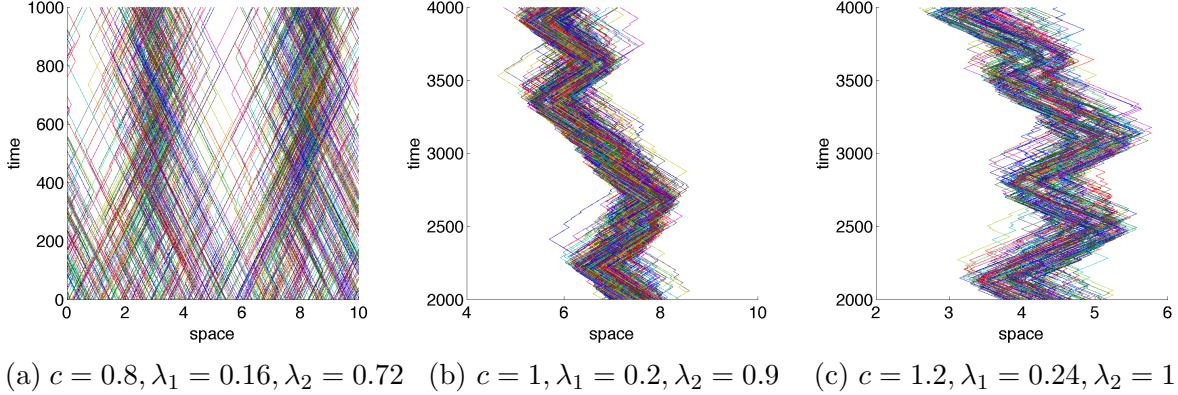


Figure 3.5: The turning rates, λ_1 and λ_2 , effect the time between direction reversals in the zigzag pulse pattern. For smaller turning rates (a), such as $c = 0.2$, individuals do not frequently change direction, but generally travel in their initial direction, $v_i(0)$. Here, the turning rates are still sufficiently large to result in some group formation. For increased turning rates (c), $c = 1.2$, the zigzag changes direction frequently.

($c = 0.2$), resulting individuals mostly traveling in their original direction. In Figure 3.5(b), the turning rates are $\lambda_1 = 0.2$ and $\lambda_2 = 0.9$ ($c = 1$), resulting in the zigzag pattern shown in Figure 3.2(g). Finally, as $\lambda_1 = 0.24$ and $\lambda_2 = 1.08$ ($c = 1.2$) are increased, the time between direction reversals is smaller, as in Figure 3.5(c).

3.4 Social Interaction Kernels

The choice of the social interaction kernels in the PDE model and IBM is biologically motivated. Individuals should be repelled by conspecifics at close ranges to avoid collisions; individuals wish to orient their velocity with individuals at intermediate distances or distances that are “just right”; individuals wish to move toward distant individuals in order to remain in contact with them. The kernels discussed above do not adequately capture this biological motivation, as neighbours very close to an individual are not weighted as heavily in the repulsion interaction force as those neighbours who are located near $\pm s_r$. To add biological realism to the repulsion kernel, we consider a shallower repulsion kernel that is centered about 0, i.e., the reference individual as illustrated in Figure 3.6. Let $\tilde{m}_r = s_r/2$ and define

$$\tilde{K}_r(s) = \frac{1}{\sqrt{2\pi\tilde{m}_r^2}} \exp\left(\frac{-s^2}{2\tilde{m}_r^2}\right). \quad (3.9)$$

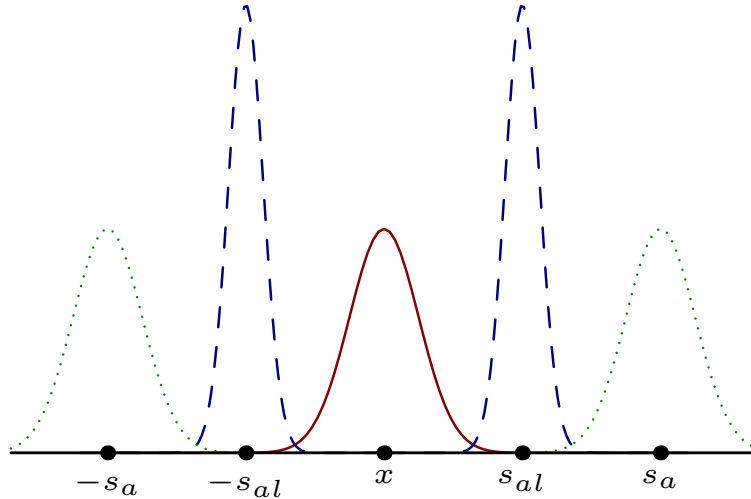


Figure 3.6: The revised repulsion kernel (red, solid) is centered over the target individual, adding biological realism as the conspecifics very close to the target individual are weighted most heavily for the repulsion social interaction force. The alignment (blue, dashed) and attraction (green, dotted) kernels remain unchanged.

Using $\tilde{K}_r(s)$ as the repulsion kernel weights nearest neighbours more strongly than other individuals for the repulsion interaction force.

This can be observed in numeric simulations with the revised repulsion kernel $\tilde{K}_r(s)$. Firstly, pattern formation is unaffected as simulations show the formation of the same patterns using the same parameters as in previous simulations. Minor differences in pattern formation exist, such as with the stationary pulse formation. In simulations with the original repulsion kernel, small high density subgroups of individuals form within the pulse; however, these small high density groups of individuals do not form using the revised repulsion kernel (compare Fig. 3.2(a) and Fig. 3.7). This results from the removal of the valley between the peaks formed by the original repulsion kernel (Fig. 2.2), as previously, individuals sufficiently close could remain together as a group without exerting a large repulsive force on each other by aggregating in this valley. The revised repulsion kernel, $\tilde{K}_r(s)$, does not permit individuals to cluster this closely without exerting a strong repulsive force upon each other.

To ensure that the complex spatial patterns form as a result from the incorporation of direction-dependent communication mechanisms and not from the specific choice of social interaction kernel, a wider range of kernels was considered. In place of the truncated Gaussian kernels as in (2.4) and (3.9), rectangular and triangular kernels were chosen. Numerical simulations reveal that the spatial patterns formed with non-Gaussian kernels have small

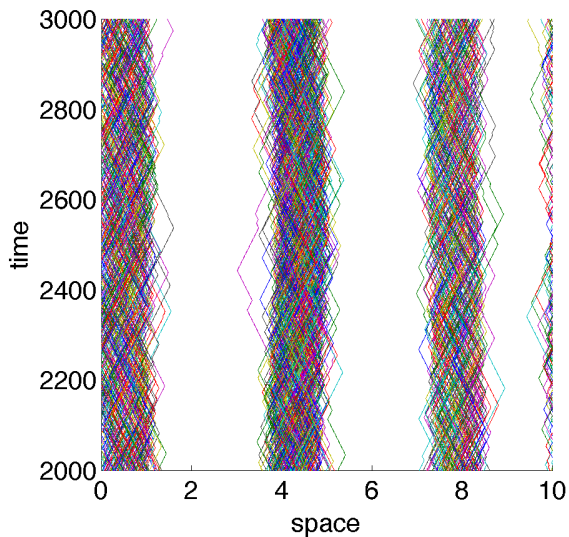


Figure 3.7: Stationary pulse formed using the revised repulsion kernel, $\tilde{K}_r(s)$. Parameters are identical to those for the stationary pulse observed in Fig. 3.2(a) (M1, $\lambda_1 = 0.2$, $\lambda_2 = 0.9$, $q_r = 2.4$, $q_{al} = 0$, $q_a = 2$). Note the loss of high-density subgroups within each stationary pulse. The revised repulsion kernel does not permit conspecifics to remain together as a small group without exerting a large repulsive force on each other.

quantitative differences. For example, the rate of direction reversal in the zigzag patterns and the small well-defined groups in the traveling train pattern differ from simulations with Gaussian kernels. Nonetheless, the patterns are qualitatively unaffected by variations in the choice of social interaction kernel.

3.5 Discussion

Existing IBMs are successful in producing spatial patterns (see Section 1.3). IBMs with additional biological background can also reproduce the most complicated behaviours, such as the amazing displays of flocking starlings [21]. However, these IBMs are unable to account for the multitude of complex spatial patterns observed in nature. Here, a one-dimensional individual-based model of collective behaviour with direction-dependent communication mechanisms was developed. The complex spatial patterns generated with our model result from the incorporation and exploration of various direction-dependent communication mechanisms.

Following the use of direction-dependent communication mechanisms as in the PDE model, we formulated the IBM on a one-dimensional domain with periodic boundary condi-

tions, upon which individuals can move to the right or left. Direction-dependent communication mechanisms were superimposed upon the traditional social interactions of repulsion, alignment, and attraction. These direction-dependent communication mechanisms describe how and how much information is received by a target individual from conspecifics. A variety of communication mechanisms can be imagined, but only five are considered as submodels.

The behaviour of the IBM is enriched by the incorporation of direction-dependent communication mechanisms. The complex spatial patterns form as a result of various submodels and varied parameter space. The IBM reproduces more classical patterns, such as stationary aggregations, ripples, traveling pulses, and traveling trains, and produces novel patterns such as feathers, zigzag pulses, breathers, and traveling breathers. The complex spatial patterns observed here are noisier than the analogous patterns formed in the PDE model. In the IBM, individuals change direction if their turning probability, $\lambda_i^\pm \Delta t$, is larger than a uniformly distributed random variable. This added stochasticity adds biological realism as it is unlikely that individuals will always respond to the stimuli from conspecifics and may act in an unpredictable manner. The effect of stochasticity can be seen very well in the traveling train pattern (Fig. 3.2(f)), as individuals will occasionally leave the group they have been traveling with and are subsequently absorbed by another group. In the zigzag pattern (Fig. 3.2(g)), the majority of individuals travel with the main zigzagging group; however, a small number of individuals continue to travel past the turning main group. Eventually, they return to the main group after being attracted by the large number of distant individuals. As defined in (3.3), in a time step individuals first update their position and secondly update their direction of travel. Considering an alternate “turn-then-move” scheme where individuals first update their direction of travel, then update their position has no observable qualitative effect on pattern formation.

Aside from the noise introduced by considering a IBM, the patterns formed throughout parameter space match those patterns formed by the PDE model. Moreover, considering alternate social interaction kernels did not have a large qualitative effect on pattern formation. Investigating three cases of parameters reveals a strong match between the behaviours of the two models. In Chapter 2, a Poisson point assumption was necessary to derive the hyperbolic PDE from the correlated random walk. This Poisson point assumption was imposed as a separate condition, as when social interactions are added, the number of individuals observed within non-overlapping intervals is not necessarily independent. Provided the movement of individuals is sufficiently random, the Poisson point assumption can be added. The incorporation of the Poisson point assumption to the PDE model is substantiated as the behaviour

of the stochastic IBM, which includes random movements of individuals, matches that of the PDE model across parameter space. Overall, the incorporation of direction dependent communication mechanisms to an IBM of collective behaviour demonstrates that the complex spatial patterns are not unique to the PDE model. Moreover, the IBM's behaviour demonstrates that the communication mechanisms modelling paradigm permits the formation of a wide variety of complex spatial patterns.

Here, individuals move with constant speed $\gamma = 0.1$ as in the PDE model from Chapter 2. This assumption may not be biologically realistic, as individuals may speed up or slow down to move towards or away from neighbours. Density-dependent movement speed is the subject of the next chapter.

Chapter 4

Density-Dependent Speed

4.1 Introduction

In this chapter, density-dependent speed is incorporated into the individual-based model with direction-dependent communication mechanisms. Animals do not move at a constant speed in nature, but rather speed up and slow down in response to their environment and the location and behaviour of conspecifics. Further motivation for investigating density-dependent speed results from the fact that it has been investigated in the context of the PDE model with direction-dependent communication mechanisms. In Chapter 2 and 3, the turning rate of an individual was assumed to depend on nonlocal social interactions with neighbours. In this chapter, we ignore environmental factors that may speed or slow an individual's movement and focus on those social interactions which may influence an individual's speed. The incorporation of density-dependent speed in the existing PDE model and the IBM studied in this thesis leads to the formation of splitting and merging groups. Splitting and merging behaviour is not observed in the PDE model described in Chapter 2 or the new IBM model described in Chapter 3.

In Section 4.2, we review the incorporation of density-dependent speed in to the PDE model as in [10] and [17]. In Section 4.3, we present a modification of the IBM with direction-dependent communication mechanism that includes density-dependent speeds. Patterns produced by the IBM with direction-dependent communication and density-dependent speeds do not exactly match those of the PDE model presented in [10]; however, density-dependent speeds in the IBM lead to aggregations that split and merge. In Section 4.4, we modify the IBM to use exponential-type kernels and present a comparison of the IBM with density-dependent speed to the results from [17].

4.2 Density-Dependent Speed in the PDE model

In [10] and [17], density-dependent speed is added to the PDE model from Chapter 2. This addition is biologically motivated by the simple fact that animals do not always move with a constant speed, but rather speed up or slow down in response to conspecifics. To incorporate density-dependent speed into the the PDE model from Chapter 2, the PDEs are modified:

$$\begin{aligned} u^+(x, t)_t + (\Gamma^+ u^+(x, t))_x &= -\lambda^+ u^+(x, t) + \lambda^- u^-(x, t), \\ u^-(x, t)_t - (\Gamma^- u^-(x, t))_x &= +\lambda^+ u^+(x, t) - \lambda^- u^-(x, t), \\ u^\pm(x, 0) &= u_0^\pm(x), \end{aligned} \quad (4.1)$$

where Γ^\pm are the density-dependent speeds. The density-dependent speed is assumed to be a positive, bounded, and increasing function of the perceived signals. That is, the speed depends on the communication signals from conspecifics in the attractive and repulsion zones. Biologically, this corresponds to the individuals speeding up to join a larger group in their attraction zone, or slowing down to avoid collision with those in front of them. In [10], the non-local speeds are $\Gamma^\pm(y^\pm) = \gamma(1 + \tanh(y_a^\pm - y_r^\pm))$. Using the communication mechanisms described by submodel M1 (see Chapters 2 and 3), the density-dependent speeds are defined in [10]:

$$\begin{aligned} \Gamma^+(y^+) &= \gamma \left(1 + \tanh \left(q_a \int_0^\infty K_a(s) (u(x+s) - u(x-s)) ds \right. \right. \\ &\quad \left. \left. - q_r \int_0^\infty K_r(s) (u(x+s) - u(x-s)) ds \right) \right), \\ \Gamma^-(y^-) &= \gamma \left(1 + \tanh \left(-q_a \int_0^\infty K_a(s) (u(x+s) - u(x-s)) ds \right. \right. \\ &\quad \left. \left. + q_r \int_0^\infty K_r(s) (u(x+s) - u(x-s)) ds \right) \right). \end{aligned} \quad (4.2)$$

Here, $u(x, t) = u^+(x, t) + u^-(x, t)$ is the total density (t -dependence omitted above for brevity), and q_a and q_r are the magnitude of attraction and repulsion signals. As before, γ is a constant baseline speed with which individuals move in the absence of attractive and repulsive interactions, and $K_j(s)$, $j = r, a$, describe the translated Gaussian kernels (2.4). The initial investigation in [10] considered two cases:

Case (a): where individuals turn only in response to conspecifics in the zone of alignment;

Pattern	Submodel	λ_1	λ_2	q_r	q_{al}	q_a
(a) Stationary Pulses	M1	0.2	0.9	0.1	0	0.5
(b) Stationary Pulses	M1	0.2	0.9	0.1	2	0.7
(c) Stationary Pulses	M1	0.2	0.9	0.1	2	0.3
(d) Splitting and Merging Groups	M1	0.2	0.9	0.05	3.5	0.2
(e) Irregular Splitting and Merging	M1	0.2	0.9	0.5	0	0.1
(f) Diagonal Grid	M1	0.2	0.9	0.1	0	0.1

Table 4.1: Sample parameter values for patterns produced by the PDE model with density-dependent speed.

Case (b): where individuals turn in response to individuals in all social interaction zones.

Numerical simulations were performed in [10], and these results are summarized here. The numerical simulations revealed no qualitative differences between the behaviour of the model in case (a) or case (b). Consequently, patterns from case (a) are presented in [10], and this is the work that is summarized in this section. As in Chapter 2, many parameters are fixed for numerical simulation, in particular, the domain size, $L = 10$, the location of the social interaction ranges, $s_r = 0.25$, $s_{al} = 0.5$, $s_a = 1$, the baseline speed $\gamma = 0.1$, and the width of the interaction kernels $m_j = \frac{s_j}{8}$. Figure 4.1 and Table 4.1 describe example patterns formed by the PDE model. Figure 4.1(a), (b), (c) show stationary pulses. The stationary pulses in Figure 4.1(a) results from large values of attraction, but without alignment. As attraction increases, the groups become more compact in Figure 4.1(b). For smaller values of attraction, the patterns become stationary, as in Figure 4.1(c), or form groups that split and merge, as in Figure 4.1(d). An irregular splitting and merging pattern forms when repulsion is larger than attraction in the absence of alignment, as in Figure 4.1(e). Finally, when repulsion and attraction are of similar magnitude, a grid-like pattern is formed by groups of individuals passing through each other. The patterns formed by the PDE model with density-dependent speed tend to be more transient than patterns formed in the PDE model without density-dependent speed. In [10], additional transient patterns are discussed. For some cases, these transient patterns evolve into more stable patterns, namely splitting and merging groups.

In [17], the PDE model with density-dependent speed is analyzed and simulated numerically. This analysis examines the solutions to (4.1) after modifying the social interaction kernels. The biological motivation for the study is to examine those cases where species form very dense groups or clusters, and the authors seek conditions for dispersive aggregations,

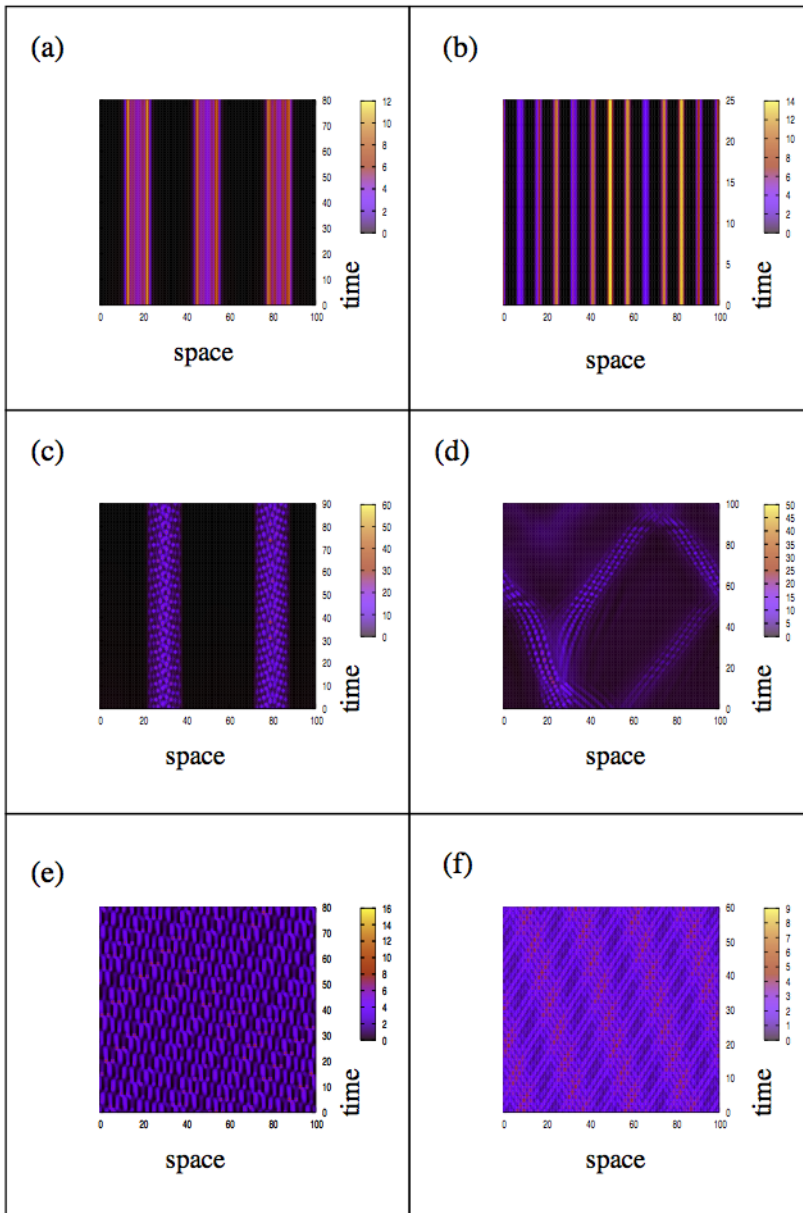


Figure 4.1: Examples of patterns produced by the PDE model with density-dependent speed. Boundary conditions are periodic, and parameters listed in Table 4.1. Figure from [10].

finite-size groups, and blow-up patterns. Solutions to the PDE that exhibit blow-up correspond to those biological aggregations that collapse to a very high-density group. These high-density groups are observed in some insect swarms and in some schools of fish. Very dense patterns appear in schools of fish when under the threat of predation. The PDE model or IBM in Chapter 2 and 3 does not exhibit blow-up behaviour in the parameter space explored.

The social interaction kernels in the PDE model or IBM, (2.4), assume that when individuals are very close together, the repulsion force is very weak (see Section 3.4). On the other hand, the PDE model with density-dependent speed assumes that the attraction and repulsion social interactions are discontinuous at the origin, accounting for the strong repulsive interactions which should act over short distances. That is, the kernel for density-dependent speed is chosen to be

$$K(x) = \text{sgn}(x) (-q_a K_a(x) + q_r K_r(x)), \quad (4.3)$$

where q_r and q_a represent the magnitudes of the repulsion and attraction forces, respectively, and

$$K_j(x) = e^{-\frac{|x|}{s_j}}, \quad (4.4)$$

where s_r and s_a represent the widths of the repulsion and attraction zones, respectively. The alignment kernel is chosen as before, as in (2.4). The social interaction kernels are depicted in Figure 4.2. The turning rates also remain unchanged.

In [17], analytical results regarding the local existence and uniqueness of solutions to (4.1) demonstrate that the model does not develop shock solutions, but rather that solutions either exist globally in time or exhibit finite-time amplitude blow-up. The behaviour of the solution depends on the relative magnitudes of repulsion and attraction, with finite-time amplitude blow-up corresponding to those groups which collapse to a very dense cluster. Equation (4.1) was analyzed and numerically simulated in two cases in [17]. The first case is with repulsion stronger than attraction ($q_r > q_a$), and second with attraction stronger than repulsion ($q_a > q_r$). In the first case, $q_r > q_a$, blow-up solutions are not possible; however, in the second case, when $q_a < q_r$, the amplitude of the solution may blow up in finite time. This is consistent with the biological interpretation of q_r and q_a . That is, if the attraction force is sufficiently stronger than repulsion, individuals will forego their “personal space” and allow neighbours at close distances. Moreover, the random turning rate, λ_1 , influences the transition between low and high density aggregations. Numerical simulations of (4.1) investigate the behaviour of the model in the case when $q_r > q_a$ or in the case when $q_r < q_a$

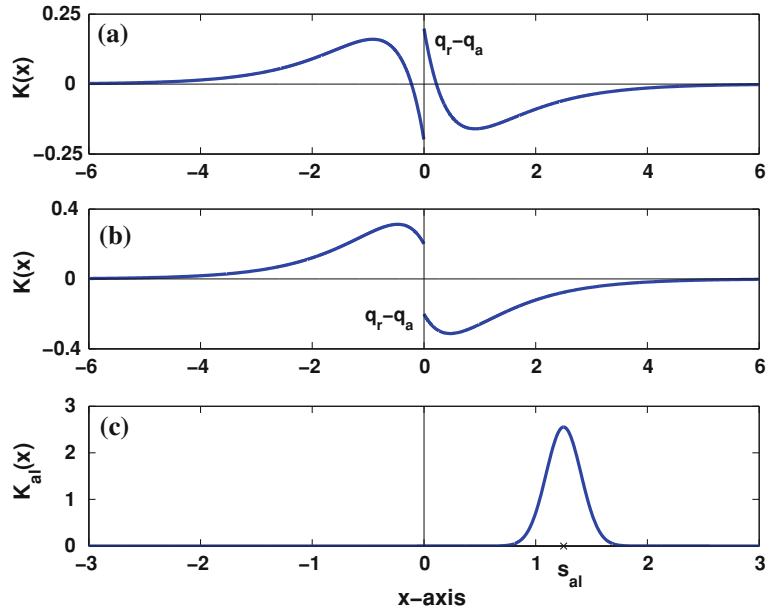


Figure 4.2: Social interaction kernels in the PDE model with density-dependent speed. These kernels are more realistic than translated Gaussian kernels, as short-range repulsion is very strong. (a) $K(x)$ from (4.3), with repulsion stronger than attraction, $q_r > q_a$; (b) $K(x)$ from (4.3), with attraction stronger than repulsion, $q_r < q_a$; (c) $K_{al}(x)$ from (2.4) is a translated Gaussian kernel. Here, $s_r = 0.5$, $s_{al} = 1.25$, $s_a = 1$, and $m_{al} = \frac{s_{al}}{8}$. Figure from [17].

Pattern	λ_1	λ_2
(a) Right- and left-moving groups	0	0
(b) Spatially homogeneous steady-state	0.2	0.5
(c) Spatially homogeneous steady-state	1	0.5
(d) Compact stationary aggregation	10	0.5

Table 4.2: Parameter values for patterns when $q_r > q_a$ (PDE model). Patterns are shown in Figure 4.3. Submodel M1 is used throughout and the fixed parameters are $q_r = 1, q_{al} = 1, q_a = 0.8, s_r = 0.5, s_{al} = 1.25, s_a = 1$ and $\gamma = 1$.

by varying the turning rates λ_1 and λ_2 .

In the first case, when $q_r > q_a$, and using parameter values as summarized in Table 4.2, the patterns observed are dispersive aggregations that approach two moving compact groups or spatially homogenous steady states, or stationary finite-size aggregations, as shown in Figure 4.3. Initial conditions for the simulations are a Gaussian distribution, as shown in Figure 4.3. In the absence of turning, individuals do not change direction, and the right- and left-moving individuals form moving aggregations. Increasing the random turning rate with respect to the bias turning rate results in the solution settling to a spatially homogeneous steady state. As the random turning rate is increased further, the solution approaches the spatially homogenous steady state but without any directed left- or right-ward movement. Finally, as the random turning rate becomes much larger than the bias turning rate, the aggregation becomes stationary and compact. This corresponds to the stationary aggregations found in nature, where individuals exhibit a large degree of random turning, like some insect swarms. This investigation reveals the influence of the random turning rate, λ_1 , on the looseness of an aggregation.

In the second case, when $q_a > q_r$, and using parameter values as summarized in Table 4.3, the patterns observed are blow-up patterns and a spatially homogenous steady state, as shown in Figure 4.4. Note that q_r is varied; this is to ensure a blow-up condition from [17] is satisfied. Initial conditions for the simulations are again Gaussian distributions. In the absence of turning, strong attraction leads to blow-up. When turning is only random and does not depend on social interactions ($\lambda_1 \neq 0$ and $\lambda_2 = 0$), moving blow-up forms. When random turning and bias turning are both included, the aggregation becomes stationary. The density of this aggregation depends on the magnitude of the random turning rate, λ_1 . The stationary aggregation becomes denser as λ_1 is increased. Another feature of the solutions in this case is the higher density at the group edges, as in Figure 4.4(c) and Figure 4.4(d).

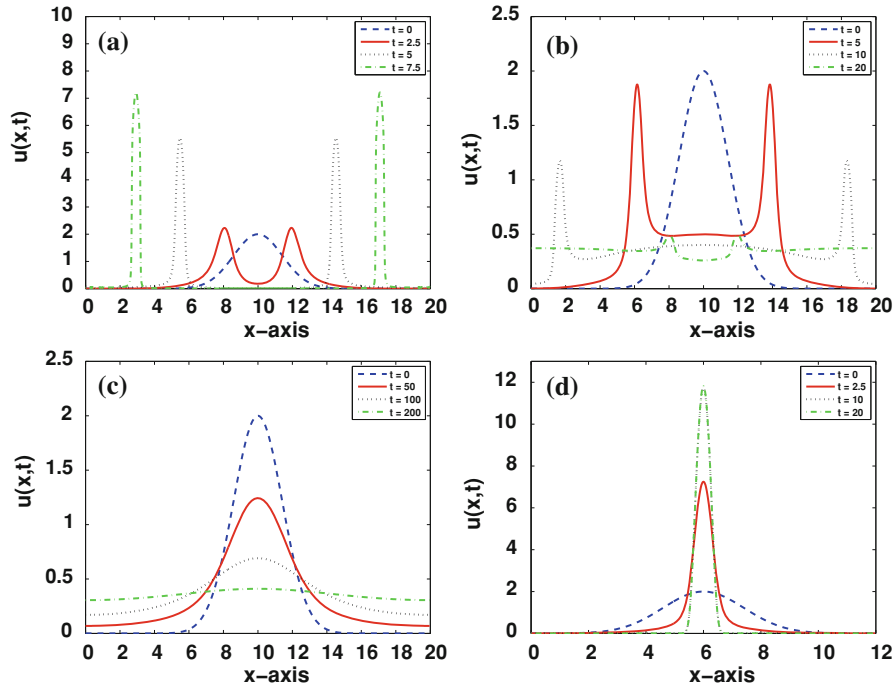


Figure 4.3: Patterns formed in the PDE model when repulsion is stronger than attraction, $q_r > q_a$. Parameter values in Table 4.2. (a) right- and left-moving groups form in the absence of turning; (b) the aggregation tends to a spatially homogenous steady state with directed left- and right-moving groups; (c) the aggregation tends to a spatially homogenous steady state without left- and right-moving groups; (d) the aggregation becomes compact and stationary. Figure from [17].

Pattern	λ_1	λ_2	q_r
(a) Blow-up	0	0	0.5
(b) Right- and left-moving blow-up	0.2	0	0.8
(c) Stationary aggregation	1	0.5	0.8
(d) Compact stationary aggregation	10	0.5	0.8

Table 4.3: Parameter values for patterns when $q_a > q_r$ (PDE model). Patterns are shown in Figure 4.4. Submodel M1 is used throughout and the fixed parameters are $q_{al} = 1, q_a = 1, s_r = 0.5, s_{al} = 1.25, s_a = 1$ and $\gamma = 1$.

This results from individuals turning around to remain in the group, and is consistent with observations in empirical studies and other models [17].

Including of density-dependent speed in the PDE model and modifying the social interaction kernels to be of exponential type explains some animal behaviour patterns. In particular, the model is able to explain the dispersion of an aggregation, the long-time existence of groups, and blow-up patterns. These patterns correspond to observed behaviours, such as foraging, grouping behaviours, and collapse of some schools of fish to tight groups, respectively. The turning rates impact the behaviour of solutions, with large random turning rates leading to dense stationary aggregations.

4.3 Density-Dependent Speed in the IBM

In this section, we modify the IBM presented in Chapter 3 to include density-dependent speed interactions. As before, individual social interactions are divided into three groups: repulsion, alignment, and attraction. Following Section 4.2, we initially consider only alignment interactions in an individual's turning rates, and allow individuals to adjust their speed as a result of repulsive and attractive interactions. Subsequently, we investigate more general turning rates which are a function of all three social interactions.

The IBM consists of a population of N individuals moving on a one-dimensional domain with periodic boundary conditions. Here, individual i has position $x_i(t)$ and direction $v_i(t)$ at time t , where $x_i(t) \in \mathbb{R}$ and $v_i(t) = \pm 1$. Recall that the social interaction forces felt by individual i are denoted $y_{j,i}^\pm$, $j = r, al, a$, where \pm indicates the individual's direction, and $j = r, al, a$ denotes repulsion (r), alignment (al), or attraction (a). A right-moving and left-moving individual i changes direction with rate λ_i^+ or λ_i^- , respectively, dependent on the

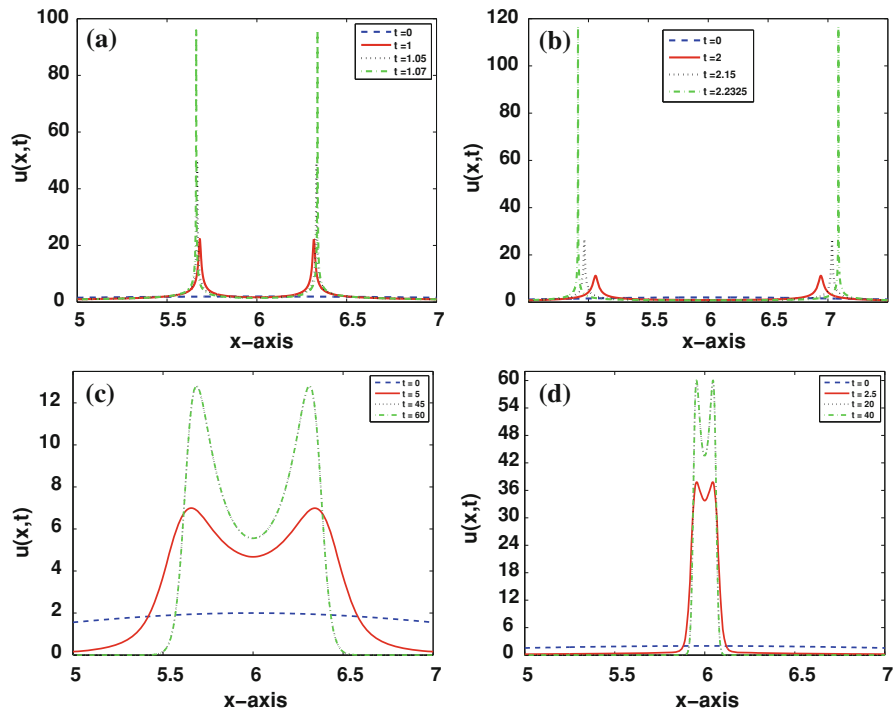


Figure 4.4: Patterns formed in the PDE model when attraction is stronger than repulsion, $q_r < q_a$. Parameter values in Table 4.3. (a) stationary blow-up (b) moving blow-up; (c) stationary aggregation; (d) very dense stationary aggregation. Figure from [17].

social interaction forces:

$$\lambda_i^\pm = \lambda_1 + \lambda_2 f(y_{al,i}^\pm), \quad (4.5)$$

where λ_1 and λ_2 describe the base-line and bias turning rate, respectively. The turning function f is chosen as before, (3.2), to be a logistic function. Here, the social interaction forces, $y_{r,i}^\pm$, $y_{al,i}^\pm$ and $y_{a,i}^\pm$, are chosen to be the social interactions from submodel M1. The exact definitions of the social interactions are can be found in Section 3.2, equations (3.5), (3.7), and (3.6).

Individuals adjust their speed by comparing individuals in the attraction and repulsion zones. It is biologically reasonable for social individuals to speed up to join distant groups, or to slow down to avoid collision with nearby individuals. Motivated thus, we let individuals move with speed $\Gamma_i^\pm(y_i^\pm)$, where

$$\Gamma_i^\pm(y_i^\pm) = \gamma (1 + \tanh(y_i^\pm)), \quad (4.6)$$

$\gamma = 0.1$ is a base-line movement speed, and $y_i^\pm = y_{a,i}^\pm - y_{r,i}^\pm$ compares the attraction and repulsion social interaction forces. To understand how the non-local speeds depend on individuals in the repulsion and attraction interaction zones, consider a right-moving individual i at x . For the sake of example, ignore conspecifics to the left of the individual. If $y_{a,i}^+ > y_{r,i}^+$, then this individual senses a large number of individuals in its zone of attraction relative to the number of individuals in its zone of repulsion. Consequently, the individual will be motivated to speed up and join the distant group. This results in the speed of individual i to increase since $\Gamma_i^+(y_i^+)$ is an increasing function. Thus, the individual increases its speed to join the distant group of individuals. On the other hand, if $y_{a,i}^+ < y_{r,i}^+$, the individual would be motivated to slow down to avoid collision. This is reflected in (4.6). To incorporate this density-dependent speed into the IBM, the position and velocity updating rule, (3.3), is modified and becomes

$$\begin{aligned} x_i(t + \Delta t) &= x_i(t) + \Gamma_i^\pm(y_i^\pm)v_i(t)\Delta t, \\ v_i(t + \Delta t) &= \begin{cases} -v_i(t), & \text{if } \lambda_i^\pm \Delta t \geq X, \\ v_i(t), & \text{otherwise,} \end{cases} \end{aligned} \quad (4.7)$$

where X is a uniformly distributed random variable on $[0, 1]$. To ensure that the individuals do not erroneously respond to conspecifics, we use a time-splitting approach. In the first half-time step, individuals respond to conspecifics by changing direction. In the second half-

step, individuals re-calculate the social interaction forces, y_i^\pm , with their new velocity, and then update their speed.

The IBM with density-dependent speed was numerically simulated to not only understand the behaviour of the model but also in an attempt to match those patterns formed by the PDE model with density-dependent speed as in Figure 4.1. To this end, the same parameter space as explored in Section 4.2 was used to numerically simulate the IBM. Moreover, the patterns presented in Figure 4.1 are produced in the case that the turning rates only depend on alignment forces and not repulsion or attraction. That is, for the initial numerical investigation, the turning rates are

$$\lambda_i^\pm = \lambda_1 + \lambda_2 f(y_{al,i}^\pm), \quad (4.8)$$

Although the same parameter space is used, we do not expect the patterns to match exactly due to the stochasticity in the IBM and how density-dependent speed is incorporated into the advection term of the PDE, (4.1). Stochasticity results in noisier patterns in the IBM than in the PDE model, as seen in the patterns presented in Figure 3.2. Density-dependent speed is incorporated inside the spatial derivative in (4.1), for instance:

$$\frac{\partial u^+}{\partial t} + \frac{\partial}{\partial x} (\Gamma^+(y^+) u^+). \quad (4.9)$$

This construction describes the flux of the population density, whereas the IBM describes the speed at which each individual moves at:

$$x_i(t + \Delta t) = x_i(t) + \Gamma_i^\pm(y_i^\pm) v_i(t) \Delta t. \quad (4.10)$$

Nonetheless, the IBM is able to reproduce the qualitative behaviour of the PDE in the same parameter space.

The patterns produced by the IBM with density-dependent speed are shown in Figure 4.5, and density plots of these patterns are presented in Figure 4.6. The patterns and parameters are given in Table 4.4. Several parameters are fixed. In particular, the domain size, $L = 10$, the location of the social interaction ranges, $s_r = 0.25$, $s_{al} = 0.5$, $s_a = 1$, the baseline speed $\gamma = 0.1$, and the width of the interaction kernels $m_j = \frac{s_j}{8}$ are fixed.

Stationary aggregations and groups that split and merge are examples of patterns formed. Splitting and merging behaviour is a new pattern which is not observed in either the PDE model or IBM with constant movement speed. In Figure 4.5(a), (b), and (c), three examples

Pattern	Submodel	λ_1	λ_2	q_r	q_{al}	q_a
(a) Stationary Pulses	M1	0.2	0.9	0.1	0	0.5
(b) Stationary Pulses	M1	0.2	0.9	0.1	2	0.7
(c) Stationary Pulses	M1	0.2	0.9	0.1	2	0.3
(d) Splitting and Merging Groups	M1	0.2	0.9	0.1	3.5	0.2
(e) Irregular Splitting and Merging	M1	0.2	0.9	0.5	0	0.1
(f) Diagonal Grid	M1	0.2	0.9	0.1	0	0.1

Table 4.4: Example parameter values for patterns produced by the IBM model with density-dependent speed. In this study, the fixed model parameters are $N = 500$, $L = 10$, and $\Delta t = 0.05$.

stationary pulses are shown. These pulses can be of a variety of sizes. In the absence of alignment, $q_{al} = 0$, individuals only turn randomly and respond to neighbours only through density-dependent speed. This results in stationary pulses as in Figure 4.5(a). When alignment is included, the size of the pulses depends on the magnitude of attraction. For relatively large attraction, the pulses are dense (Figure 4.5(b)) and for relatively small attraction, the pulses remain large (Figure 4.5(c)). The behaviour of the IBM and PDE model match well in these cases.

Figure 4.5(d) appears to be an aggregation without order or patterning; however, the corresponding density plot in Figure 4.6(d) shows a high-density aggregation splitting and merging. The density plot for the pattern in Figure 4.6(e) is not particularly revealing of pattern formation or group behaviour, but the plot of the individuals' trajectories in Figure 4.5(e) reveals small groups that split apart and merge with other small groups repeatedly. This behaviour is shown in detail in Figure 4.7. A diagonal grid pattern forms in the plot of the individual trajectories, Figure 4.5(f); however, the corresponding density plot in Figure 4.6(f) reveals some level of grouping with an expansion and contraction similar the breather pattern as observed in the PDE model and IBM without density-dependent speed.

The IBM with density-dependent speed generally reproduces the patterns produced by the PDE model. In Figure 4.1(d), the spitting and merging behaviour appears to consist of very well-defined groups that travel throughout the domain. Using the same parameters in the IBM the splitting and merging behaviour is not immediately apparent in Figure 4.5(d). Instead, we find many individuals outside these main aggregations. Upon closer investigation, this is also the case with the PDE model, as in Figure 4.1(d) a non-zero density outside of the main aggregations is observed.

The initial numerical investigation of the behaviour of the IBM considered the turning

rates λ_i^\pm to be a function of the alignment interaction force, see (4.8). Attraction and repulsion were excluded from the turning as this is how the PDE model was investigated in [10]. Nonetheless, using all social interactions for the turning rates as in (4.5) does not qualitatively change pattern formation using the parameters in Table 4.4.

By relaxing the restriction on using the social interaction forces from submodel M1, we introduce alternate communication mechanisms to the density-dependent speed model. Using the parameters that produce the patterns using the IBM with constant movement speed as presented in Figure 3.2, we investigated the behaviour of the IBM with density-dependent speed. Although the constant speed and density-dependent speed models are fundamentally different, it would not be unexpected if the density-dependent speed model also produced a wide variety of patterns. A numerical investigation reveals a smaller array of patterns. The patterns formed consist of groups that are typically more stationary, and may exhibit some traveling or meandering behaviour. The wide variety of patterns similar to those obtained in Figure 3.2 may result from the IBM with density-dependent speed, however, a much larger parameter space exploration would be required.

Splitting and merging groups are a new feature of both the PDE model and IBM with density-dependent speed and direction-dependent communication mechanisms. Interestingly, splitting and merging groups can result from either the inclusion or exclusion of alignment. This is revealed by the numerical investigation of the IBM with density-dependent speed. Splitting and merging groups are observed when $q_{al} = 3.5$, and irregular splitting and merging behaviour is also observed when $q_{al} = 0$ (see Table 4.4(d) and (e)). The turning rates in the investigation that produces the splitting and merging patterns and the irregular splitting and merging patterns depend only on alignment. Since splitting and merging behaviours result with and without alignment, we conclude that density-dependent speed, not direction-dependent communication, is responsible for splitting and merging behaviours.

4.4 Density-Dependent Speed and Exponential Kernels

In this section, the IBM is adapted to incorporate exponential-type kernels as in [17]. In Section 4.2, the motivation of the study in [17] was summarized. The main idea is to look for conditions for the dispersal of aggregations, the formation of groups, or exhibit blow-up behaviour. In the context of an individual-based model, blow-up behaviour corresponds to a very dense group interacting over a small area, that is, a very high-density group. These

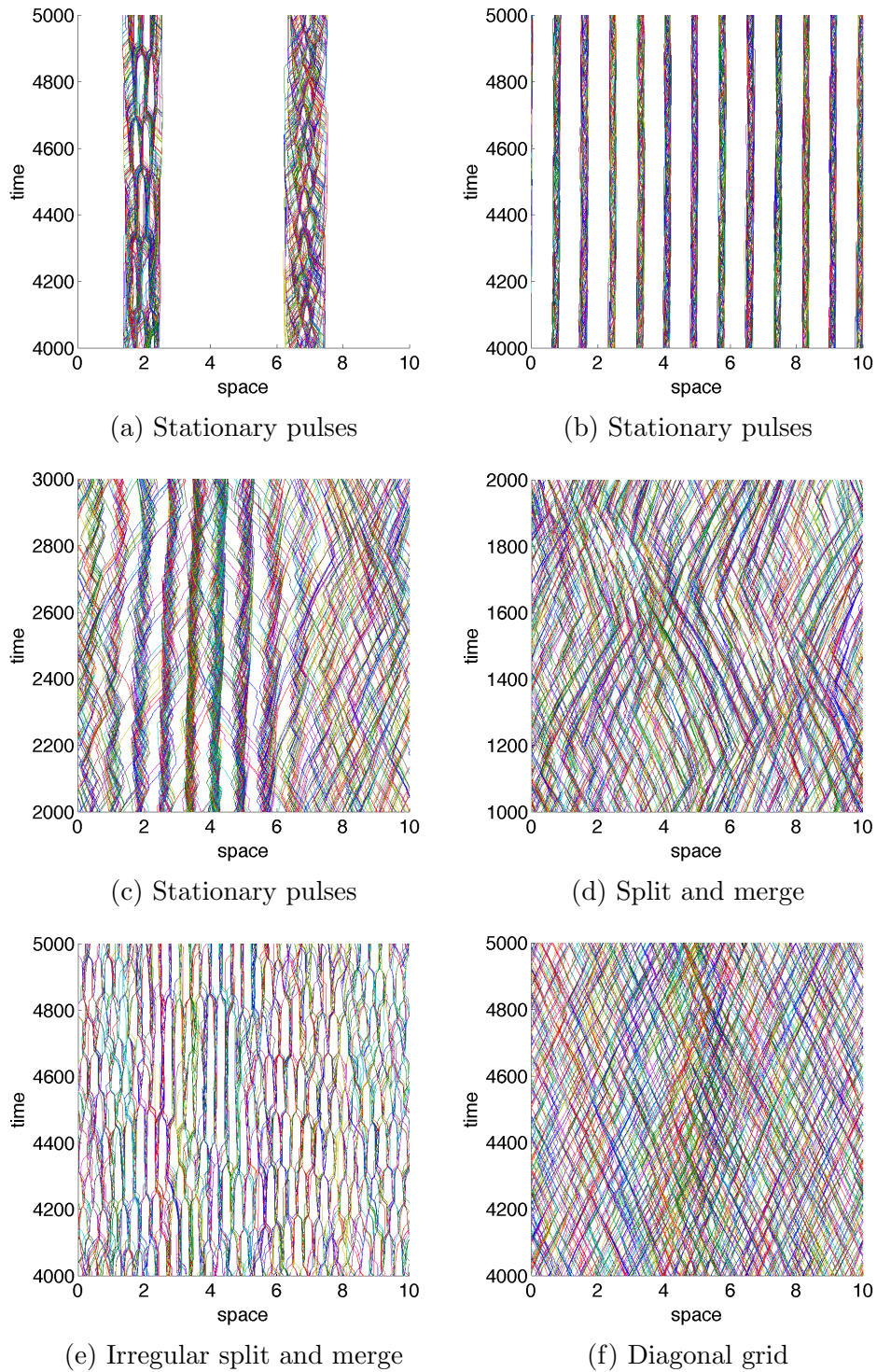


Figure 4.5: Examples of patterns obtained by the IBM with various communication mechanisms and density-dependent speed. Parameters and communication mechanism (submodel) are listed in Table 4.4, and boundary conditions are periodic.

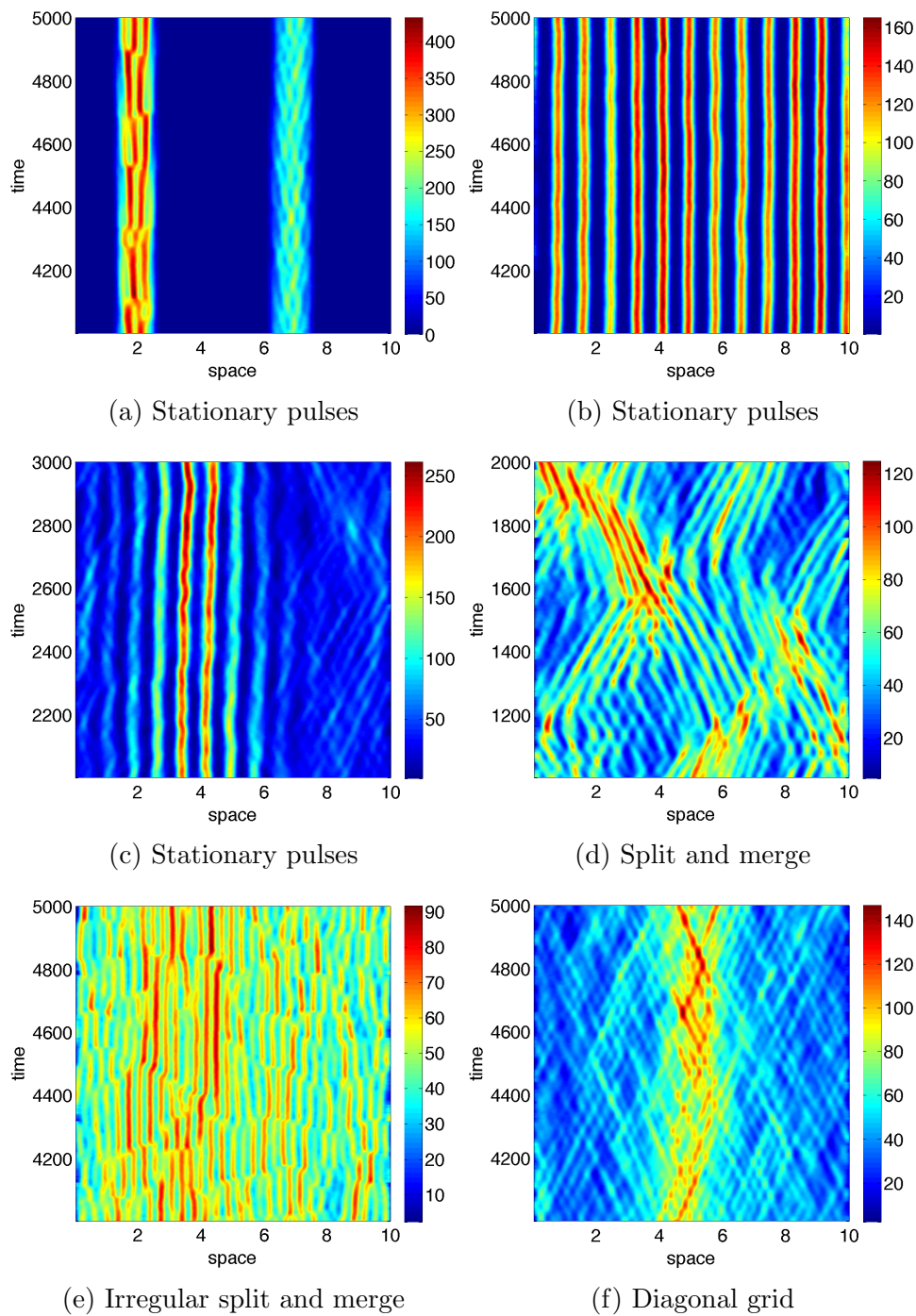


Figure 4.6: Density plots of examples of patterns obtained by the IBM with various communication mechanisms and density-dependent speed. Parameters and communication mechanism (submodel) are listed in Table 4.4, and boundary conditions are periodic.

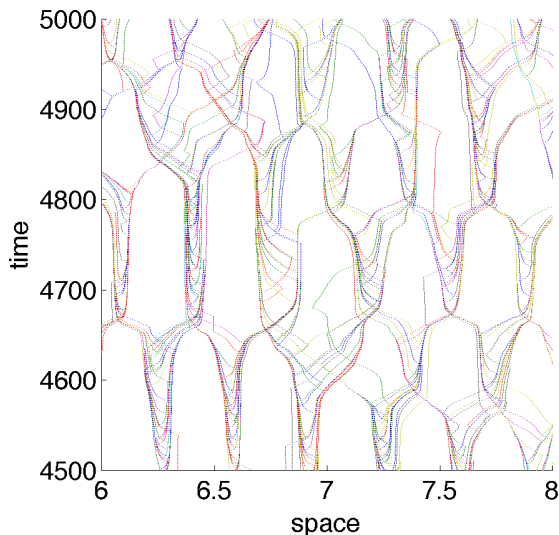


Figure 4.7: Splitting and merging behaviour in the IBM with density-dependent speed. Magnifying a section of Figure 4.6(e) reveals small groups of individuals merging and splitting over time.

very high-density groups can be viewed to be analogous to some schools of fish or swarms of insects that form tightly-packed clusters. The major modification is to incorporate social interaction kernels that better model the repulsion force. The translated Gaussian kernels, (2.4), assume that when individuals are very close together the repulsion force is very weak, whereas it should be strongest. The kernel for density-dependent speed is chosen to be

$$K(x) = \text{sgn}(x)(-q_a K_a(x) + q_r K_r(x)), \quad (4.11)$$

where q_r and q_a are magnitudes of the repulsion and attraction forces, and

$$K_j(x) = e^{-\frac{|x|}{s_j}}, \quad (4.12)$$

where s_r and s_a represent the widths of the repulsion and attraction zones. The movement speed is assumed to only be a function of the repulsion and attractive interactions, and the turning rates only a function of the alignment social interaction force. The translated Gaussian alignment kernel remains suitable. This choice of social interaction kernel is sketched in Figure 4.2.

Numerical simulations of the IBM with density-dependent speed and exponential-type kernels consider two cases, as in the investigation of the PDE model. We use the same

Pattern	λ_1	λ_2
(a) Right- and left-moving groups	0	0
(b) Stationary aggregation	0.2	0
(c) Compact stationary aggregation	1	0.5
(d) High-density stationary aggregation	10	0.5

Table 4.5: Parameter values for patterns when $q_a < q_r$ (IBM model). Patterns are shown in Figure 4.8 and in Figure 4.9. Submodel M1 is used throughout and the fixed parameters are $q_r = 1, q_{al} = 1, q_a = 0.8, s_r = 0.5, s_{al} = 1.25, s_a = 1$ and $\gamma = 1$.

Pattern	λ_1	λ_2
(a) Right- and left-moving groups	0	0
(b) Dispersive aggregation	0.2	0
(c) Compact stationary aggregation	1	0.5
(d) High-density stationary aggregation	10	0.5

Table 4.6: Parameter values for patterns when $q_a > q_r$ (IBM model). Patterns are shown in Figure 4.10 and in Figure 4.11. Submodel M1 is used throughout and the fixed parameters are $q_r = 0.8, q_{al} = 1, q_a = 1, s_r = 0.5, s_{al} = 1.25, s_a = 1$ and $\gamma = 1$.

parameters as in [17] and in Section 4.2 to compare the PDE model and IBM behaviours. In [17], the authors seek conditions which lead to the formation of blow-up patterns, finite-size groups, and dispersive aggregations. In the first case, repulsion is stronger than attraction, $q_r > q_a$, and blow-up patterns are not expected. Thus, we investigate the effect of varying the turning rates on the group structure. Conversely, when attraction is stronger than repulsion, $q_r < q_a$, blow-up solutions are possible, and again, we investigate the effect of varying the turning rates on the group structure.

Parameters for the investigation of the IBM in the case $q_r > q_a$, and in the case $q_r < q_a$, can be found in Table 4.5 and Table 4.6, respectively. As we will see below, patterns obtained in the case when $q_r > q_a$ are moving groups, stationary aggregations, and high-density stationary groups. When $q_r < q_a$, not only are moving groups and stationary aggregations found but dispersive aggregations as well. The turning rates have an impact on the structure of the group in both cases.

When repulsion is stronger than attraction, $q_r > q_a$, we fix $q_r = 1, q_{al} = 1, q_a = 0.8, s_r = 0.5, s_{al} = 1.25, s_a = 1$ and $\gamma = 1$. The initial conditions for this investigation are again a small translated Gaussian, with $N = 500$ individuals, chosen to investigate the dispersal or collapse of a group to a very dense cluster. Pattern formation is presented in

two ways. Firstly, plots of individual trajectories are shown in Figure 4.8, and the estimated probability density is shown in Figure 4.9, to better compare with Figure 4.3 and Figure 4.4. The estimated probability density plots are produced via a kernel smoothing method. The method used is the MATLAB subroutine, `ksdensity`, which computes a probability density estimate from a sample [3].

In Figure 4.8(a), $\lambda_1 = \lambda_2 = 0$, so individuals do not change direction. Here, although repulsion is stronger than attraction, two groups form, one of right-moving individuals and the other of left-moving individuals. This can be seen in Figure 4.9(a). In Figure 4.8(b) and Figure 4.9, $\lambda_1 = 0.2$ and $\lambda_2 = 0$. In this case, the nonzero random turning rate is sufficient to stop the formation of a right- and left-moving group, and instead results in a loose stationary aggregation. The last two cases look at the effect of including turning in response to neighbours, that is, $\lambda_2 \neq 0$. In Figure 4.8(c) and Figure 4.9(c), $\lambda_1 = 1$ and $\lambda_2 = 0.5$, resulting in a stationary aggregation. Finally, in Figure 4.8(d) and Figure 4.9(d), $\lambda_1 = 10$ and $\lambda_2 = 0.5$ resulting in a high-density stationary aggregation. The large value of $\lambda_1 = 10$ in (d) leads to a very dense aggregation as individuals change direction with a very high probability. The stationary groups obtained using parameters in (b) and (c) differ from the patterns obtained with the PDE model (Figure 4.3(b) and (c)). In the PDE model, parameters in (b) and (c) lead to spatially homogenous steady-states, i.e., dispersive aggregations. In the IBM, parameters in case (b) and (c) lead to compact stationary groups; however, the group in (b) tends to be more dispersive.

When attraction is stronger than repulsion, $q_a > q_r$, we fix parameters are $q_r = 0.8$, $q_{al} = 1$, $q_a = 1$, $s_r = 0.5$, $s_{al} = 1.25$, $s_1 = 1$, and $\gamma = 1$. The initial conditions for this investigation are again chosen to be a small translated Gaussian, with $N = 500$ individuals, chosen to investigate the dispersal or collapse of a group to a very dense cluster. As in the case when $q_r < q_a$, the results of the numerical simulations are presented in two ways: the individual trajectories are plotted in Figure 4.10, and an estimated probability density is plotted in Figure 4.11.

In Figure 4.10(a) and Figure 4.11(a), the turning rates are zero, $\lambda_1 = \lambda_2 = 0$, and the aggregation splits into a right- and left-moving group. Non-zero random turning rates lead to a dispersive group, as seen in Figure 4.10(b) and Figure 4.11(b). Stationary groups form in Figure 4.10(c) and (d) (see also Figure 4.11(c) and (d)), with $\lambda_1 = 1$ and $\lambda_2 = 0.5$ in (c), and $\lambda_1 = 10$ and $\lambda_2 = 0.5$ in (d). In this case, pattern formation matches the PDE model reasonably well, except in case (a) and (b). In case (a), the PDE model exhibits blow-up solutions, and right- and left- moving groups form in the IBM. In case (b), right- and left-

moving blow-up is exhibited in the PDE model; however, a dispersive aggregation forms in the IBM.

4.5 Discussion

In the first part of this Chapter, we reviewed how density-dependent speed was incorporated into the PDE model with direction-dependent communication mechanisms in [10, 17]. This material was reviewed to provide background for the second part of this Chapter, namely incorporating density-dependent speed into the new IBM with direction-dependent communication mechanisms.

Motivated by the biological fact that individuals in a group do not travel at a constant speed, and the splitting and merging behaviour described in [20], density-dependent speed is incorporated into the PDE model with direction-dependent communication mechanisms in [10, 17]. In [10], density-dependent speed is assumed to be a function of the difference between attractive and repulsive social interactions, and the turning rates dependent only on the alignment interactions. Numerical simulations reveal that the patterns formed with density-dependent speed included are mostly stationary pulses and groups that split and merge. Splitting and merging groups form when alignment is included and excluded, demonstrating the importance of density-dependent movement speeds for splitting and merging behaviours. Additional analysis of the PDE model with density-dependent speed is presented in [17]. Here, the repulsion and attraction social interaction kernels are modified to be of exponential type, i.e., Laplace distributions. This modification attempts to address the shortfall that translated Gaussian kernels do not sufficiently weight very close range repulsion. This investigation is placed in the biological context of aggregations that remain stationary, disperse, or collapse to a high-density cluster, and so blow-ups and steady state solutions are sought. These patterns are investigated through two cases. Case one is when repulsion is stronger than attraction, and case two is when attraction is stronger than repulsion. Initial conditions for analysis are groups with Gaussian density, and this group remains stationary, moves, disperses or collapses to a high-density group depending on the turning rates λ_1 and λ_2 .

In Section 4.3, density-dependent speed is introduced into the IBM with direction-dependent communication. The turning rates are assumed to depend only on the alignment interaction force and the density-dependent speed on the difference between the attraction and repulsion forces, as in the PDE model. Numerical simulations of the IBM reveal a

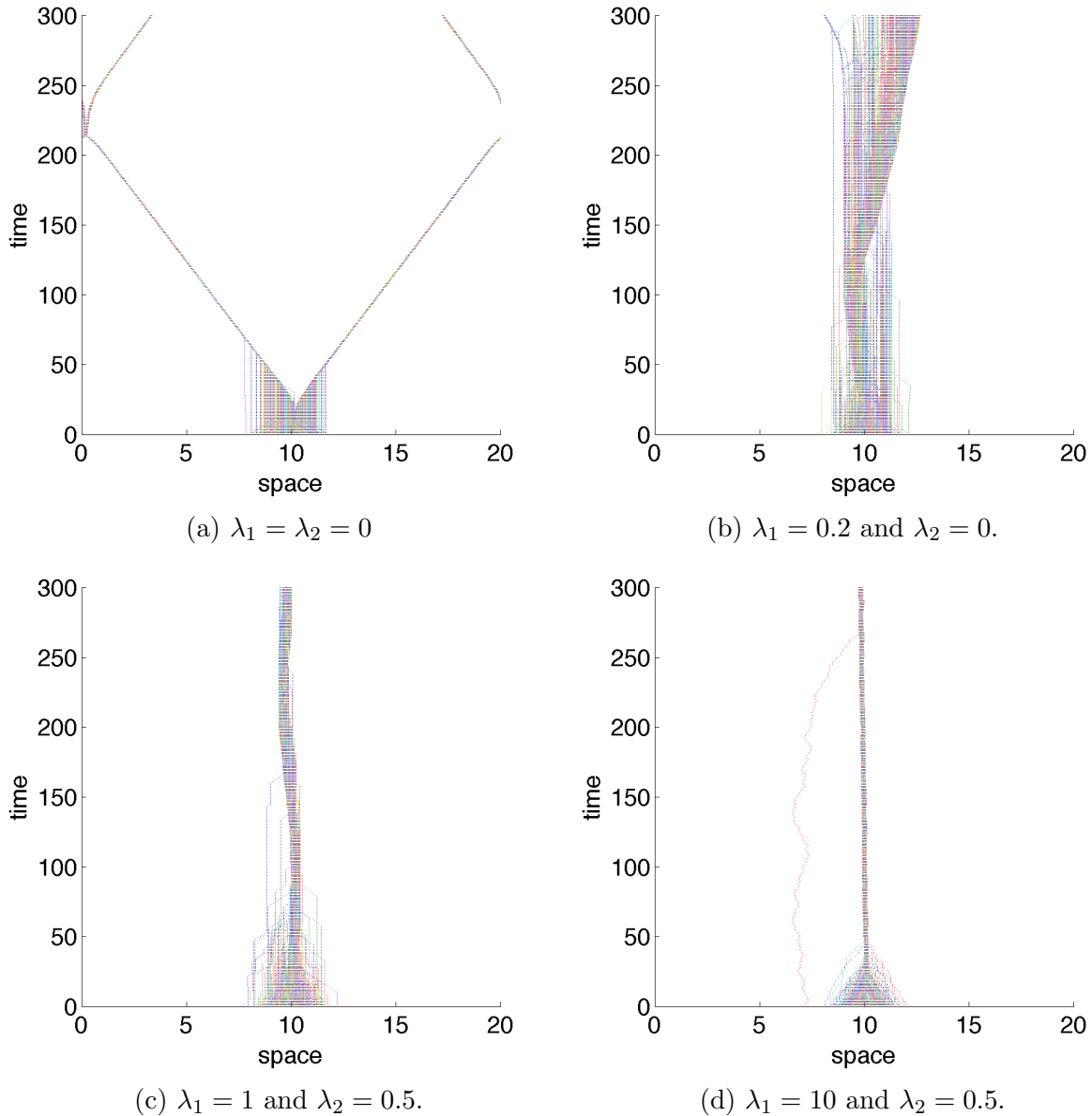


Figure 4.8: Patterns formed in the IBM model when repulsion is stronger than attraction. The effect of changing the base-line (random) turning rates, λ_1 , and the bias turning rate, λ_2 , is investigated. Parameters are listed in Table 4.5. In (a), the absence of turning rates lead to compact left- and right-moving groups. In (b), small random turning leads to a stationary aggregation. In (c), a small random turning rate and a small bias turning rate leads to a compact stationary aggregation, and in (d), a large random turning rate leads to a high-density stationary aggregation.

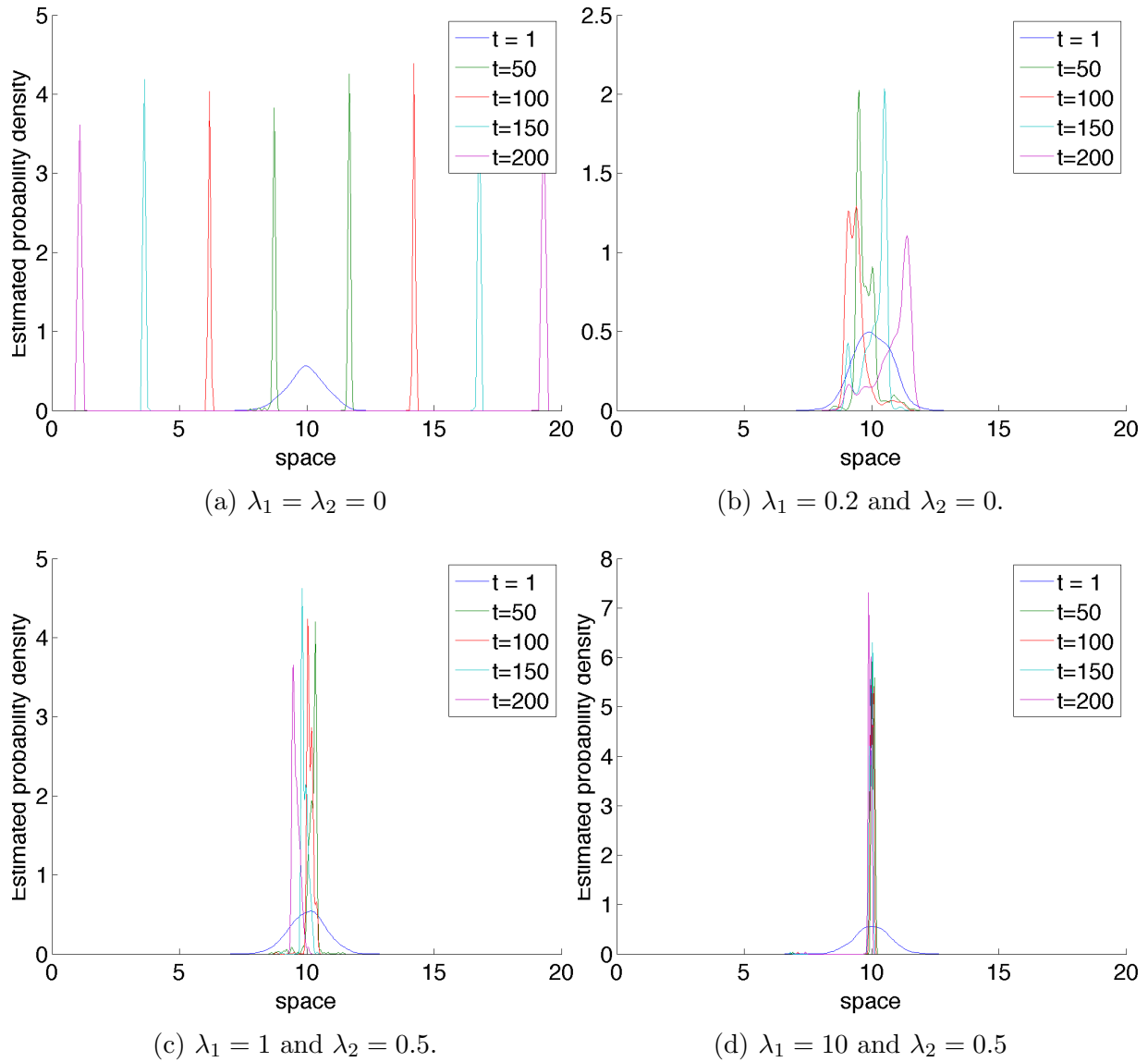


Figure 4.9: Estimated probability density corresponding to the trajectories shown in Figure 4.8. In (a), the initial group turns into a right-moving and left-moving group. In (b), (c), and (d), the group becomes compact and remains stationary. The group in (b) does not become as compact as in (c) or (d) and become more dispersive as time progresses.

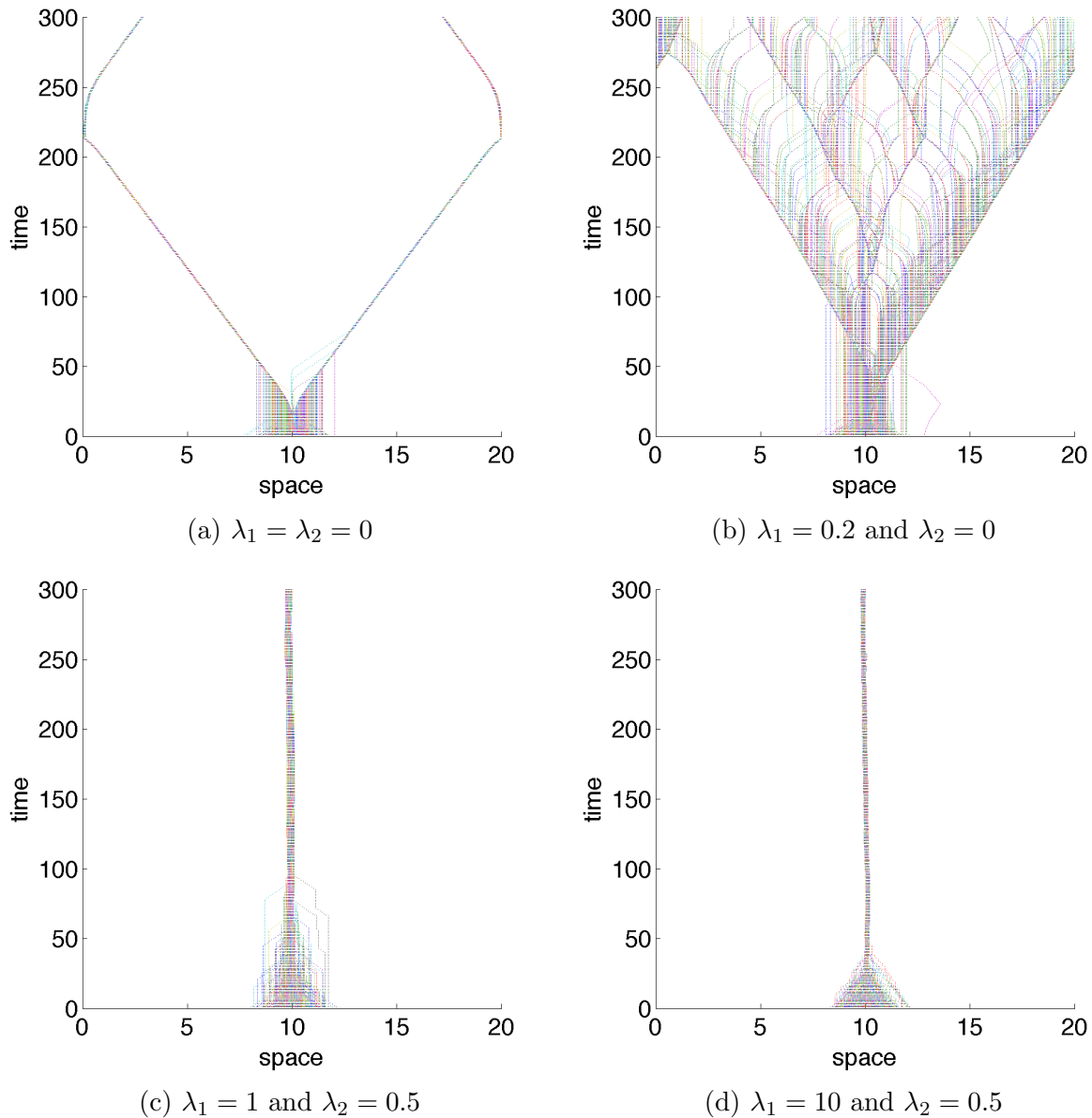


Figure 4.10: Patterns formed in the IBM model when attraction is stronger than repulsion. The effect of changing the base-line (random) turning rates, λ_1 , and the bias turning rate, λ_2 , is investigated. Parameters are listed in Table 4.6. In (a), the absence of turning rates lead to compact left- and right-moving groups. In (b), small random turning leads to a dispersive aggregation. In (c), a small random turning rate and a small bias turning rate leads to a compact stationary aggregation, and in (d), a large random turning rate leads to a high-density stationary aggregation.

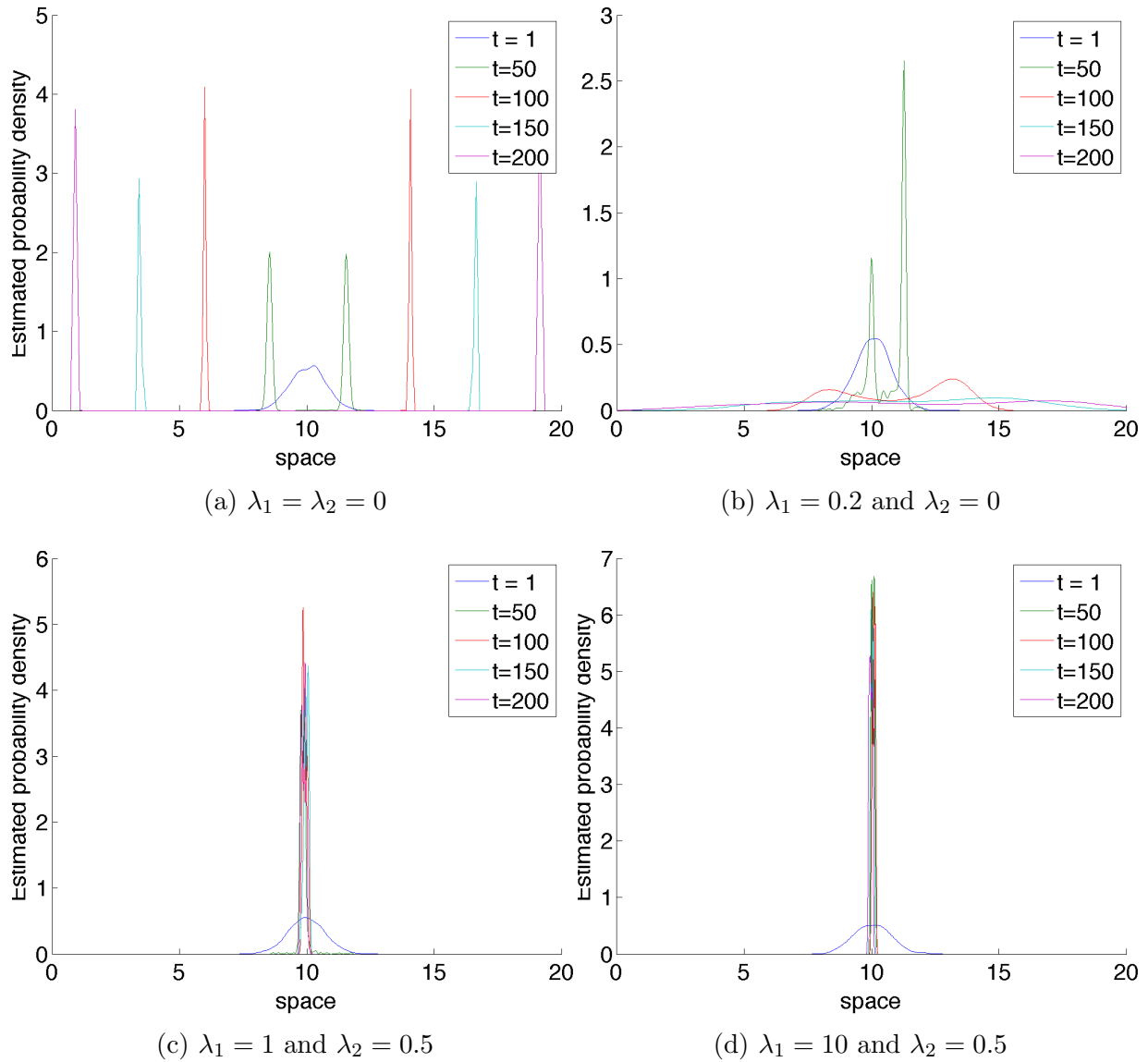


Figure 4.11: Estimated probability density corresponding to the trajectories shown in Figure 4.10. In (a), the initial group splits into a right-moving group and left-moving group. In (b), the group disperses. In (c) and (d), the group becomes compact and remains stationary.

qualitative match to the behaviour of the PDE model with density-dependent speed. This demonstrates that the splitting and merging behaviour is again a result of the incorporation of density-dependent speed. The numerical simulations also reveal the nature of how individuals behave with respect to density-dependent speed. Comparing the stationary pulses in Figure 4.5(a), for example, with those stationary pulses in Figure 3.2(a) reveals that without density-dependent speed, individuals near the edge of the group may escape due to repulsion only to later turn and rejoin the group due to attraction. However, with density-dependent speed, individuals near the edge of the group do not escape the pulse, but rather form a well-defined edge. If an individual nears the edge, they tend to be moving slowly, and at some point will change direction and speed up to return to the dense group centre. Splitting and merging behaviour is not seen in the IBM without density-dependent speed, again alluding to the importance of density-dependent movement speeds. Interestingly, when density-dependent speed is combined with a wide variety of direction-dependent communication mechanisms, the patterns obtained with constant speed, as in Figure 3.2, do not form using the same parameters. Instead, the patterns that form are typically stationary or may be slowly traveling groups, with qualitatively less direction-switching. This suggests that group formation and group dispersal may rely on speeding and slowing behaviours resulting from density-dependent speed mechanisms, whereas detailed pattern formation may rely on direction-switching mechanisms resulting from non-local communication mechanisms.

The IBM with modified repulsion and attraction kernels of exponential type, studied in Section 4.4, does not match the behaviour of the PDE model with modified social interaction kernels across parameter regimes quantitatively. Nonetheless, the two models behaviour matches in the types of patterns obtained: dispersive aggregations, moving groups, and very dense stationary aggregations. The turning rates, λ_1 and λ_2 influence pattern formation in either case: $q_a < q_r$ or $q_r < q_a$. Even when attraction is weaker than repulsion, high random turning rates, $\lambda_1 = 10$, for example, result in stationary groups. Paradoxically, in the case when the turning rates are small and turning does not depend on social interactions, $\lambda_1 = 0.2$ and $\lambda_2 = 0$, a loose stationary aggregation forms when $q_a < q_r$, while a dispersive aggregation forms when $q_r < q_a$. Intuition dictates that repulsion forces should lead to the dispersion of the aggregation. Instead, the dispersion in Figure 4.10(b) appears to result from individuals leaving the traveling high-density groups and subsequently attracted to other escapees.

Previously, the added stochasticity in the IBM was hypothesized to play a role in the not-so-perfect match of patterns between the two models in the same parameter regimes, and this may again be the case here. A larger parameter exploration could clarify the behaviour

of both the PDE model and IBM. Another hypothesis for the variation is that density-dependent speed is introduced ad hoc to the IBM. As discussed in Section 4.3 (equation (4.9)), the density-dependent speed appears within the advection term of the PDE model (4.1). This construction describes the flux of the population density through space and does not prescribe the speeds at which individuals move at. The IBM, on the other hand, describes the speeds at which individuals move, and is not concerned with a spatial change in population density. A better understanding of the first principles that lead to the non-local hyperbolic PDE with density-dependent speed and direction-dependent turning rates, (4.1), may better describe the speeds at which individuals move at. A random walk with density-dependent speeds and the resulting limiting PDE is studied in [6], and may provide insight to the nature of density-dependent speeds in the IBM.

Chapter 5

2-Particle Model with Communication Mechanisms

5.1 Introduction

In this chapter, we continue to focus on understanding the behaviour of individuals in response to social interactions, specifically direction-dependent communication mechanism as studied in Chapters 2 and 3. The modelling approaches in the previous chapters have been focused on population-density and group level pattern formation. Studying pattern formation reveals, for instance, how different direction-dependent communication mechanisms result in stationary versus moving groups. The disadvantage to studying pattern formation as an emergent group-level phenomena is that it does not reveal how each individual in the group responds to others. Understanding interactions and responses on an individual-to-individual level is equally as important as understanding the collective behaviour. For instance, in [27], a group of robots without centralized control worked collectively to accomplish a complex task, which they are unable to complete individually. In this case, the group level task has priority over the organization of the individuals; however, when thinking of modern applications, such as a system of driverless cars, the collective task of transport is equally as important as the car-to-car individual interactions. Focusing on individual-to-individual interactions allows for a complete understanding of how direction-dependent communication mechanisms affect collective behaviour.

To study individual-to-individual interactions, we focus on 2-particle models in this Chapter. In Section 5.2, we review an anti-symmetric exclusion process, which was defined by Potts *et al.* in [34] and completely solved. This review provides background for introducing

social interactions to 2-particle systems, as in Section 5.3, and direction-dependent communication, as in Section 5.4. In Section 5.5, the main ideas from the Eftimie model (Chapter 2 and Chapter 3) are studied in the context of a 2-particle model. Finally, in 5.6, the significance and limitations of these results are discussed.

5.2 Anti-symmetric Exclusion Process

In this section, we review work from Potts *et al.* [34], where an anti-symmetric exclusion process for two particles on an infinite one-dimensional lattice is studied. Potts extends the work of Aslangul [1], who completely characterized the diffusion of two repulsive particles on a one-dimensional lattice. Aslangul solves this problem by deriving a master equation and solving it using elementary methods. Potts follows Aslangul's construction and methodology; however, Aslangul only considers unbiased movement while Potts considers a movement bias. The purpose of this summary is to provide background for including social interactions and direction-dependent interactions in a 2-particle system.

Exclusion processes are common in applications such as RNA transcription, wireless networking, and in the case of [34], territorial behaviour in the animal kingdom. The primary characteristic of exclusion processes is that the agents in the system exclude each other from the space they occupy. If, in one dimension, the individuals hop to the right or left with equal probability, we call the movement unbiased. If the probability of hopping to the right or to the left is not equal, the movement is called biased. Potts *et al.* studies an anti-symmetric exclusion process where the two particles have a directional bias, but the bias of each particle is the opposite of the other, i.e., the particles have anti-symmetric biases.

The anti-symmetric exclusion process is studied by considering two particles, that randomly walk on an infinite one-dimensional lattice. The probability of the left-hand particle jumping to the right at each step is p and the right-hand particle jumping to the left at each step is p . Thus, the probability of the left-hand particle jumping to the left at each step is $1 - p$ and the probability of the right-hand particle jumping to the right at each step is $1 - p$. Figure 5.1 shows the two particles and their anti-symmetric movement biases. If $p > \frac{1}{2}$, then the two particles are biased to hop towards each other; and if $p < \frac{1}{2}$, then the two particles are biased to hop away from each other.

The model assumes that both particles cannot occupy the same site at the same time, the hopping rate is F , and the lattice spacing is a . Ensuring that the two particles cannot occupy the same site is the same as assuming a contact-based repulsion mechanism. The beginning of

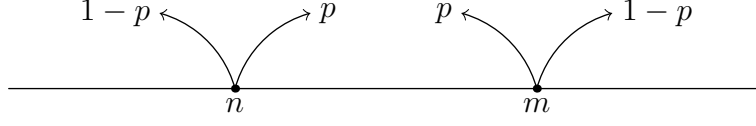


Figure 5.1: Cartoon depiction of the one-dimensional anti-symmetric exclusion process. The left-hand particle is at lattice site n , hops to the right with probability p , and hops to the left with probability $1 - p$. The right-hand particle is at lattice site m , hops to the right with probability $1 - p$, and hops to the left with probability p .

this investigation is to write a master equation for the joint occupation probability $P(n, m, t)$ of the two particles being at lattice site n and m at time t . The master equation for $P(n, m, t)$ is

$$\begin{aligned}
P(n, m, t + \Delta t) = & P(n, m, t) \\
& - F\Delta t p P(n, m, t) (1 - \delta_{n, m-1}) (1 - \delta_{n, m}) \\
& - F\Delta t (1 - p) P(n, m, t) (1 - \delta_{n, m+1}) (1 - \delta_{n, m}) \\
& - F\Delta t (1 - p) P(n, m, t) (1 - \delta_{n, m+1}) (1 - \delta_{n, m}) \\
& - F\Delta t p P(n, m, t) (1 - \delta_{n, m-1}) (1 - \delta_{n, m}) \\
& + F\Delta t (1 - p) P(n + 1, m, t) (1 - \delta_{n, m-1}) (1 - \delta_{n, m}) \\
& + F\Delta t p P(n - 1, m, t) (1 - \delta_{n, m+1}) (1 - \delta_{n, m}) \\
& + F\Delta t p P(n, m + 1, t) (1 - \delta_{n, m+1}) (1 - \delta_{n, m}) \\
& + F\Delta t (1 - p) P(n, m - 1, t) (1 - \delta_{n, m-1}) (1 - \delta_{n, m}) \\
& + O(\Delta t^2). \tag{5.1}
\end{aligned}$$

Here, $\delta_{n, m} = 1$ if $n = m$ and $\delta_{n, m} = 0$ if $n \neq m$. This master equation looks at how individuals end up at lattice sites n and m at time $t + \Delta t$, and how individuals at lattice sites n and m at time t leave these lattice sites. There are eight possible hops, as depicted in Figure 5.2. These hops and the corresponding term in the master equation are:

1. n hops to $n + 1$: $-F\Delta t p P(n, m, t) (1 - \delta_{n, m-1}) (1 - \delta_{n, m})$
2. n hops to $n - 1$: $-F\Delta t (1 - p) P(n, m, t) (1 - \delta_{n, m+1}) (1 - \delta_{n, m})$
3. m hops to $m + 1$: $-F\Delta t (1 - p) P(n, m, t) (1 - \delta_{n, m+1}) (1 - \delta_{n, m})$
4. m hops to $m - 1$: $-F\Delta t p P(n, m, t) (1 - \delta_{n, m-1}) (1 - \delta_{n, m})$

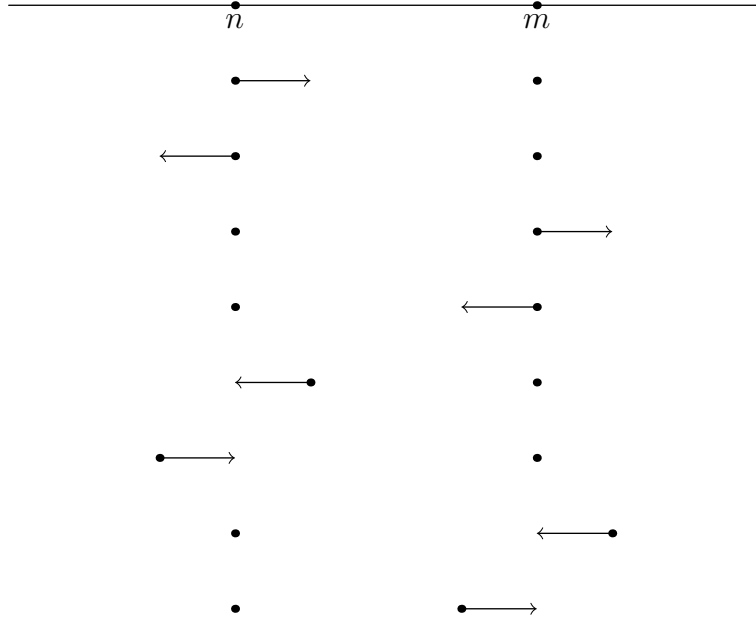


Figure 5.2: Cartoon depiction of particle movement in the anti-symmetric exclusion process. Each row represents a possible hop that occurs in time step Δt .

$$5. \ n + 1 \text{ hops to } n: F\Delta t (1 - p) P(n + 1, m, t) (1 - \delta_{n, m-1}) (1 - \delta_{n, m})$$

$$6. \ n - 1 \text{ hops to } n: F\Delta t p P(n - 1, m, t) (1 - \delta_{n, m+1}) (1 - \delta_{n, m})$$

$$7. \ m + 1 \text{ hops to } m: F\Delta t p P(n, m + 1, t) (1 - \delta_{n, m+1}) (1 - \delta_{n, m})$$

$$8. \ m - 1 \text{ hops to } m: F\Delta t (1 - p) P(n, m - 1, t) (1 - \delta_{n, m-1}) (1 - \delta_{n, m})$$

These hops occur with rate F and probability p or $1 - p$. To ensure that each of these hops occur only when allowed, Potts includes factors of the form $(1 - \delta_{n, m})$, $(1 - \delta_{n, m-1})$, and $(1 - \delta_{n, m+1})$. The factors of the form

- $(1 - \delta_{n, m})$ ensure that individuals do not hop to the same lattice site;
- $(1 - \delta_{n, m-1})$ ensure that if the left-hand particle is adjacent to the right-hand particle that they do not hop toward each other ($n = m - 1$);
- and $(1 - \delta_{n, m+1})$ ensure that if the right-hand particle is adjacent to the left-hand particle that they do not hop toward each other ($n = m + 1$).

For example, if at time t a particle hops from n to $n + 1$, the term it contributes to the master equation is

$$\underbrace{-F\Delta t p}_{\text{hopping probability}} \underbrace{P(n, m, t)}_{\text{probability of particles at } n \text{ and } m} \underbrace{(1 - \delta_{n, m-1})}_{\text{do not hop if adjacent}} \underbrace{(1 - \delta_{n, m})}_{\text{exclude from the same spot}}. \quad (5.2)$$

Here, the minus sign indicates that this particle is leaving site n , $F\Delta t p$ gives the hopping probability, $P(n, m, t)$ gives the probability that the particles are at n and m . $(1 - \delta_{n, m-1}) = 0$ if $n = m - 1$, that is, the particle at n cannot hop to site $n + 1$ as the two particles are adjacent (the left-hand particle is at n , and the right-hand particle is at $n + 1 = m$). $(1 - \delta_{n, m}) = 0$ ensures the particles exclude each other.

Re-writing (5.1), we find

$$\begin{aligned} \frac{P(n, m, t + \Delta t) - P(n, m, t)}{\Delta t} &= -2FpP(n, m, t)(1 - \delta_{n, m-1})(1 - \delta_{n, m}) \\ &\quad - 2F(1 - p)P(n, m, t)(1 - \delta_{n, m+1})(1 - \delta_{n, m}) \\ &\quad + F(1 - p)[P(n + 1, m, t) + P(n, m - 1, t)](1 - \delta_{n, m-1})(1 - \delta_{n, m}) \\ &\quad + Fp[P(n - 1, m, t) + P(n, m + 1, t)](1 - \delta_{n, m+1})(1 - \delta_{n, m}) \\ &\quad + O(\Delta t). \end{aligned} \quad (5.3)$$

Hence, as $\Delta t \rightarrow 0$,

$$\begin{aligned} \frac{dP(n, m, t)}{dt} &= -2FpP(n, m, t)(1 - \delta_{n, m-1})(1 - \delta_{n, m}) \\ &\quad - 2F(1 - p)P(n, m, t)(1 - \delta_{n, m+1})(1 - \delta_{n, m}) \\ &\quad + F(1 - p)[P(n + 1, m, t) + P(n, m - 1, t)](1 - \delta_{n, m-1})(1 - \delta_{n, m}) \\ &\quad + Fp[P(n - 1, m, t) + P(n, m + 1, t)](1 - \delta_{n, m+1})(1 - \delta_{n, m}). \end{aligned} \quad (5.4)$$

The method of solution to (5.4) is given in [34]. Asymptotic analysis of the solution allows for the mean position of the left-hand (or right-hand) particle as well as the second moment of the distribution. Dimensionless time $\tau = tF$ is considered, and $x_1(\tau)$ and $x_2(\tau)$ are defined to be the positions of the left- and right-hand particles at time τ , respectively. The mean separation distance is defined to be $d(\tau) = \langle x_2(\tau) - x_1(\tau) \rangle$. Potts *et al.* states that the second moments of the positions of the particles coincide and this is denoted as $\langle x^2(\tau) \rangle$. The mean square displacement (MSD) is defined as $\Delta x^2(\tau) = \langle x^2(\tau) - \langle x(\tau) \rangle^2 \rangle$, where $x^2(\tau)$ is

the second moment and $\langle x(\tau) \rangle$ is the first moment of the position probability distribution. Recall that a is the lattice spacing. For $\tau \gg 1$, the following asymptotic expressions are reported in [34]:

$$d(\tau) \sim \begin{cases} 4a(1-2p)\tau & \text{if } 0 < p < \frac{1}{2}, \\ \sqrt{\frac{8}{\pi}}a\sqrt{\tau} & \text{if } p = \frac{1}{2}, \\ \frac{p}{2p-1}a & \text{if } \frac{1}{2} < p < 1, \end{cases} \quad (5.5)$$

$$\langle x^2(\tau) \rangle \sim \begin{cases} 4a^2(1-2p)^2\tau^2 & \text{if } 0 < p < \frac{1}{2}, \\ 2a^2\tau & \text{if } p = \frac{1}{2}, \\ 2a^2(1-p)\tau & \text{if } \frac{1}{2} < p < 1. \end{cases} \quad (5.6)$$

$$\Delta x^2(\tau) \sim \begin{cases} 2a^2\tau & \text{if } 0 < p < \frac{1}{2}, \\ 2a^2\left(1 - \frac{1}{\pi}\right)\tau & \text{if } p = \frac{1}{2}, \\ 2a^2(1-p)\tau & \text{if } \frac{1}{2} < p < 1. \end{cases} \quad (5.7)$$

The asymptotic results reveal that the behaviour of the anti-symmetric exclusion process is influenced by the value of p . In particular, the separation distance and mean square displacement (MSD) differ depending on the value of p . When $0 < p < \frac{1}{2}$, the separation distance is asymptotically linear in time; when $p = \frac{1}{2}$, the separation distance increases with the square root in time; and when $\frac{1}{2} < p < 1$, the separation distance saturates. These results coincide with the bias of the particles. For instance, when $0 < p < \frac{1}{2}$, the particles are biased to hop apart and we expect the distance between the particles to grow. On the other hand, when $\frac{1}{2} < p < 1$, the particles are biased to hop toward each other. Since the particles cannot cross, they achieve a steady state at a separation distance that depends on the value of p . The asymptotic expression for the MSD reveals that the asymptotic diffusion constant, $\frac{\Delta x^2(t)}{2t}$, takes a different value depending on the value of p . These results are summarized in detail in [34]. The separation distance and MSD allow for the anti-symmetric exclusion process to be studied quantitatively.

Most importantly, we can interpret these results in a biological context. In terms of collective behaviour, the particles in the anti-symmetric exclusion process discussed above can be considered to be two randomly walking individuals each having an intrinsic bias to hop toward or away from each other, depending on the value of p . These individuals thus can have an intrinsic attractive force or an intrinsic repulsive force. Moreover, since the individuals exclude each other from the same lattice sites, they also interact via a contact-

repulsion process. This is easily seen to be analogous to individuals in a population that change direction upon bumping into each other. In this way, the anti-symmetric exclusion process provides a framework for a 2-particle collective behaviour model. In this model, when $\frac{1}{2} < p < 1$, the individuals exhibit grouping and the mean separation distance between them approaches a constant value; when $p = \frac{1}{2}$, the individuals drift apart with the square root of time; and when $0 < p < \frac{1}{2}$, the individuals are repelled away from each other and the mean separation distance between them grows linearly in time.

5.3 Anti-symmetric Exclusion Process with Social Interactions

The anti-symmetric exclusion process reviewed in Section 5.2 provides a framework for studying how individuals respond to animal communication mechanisms. To study the process, a master equation for the joint occupation probability, $P(n, m, t)$, the probability that the left-hand particle is at n and the right-hand particle at m at time t , was derived and studied. This probability distribution describes the likelihood of finding the two individuals at lattice sites n and m . Understanding the time evolution of this probability distribution is analogous to understanding the particle's interactions. In the anti-symmetric exclusion process, each walker hopped toward the other with probability p , and away from each other with probability $1 - p$. Moreover, the individuals excluded each other from adjacent lattice sites, that is, they experienced contact repulsion. This short-range repulsion can be considered a social interaction, although it is not non-local like the repulsion force in the PDE model or IBM from Chapter 2 or Chapter 3.

In this section, we extend the contact repulsion to be non-local and add a non-local attraction interaction to the anti-symmetric exclusion process, by modifying the probability p of the individuals hopping toward each other to be a function of the distance between the particles, $d = m - n$. A cartoon of this process is presented in Figure 5.3. To understand this new process, we will write a master equation for the joint occupation probability, $P(n, m, t)$. In place of an analysis of the master equation, stochastic simulations of the process reveal the behaviour of the model, and provide statistics that reveal the characteristics of the probability distribution.

Consider two particles on an infinite one-dimensional lattice, with lattice sites separated by a . We assume that both particles cannot occupy the same site at the same time, exhibit contact repulsion, and hop with rate F . Additionally, we assume that each hop depends

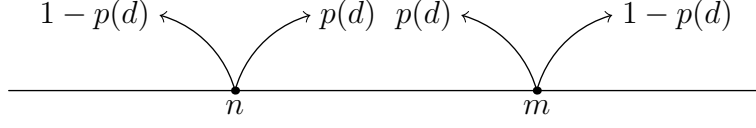


Figure 5.3: Cartoon depiction of the one-dimensional anti-symmetric exclusion process with social interactions. The left-hand particle is at lattice site n , hops to the right with probability $p(d)$, and hops to the left with probability $1 - p(d)$. The right-hand particle is at lattice site m , hops to the right with probability $1 - p(d)$, and hops to the left with probability $p(d)$.

only on the distance between the particles, and that each hop is independent of any other hops. As in Section 5.2, we write a master equation for the joint occupation probability $P(n, m, t)$ for the left-hand particle to be at n and the right-hand particle to be at m at time t . Accounting for all the possible hops, we find:

$$\begin{aligned}
P(n, m, t + \Delta t) = & P(n, m, t) \\
& - F\Delta t p(d) P(n, m, t) (1 - \delta_{n, m-1}) (1 - \delta_{n, m}) \\
& - F\Delta t (1 - p(d)) P(n, m, t) (1 - \delta_{n, m+1}) (1 - \delta_{n, m}) \\
& - F\Delta t (1 - p(d)) P(n, m, t) (1 - \delta_{n, m+1}) (1 - \delta_{n, m}) \\
& - F\Delta t p(d) P(n, m, t) (1 - \delta_{n, m-1}) (1 - \delta_{n, m}) \\
& + F\Delta t (1 - p(d)) P(n + 1, m, t) (1 - \delta_{n, m-1}) (1 - \delta_{n, m}) \\
& + F\Delta t p(d) P(n, m + 1, t) (1 - \delta_{n, m+1}) (1 - \delta_{n, m}) \\
& + F\Delta t p(d) P(n - 1, m, t) (1 - \delta_{n, m+1}) (1 - \delta_{n, m}) \\
& + F\Delta t (1 - p(d)) P(n, m - 1, t) (1 - \delta_{n, m-1}) (1 - \delta_{n, m}) \\
& + O(\Delta t^2), \tag{5.8}
\end{aligned}$$

where $d = m - n$ is the distance between the particles and $p: \mathbb{R}^+ \rightarrow [0, 1]$ is a function describing the non-local repulsion and attraction interactions. In (5.8), the factors $(1 - \delta_{n, m}) = 0$ whenever $n = m$, to ensure that individuals do not hop to the same lattice site, and the factors $(1 - \delta_{n, m-1})$ and $(1 - \delta_{n, m+1})$ ensure that the particles hop away from each

other if they are adjacent. Re-writing (5.8), we find

$$\begin{aligned}
\frac{P(n, m, t + \Delta t) - P(n, m, t)}{\Delta t} &= -2F p(d) P(n, m, t) (1 - \delta_{n, m-1}) (1 - \delta_{n, m}) \\
&\quad - 2F (1 - p(d)) P(n, m, t) (1 - \delta_{n, m+1}) (1 - \delta_{n, m}) \\
&\quad + F (1 - p(d)) [P(n + 1, m, t) + P(n, m - 1, t)] (1 - \delta_{n, m-1}) (1 - \delta_{n, m}) \\
&\quad + F p(d) [P(n, m + 1, t) + P(n - 1, m, t)] (1 - \delta_{n, m+1}) (1 - \delta_{n, m}) \\
&\quad + O(\Delta t),
\end{aligned} \tag{5.9}$$

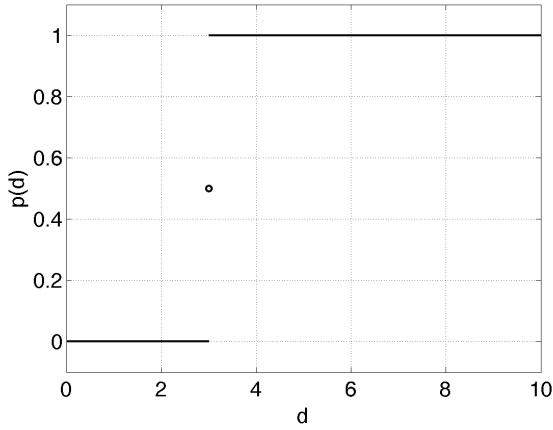
so that as $\Delta t \rightarrow 0$, we find the master equation for the joint occupation probability:

$$\begin{aligned}
\frac{dP(n, m, t)}{dt} &= -2F p(d) P(n, m, t) (1 - \delta_{n, m-1}) (1 - \delta_{n, m}) \\
&\quad - 2F (1 - p(d)) P(n, m, t) (1 - \delta_{n, m+1}) (1 - \delta_{n, m}) \\
&\quad + F (1 - p(d)) [P(n + 1, m, t) + P(n, m - 1, t)] (1 - \delta_{n, m-1}) (1 - \delta_{n, m}) \\
&\quad + F p(d) [P(n, m + 1, t) + P(n - 1, m, t)] (1 - \delta_{n, m+1}) (1 - \delta_{n, m}).
\end{aligned} \tag{5.10}$$

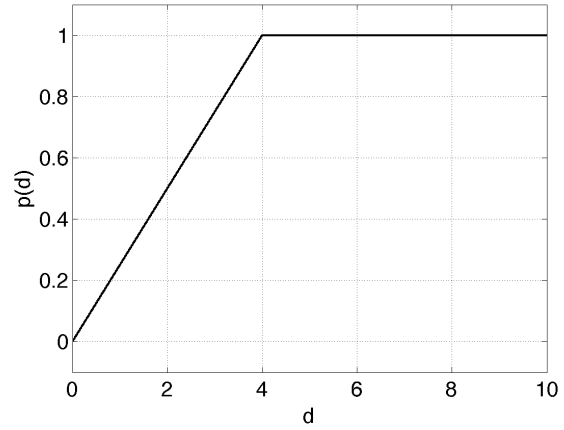
To fully describe the system, it is necessary to prescribe an initial condition, $P(n, m, 0)$, as well as to choose a suitable function $p(d)$. For the initial condition, we seek to release two particles at lattice sites n_0 and m_0 . That is, $P(n, m, 0) = \delta_{n-n_0} + \delta_{m-m_0}$, where δ_x is the Kronecker delta function ($\delta_x = 1$ if $x = 0$ and $\delta_x = 0$ if $x \neq 0$).

The choice of the interaction function $p(d)$ is motivated by the biological meaning of repulsion and attraction, as well as the results from Section 5.2. In the anti-symmetric exclusion process, Potts found that the asymptotic distance between particles depends on the value of p . When $0 < p < \frac{1}{2}$, the particles drift apart linearly in time; when $p = \frac{1}{2}$, the particles drift apart with the square root of time; and when $\frac{1}{2} < p < 1$, the distance between particles is asymptotic to a constant. This motivates the choice of $p(d)$. For small d , the particles should drift apart in order to avoid collision, hence $p(d)$ should be less than $\frac{1}{2}$ in the zone of repulsion. When the distance between the particles is such that they are in each other's zone of attraction, $p(d)$ should be greater than $\frac{1}{2}$ to ensure that the particles hop toward each other. For larger distances, we can allow $p(d) \rightarrow 1$ as $d \rightarrow \infty$, or choose more complicated $p(d)$. We expect the choice of $p(d)$ to strongly impact the behaviour of the model, and explore several choices. These functions are sketched in Figure 5.4.

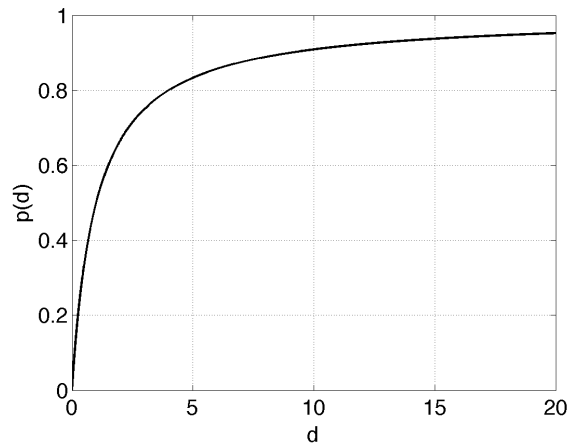
In Figure 5.4, three choices of $p(d)$ are presented. In Figure 5.4(a), the Heaviside function



(a) Heaviside



(b) Piecewise linear



(c) Saturating

Figure 5.4: Example interaction functions, $p(d)$. In (a), a Heaviside function is chosen: $p(d) = H(d - s_r)$, with $s_r = 3$ representing the width of the repulsion zone. In (b), a linear function is chosen: $p(d) = \frac{d}{s_r} \chi_{[0, s_r)}(d) + \chi_{[s_r, \infty)}(d)$, with $\chi_{(a, b)}(d)$ is an indicator function on (a, b) , with $s_r = 4$. In (c), a saturating function is chosen: $p(d) = \frac{d}{1+d}$.

is used to model the repulsion and attraction interaction forces. Specifically,

$$p(d) = H(d - s_r) = \begin{cases} 1, & d > s_r, \\ \frac{1}{2} & d = s_r, \\ 0, & d < s_r. \end{cases} \quad (5.11)$$

Effectively, the parameter $s_r = 3$ gives the length of the repulsion zone: if the particles are at a distance $d < s_r$, then $p(d) = 0$, ensuring that the particles do not hop toward each other. On the other hand, if $d \geq s_r$, then $p(d) = 1$, and the particles hop toward each other with probability 1. In Figure 5.4(b), a piecewise linear function is chosen:

$$p(d) = \begin{cases} \frac{d}{s_r}, & d \leq s_r, \\ 1, & d > s_r. \end{cases} \quad (5.12)$$

Again, s_r is a parameter modifying the length of the repulsion zone. In this case, $s_r = 4$ is chosen differently than $s_r = 3$ in the Heaviside function due to the model assumptions. If $s_r = 3$ and $p(d)$ is piecewise linear as in (5.12), and the particles are 1 lattice site apart, then at the first time step they will hop apart and sit separated by 3 lattice sites. If $s_r = 3$, then $p(3) = 1$, and the two particles will hop toward each other again, only to be separated by one lattice site. This cycle will dominate the movement of the particles for all time t . A final choice of $p(d)$ is presented in Figure 5.4(c). In this case,

$$p(d) = \frac{d}{1 + d} \quad (5.13)$$

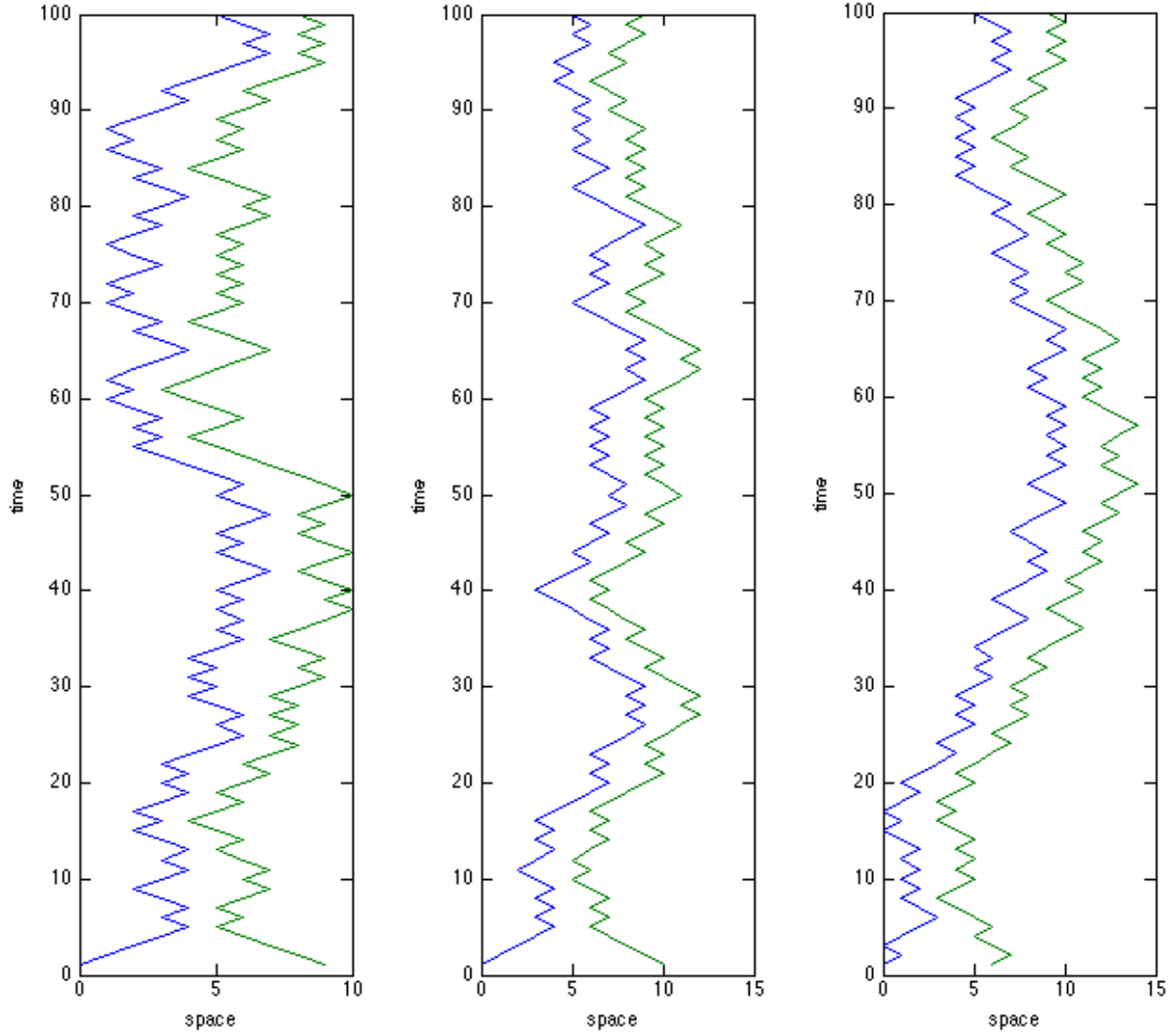
is a saturating function, with the probability of hopping toward each other increasing as the inter-particle distance increases.

In place of an analysis of (5.10) explicitly describing the time evolution of $P(n, m, t)$, we use stochastic simulations to understand the model behaviour. Using MATLAB, we simulate the 2-particle model by ensuring particles exclude each other from space, by calculating $p(d)$ at each time step, and deciding to hop to the right or the left by comparing $p(d)$ to a uniform random variable. Sample particle trajectories are presented in Figure 5.5; however, to understand the joint probability distribution, $P(n, m, t)$, we measure statistics over many runs of the stochastic simulation, as the sample trajectories do not appear qualitatively different. The quantities of interest are the average distance between the particles, the variance of one of the particles position, and the mean square displacement (MSD) of one of

the particles. These quantities are of interest in this case, as they allow us to characterize $P(n, m, t)$ given a certain choice of social interaction, that is, given a choice of $p(d)$.

Let $x_1(t)$ and $x_2(t)$ represent the position of the left-hand and right-hand particles respectively. Define $d(t) = x_2(t) - x_1(t)$ to be the distance between the particles at time t . The quantities measured over many runs of the stochastic simulations are $d(t)$, the mean separation distance, and $\Delta x^2(t)$, the MSD of the left-hand particle. Figure 5.6, Figure 5.7, and Figure 5.8 present average values from 10000 runs of the stochastic simulations, with $p(d)$ the Heaviside function, (5.11), piecewise linear function, (5.12), and saturating function, (5.13), respectively. The initial conditions for these simulations are that the left-hand particle is at $n = 0$ and the right-hand particle's position is randomly chosen from the set $A = \{1, 2, \dots, 10\}$. This choice is made randomly to ensure that the initial condition does not affect the results. The size of the set A was chosen $|A| = 10$ to limit the size of the transient before the particles approached their asymptotic mean separation distance. In each of Figure 5.6, Figure 5.7, and Figure 5.8, the mean separation distance as a function of time, $\langle d(t) \rangle$ is shown in (a); and sample displacements for the left-hand particle trajectories are shown as blue curves and three lines representing the diffusion coefficients in part (b). These diffusion coefficients are calculated using least squares regression. The slope of the green line is D_m , the short-term (or microscopic) diffusion coefficient, calculated by using only the first 4 displacements. The slope of the red line is D_M , the long-term (or macroscopic) diffusion coefficient, calculated by using one-third of the displacements. Lastly, the slope of the black line is D_f , a diffusion coefficient calculated using all of the displacements (f subscript refers to full time). For a discussion on estimating diffusion coefficients from random walk data, see [36] or Rajani's thesis on single particle tracking [35].

The behaviour of the 2-particle system depends on the choice of $p(d)$. The differing behaviour is evident in the statistics shown in Figure 5.6, 5.7, and 5.8. These statistics are summarized in Table 5.1. The time-averaged mean separation distance was obtained by averaging the mean separation distance after excluding the first 10 time steps. The average separation distance for the Heaviside function is largest, around 3 lattice sites. This is consistent with the choice of the Heaviside $p(d)$: if the particles are separated by exactly 3 lattice sites, they hop symmetrically; if the particles are separated by less than 3 lattice sites, the particles hop apart with probability 1; and if the particles are separated by more than 3 lattice sites, the particles hop toward each other with probability 1. The average separation distance for the piecewise linear function and the saturating function is less than the Heaviside function; however, the piecewise linear function has the lowest average sepa-

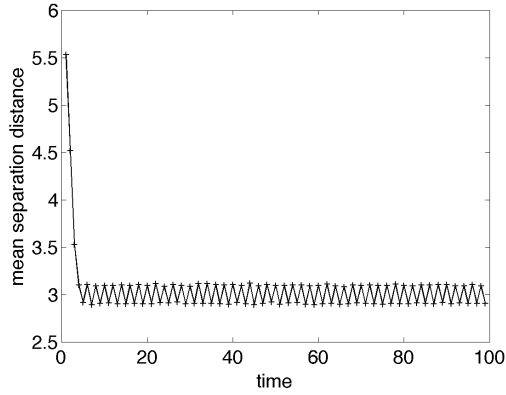


(a) Heaviside

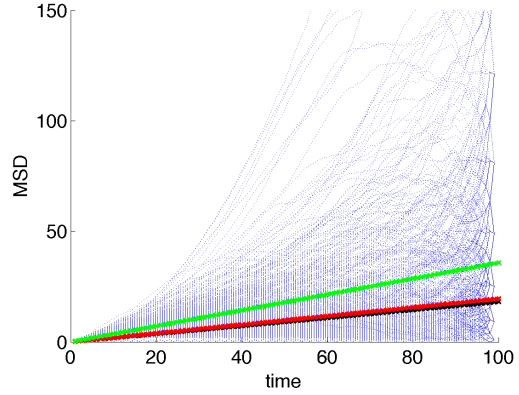
(b) Piecewise linear

(c) Saturating

Figure 5.5: Sample trajectories of the 2-particle model with social interactions. In (a), $p(d)$ is chosen to be the Heaviside function, (5.11). In (b), $p(d)$ is chosen to be the piecewise linear function, (5.12). In (c), $p(d)$ is chosen to be the saturating function, (5.13).

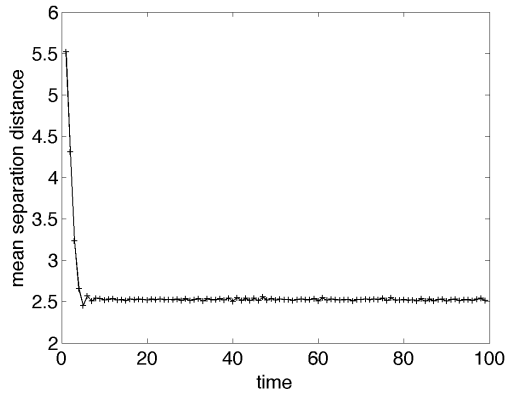


(a) Separation distance $\langle d(t) \rangle$

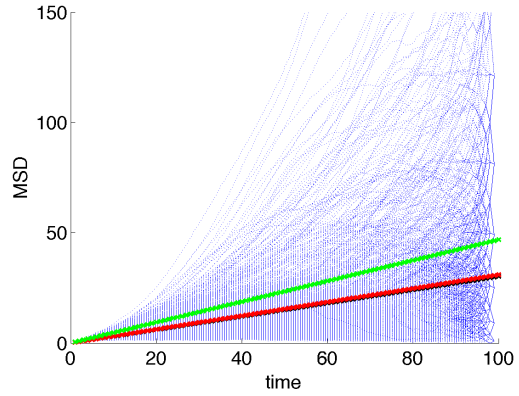


(b) MSD $\Delta x^2(t)$

Figure 5.6: Statistics for 10000 samples with the Heaviside $p(d)$, (5.11). In (a), mean separation distance, $d(t)$, is shown as a function of time. In (b), the MSD of the left-hand particle is shown for several trajectories (blue curves). The slope of the green line is D_m , the slope of the red line is D_M , and the slope of the black line is D_f .



(a) Separation distance $d(t)$



(b) MSD $\Delta x^2(t)$

Figure 5.7: Statistics for 10000 samples with the piecewise linear $p(d)$, (5.12). In (a), mean separation distance, $d(t)$, is shown as a function of time. In (b), the MSD of the left-hand particle is shown for several trajectories (blue curves). The slope of the green line is D_m , the slope of the red line is D_M , and the slope of the black line is D_f .

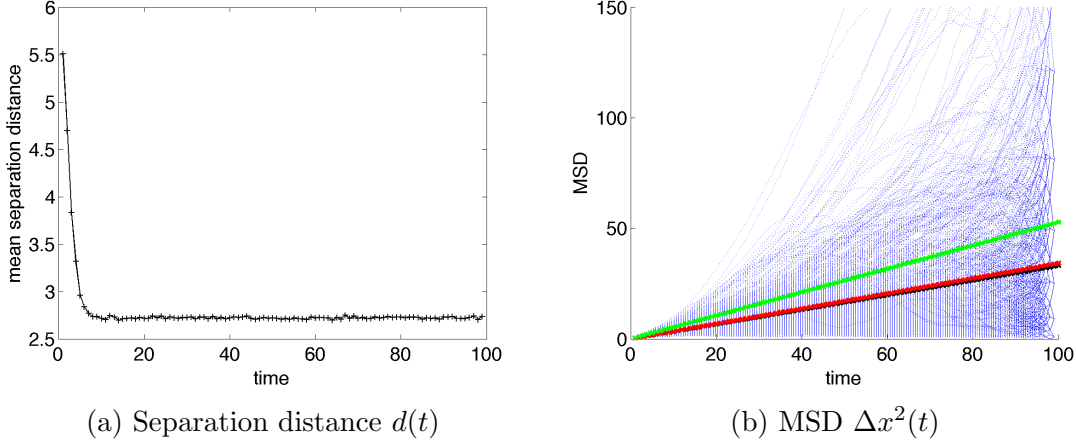


Figure 5.8: Statistics for 10000 samples with the saturating $p(d)$, (5.13). In (a), mean separation distance, $d(t)$, is shown as a function of time. In (b), the MSD of the left-hand particle is shown for several trajectories (blue curves). The slope of the green line is D_m , the slope of the red line is D_M , and the slope of the black line is D_f .

$p(d)$	average $d(t)$	D_m	D_M	D_f
(a) Heaviside	3.0010	0.3595	0.1991	0.1840
(b) Piecewise linear	2.5263	0.4679	0.3084	0.2982
(c) Saturating	2.7177	0.5325	0.3465	0.3296

Table 5.1: Mean separation and diffusion coefficients for 10000 samples with different $p(d)$. The time-averaged mean separation distance was obtained by averaging $d(t)$ over time after excluding the first 10 steps. Diffusion coefficients are calculated by least squares regression.

ration distance. The choice of s_r likely plays a role in the model behaviour. The calculated diffusion coefficients agree with expected model behaviour. The Heaviside $p(d)$ interaction function is the most restrictive as $p(d) = 1$ or $p(d) = 0$ for almost all d . This prescribes the movement and interaction of the individuals very well, and hence does not let them diffuse greatly. On the other hand, the saturating interaction function $p(d) = 0$ only when $d = 0$ and $p(d) < 1$ for all d . This allows for stochasticity in the individuals' response to each other, i.e., even if they are strongly attracted to each other, they may still jump apart. This leads to a higher diffusion coefficient, D_M (or D_f).

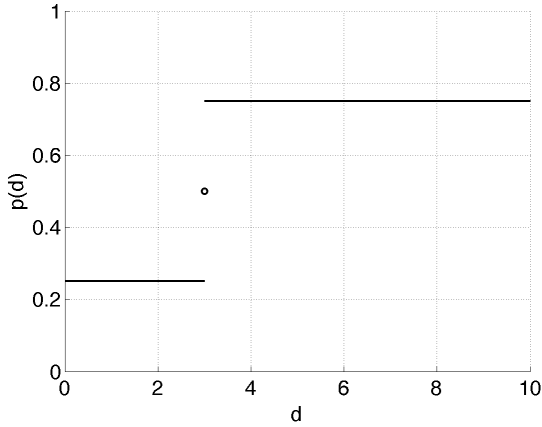
Incorporating attractive and repulsive interactions into the anti-symmetric exclusion process alters the model behaviour. Without these interactions, the anti-symmetric exclusion behaviour exhibited two behaviours. The separation distance between the particle either saturated (when $\frac{1}{2} < p < 1$) or the distance between the particles increased (linearly in

time when $0 < p < \frac{1}{2}$ or with the square root of time when $p = \frac{1}{2}$). Attraction-repulsion interactions lead to a constant mean separation distance, i.e., a grouping behaviour with a preferred inter-individual distance.

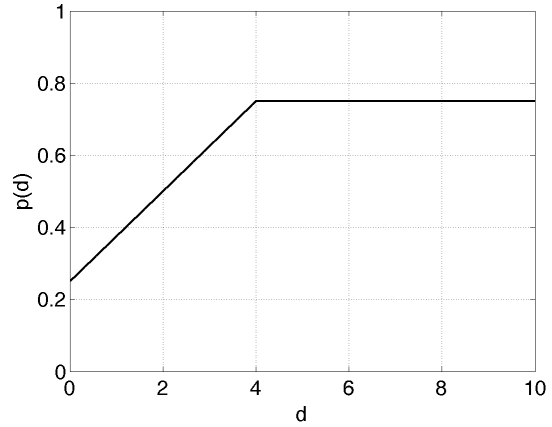
The choices of $p(d)$ studied above model an infinite zone of attraction. For large distances between particles, $p(d) = 1$ in the case of the Heaviside and piecewise linear functions, and $p(d) \approx 1$ for the saturating function. The Heaviside and piecewise linear $p(d)$ prescribe that the particles may not move apart from each other if they are in each other's zone of attraction, and if d is sufficiently large, it is very unlikely that the particles will move apart when $p(d)$ is chosen to be saturating. Although this is not biologically realistic, as individuals do not have infinite interaction zones. Moreover, it is unlikely that individuals will always respond to neighbours. Instead, some stochasticity is expected. To adjust for this, we choose $p(d)$ with restricted range. This incorporates stochasticity as $p(d)$ is never 0 or 1. We modify the choices of the Heaviside, piecewise linear, and saturating function to have range in the interval $[0.25, 0.75]$, and repeat our investigation. It is expected that on average, grouping will still occur, but the separation distance and diffusion coefficients will be larger. These modified interaction functions are plotted in Figure 5.9.

In Figures 5.10, 5.11, and 5.12, the behaviour of the 2-particle model with $p(d)$ with range in $[0.25, 0.75]$ is shown. The two quantities most revealing of behaviour are the mean separation distance and the MSD. From these quantities, the asymptotic spacing between individuals and the diffusivity of the individuals can be measured. In part (a) of Figures 5.10, 5.11, and 5.12, the mean separation distance is shown as a function of time. In part (b), the MSD of the left-hand particle is shown. Blue curves show sample displacements, and the slopes of the lines give diffusion coefficients. The slope of the green line is the short-time diffusion coefficient, D_m ; the slope of the red line is the long-time diffusion coefficient, D_M , measured using the first one-third time steps; and the slope of the black-line is a diffusion coefficient calculated by considering all the time steps, D_f .

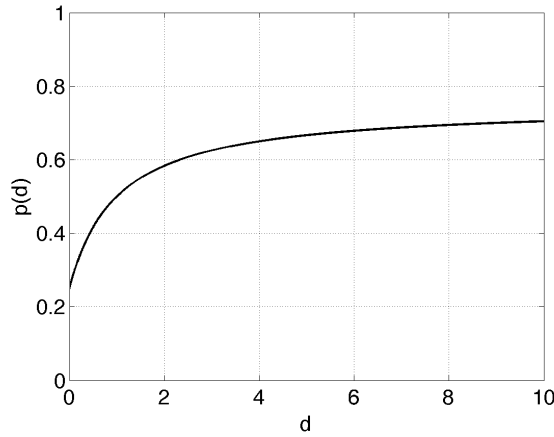
In Table 5.2, we present statistics from 10000 samples of the random walk model with different $p(d)$ with restricted range in $[0.25, 0.75]$. In this case, the piecewise linear function exhibits the smallest mean separation distance. The Heaviside function and saturating function exhibit similar mean separation distances, with the saturating function slightly larger. Diffusion coefficients follow a different trend: the Heaviside function resulting in the least diffuse system over long time periods, followed by the piecewise linear system and the saturating function. Interestingly, over short-time, we find that the piecewise linear function is the least diffuse system, followed by the Heaviside and the saturating system.



(a) Heaviside



(b) Piecewise linear



(c) Saturating

Figure 5.9: Example interaction functions, $p(d)$, with range $[0.25, 0.75]$. In (a), a modified Heaviside function is chosen: $p(d) = \frac{H(d-s_r)}{2} + \frac{1}{4}$, with $s_r = 3$ representing the width of the repulsion zone. In (b), a linear function is chosen: $p(d) = \frac{d}{2s_r}\chi_{[0,s_r)}(d) + \frac{1}{4} + \frac{3\chi_{[s_r,\infty)}(d)}{4}$, with $\chi_{(a,b)}(d)$ is an indicator function on (a, b) , with $s_r = 4$. In (c), a saturating function is chosen: $p(d) = \frac{d}{2(1+d)} + \frac{1}{4}$.

$p(d)$	average $d(t)$	D_m	D_M	D_f
(a) Heaviside	3.3108	0.6570	0.4305	0.4029
(b) Piecewise linear	3.0199	0.6484	0.4333	0.4128
(c) Saturating	3.4009	0.7153	0.4773	0.4461

Table 5.2: Mean separation and diffusion coefficients for 10000 samples with different $p(d)$ with range $[0.25, 0.75]$. The time-averaged mean separation distance was obtained by averaging $d(t)$ over time after excluding the first 10 steps. Diffusion coefficients calculated by least squares regression.

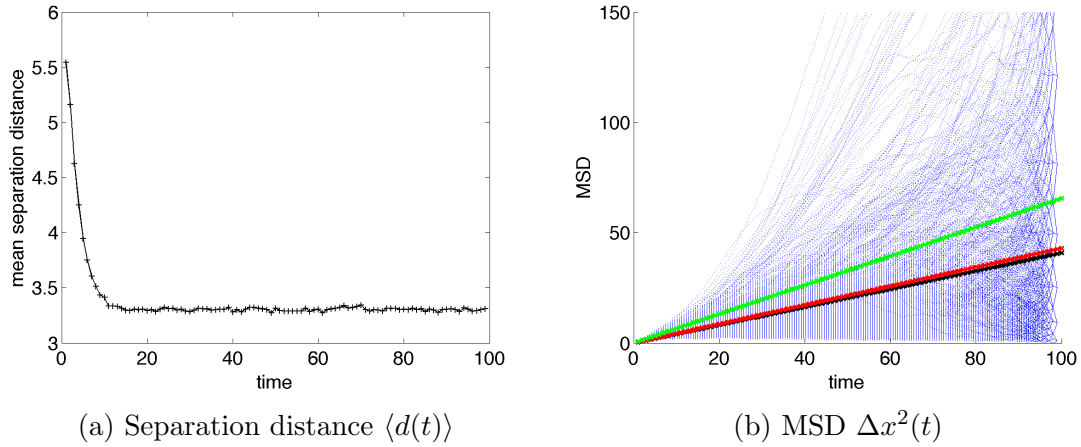


Figure 5.10: Statistics for 10000 samples with the modified Heaviside $p(d)$ with range $[0.25, 0.75]$. In (a), mean separation distance, $d(t)$, is shown as a function of time. In (b), the MSD of the left-hand particle is shown for several trajectories (blue curves). The slope of the green line is D_m , the slope of the red line is D_M , and the slope of the black line is D_f .

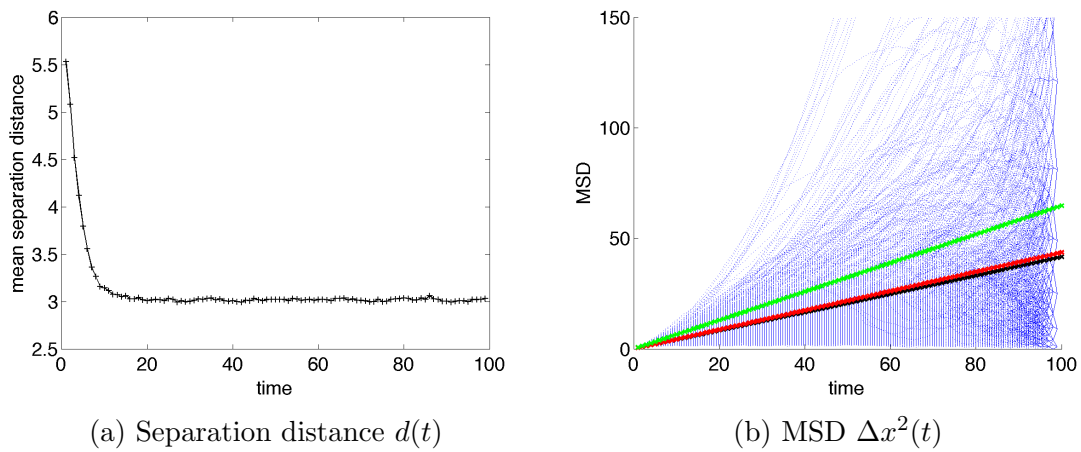


Figure 5.11: Statistics for 10000 samples with the modified piecewise linear $p(d)$ with range $[0.25, 0.75]$. In (a), mean separation distance, $d(t)$, is shown as a function of time. In (b), the MSD of the left-hand particle is shown for several trajectories (blue curves). The slope of the green line is D_m , the slope of the red line is D_M , and the slope of the black line is D_f .

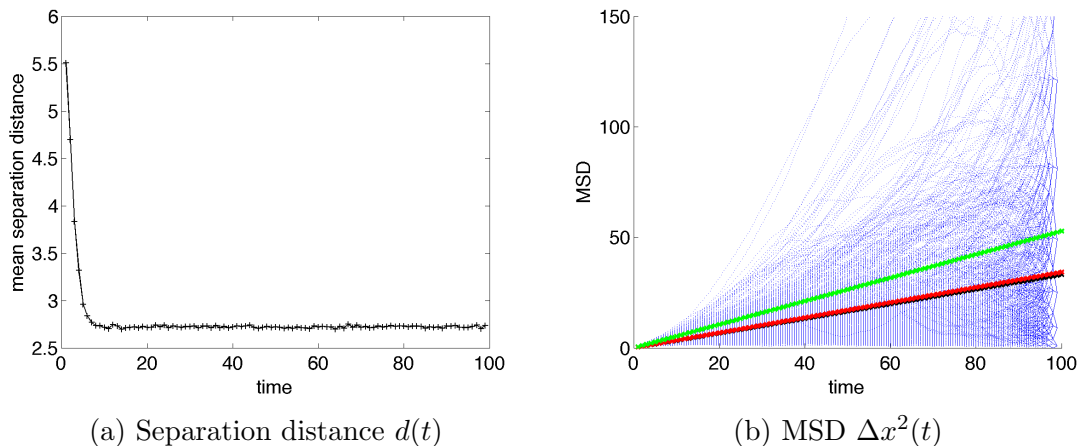


Figure 5.12: Statistics for 10000 samples with the modified saturating $p(d)$ with range $[0.25, 0.75]$. In (a), mean separation distance, $d(t)$, is shown as a function of time. In (b), the MSD of the left-hand particle is shown for several trajectories (blue curves). The slope of the green line is D_m , the slope of the red line is D_M , and the slope of the black line is D_f .

In this section, distance-dependent social interactions were added to the anti-symmetric exclusion process. The choice of the interaction function $p(d)$ affects the behaviour of the model. Even so, the choices of functions investigated here reveal that there is a relationship between the choice of $p(d)$, the mean separation distance, $d(t)$, and the diffusion coefficient of the left-hand particle, D_M . It is difficult to quantify the relationship between $p(d)$ and these quantities; however, as shown in Figure 5.13, there may be a linear relationship between the diffusion coefficient and the separation distance between individuals. Investigating distance-dependent social interactions in this context raises several questions. For instance, is it possible to predict the characteristics of the joint occupation probability from the choice interaction function? Another question is whether mean separation distance and diffusion coefficients can be measured from biological aggregations and the social interactions subsequently inferred. Most importantly, we find the 2-particle framework useful for investigating the behaviour of individuals in response to social interactions.

5.4 Incorporating Directionality

In this section, we continue investigating the anti-symmetric exclusion process. In Section 5.3, we added distance-dependent social interactions to the anti-symmetric exclusion process, and we investigated the behaviour of the 2-particle system. The choice of the interaction

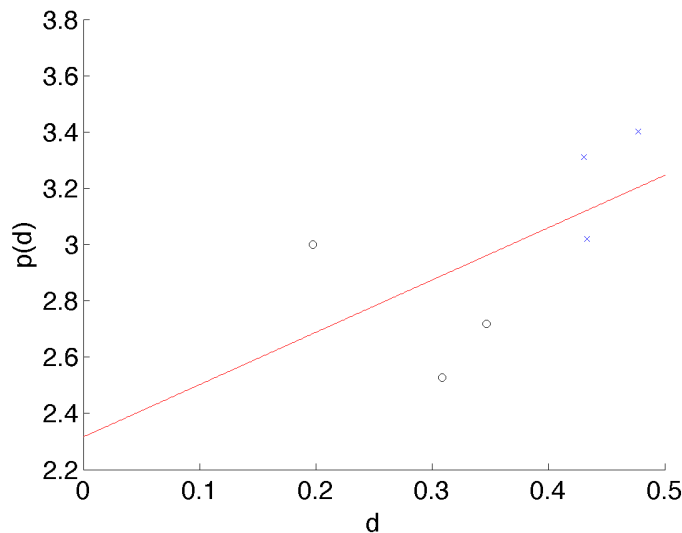


Figure 5.13: Relationship between mean separation distance and D_M . Black circles are pairs $(D_M, \langle d(t) \rangle)$ for $p(d)$ with range in $[0, 1]$. Blue markers are pairs $(D_M, \langle d(t) \rangle)$ for $p(d)$ with range in $[0.25, 0.75]$. The red line is best fit to these data points.

function, $p(d)$, greatly impacted the behaviour of the model, especially the inter-individual distance, and the diffusivity of the individuals. The goal of this section is to modify the interaction function to include alignment interactions, as studied throughout this thesis.

To incorporate directionality, we add an alignment interaction force to the anti-symmetric exclusion process with social interactions. The biological motivation for incorporating an alignment term comes from the relatively constant inter-individual distance observed in many animal groupings. The alignment interaction models the tendency of individuals to travel in the same direction as neighbours, provided the inter-individual distance is not too small, which would lead to repulsion, or not too big, which would lead to attraction.

The foundation for the model consists of two particles on an infinite one-dimensional lattice with spacing a . Let n denote the position of the left-hand particle and m denote the position of the right-hand particle. The model assumes that both particles cannot occupy the same site, and hop toward each other with probability $p(d)$, where $d = m - n$ is the distance between the particles. The choice of $p(d)$ will have an impact on the model behaviour, and this will be investigated below. Recall that the individuals in the 2-particle anti-symmetric exclusion process hop toward each other with probability p and away from each other with probability $1 - p$. Directionality is not a characteristic of the particles; they simply hop to the right or to the left, but do not “face” in a certain direction. To incorporate alignment,

each particle requires a direction. Let v_n and v_m be the direction (v representing velocity) of the left-hand and right-hand individual, respectively. In a one-dimensional setting, the two directions are right and left, whence $v_n, v_m \in \{-1, 1\}$. To flush out the social interactions, we introduce constants $s_r \in \mathbb{R}$ and $s_{al} \in \mathbb{R}$ which represent the width of the repulsion and alignment zones. Repulsion acts on shorter distances than alignment, and for biologically meaningful interaction zones we require $s_r < s_{al}$. We assume that the two particles interact according to the anti-symmetric exclusion process when in the zone of repulsion or attraction, i.e., $d \in [0, s_r) \cup [s_{al}, \infty)$. However, when the particles are in the zone of alignment, i.e., $d \in [s_r, s_{al})$, we forgo the anti-symmetric hopping if both the left-hand particle and right-hand particle are traveling in the same direction, that is, if $v_n v_m = 1$. In this case, we allow the individuals to continue moving in their direction of travel. If the two individuals are in the zone of alignment but are not traveling in the same direction, we allow them to interact according to the anti-symmetric exclusion process.

Again, the distribution of interest is $P(n, m, t)$, the joint occupation probability at time t . Writing a master equation for this process is not as straightforward as the master equation for the anti-symmetric exclusion process with social interactions. Previously, in (5.8), we assumed that an individual's hop is independent of any other hop and only depends on the distance between individuals. Here, not only do we assume that each hop is independent of the previous one, but we also assume that each hop depends only on the distance between particles and the direction of each particle. This leads to a much more complicated master equation:

$$\frac{dP(n, m, t)}{dt} = \begin{cases} g(n, m, t), & d \in [s_r, s_{al}) \text{ and } v_n v_m = 1, \\ f(n, m, t), & \text{otherwise,} \end{cases} \quad (5.14)$$

where $f(n, m, t)$ is the right-hand side of the master equation for the anti-symmetric random walk, (5.10), and $g(n, m, t)$ describes the hopping process when the two particles are in the alignment zone. In this case,

$$\begin{aligned} g(n, m, t) = & -2FP(n, m, t) \\ & + F(P(n+1, m, t) + P(n, m+1, t)) \delta_{v_n, -1} \\ & + F(P(n-1, m, t) + P(n, m-1, t)) \delta_{v_n, 1}, \end{aligned} \quad (5.15)$$

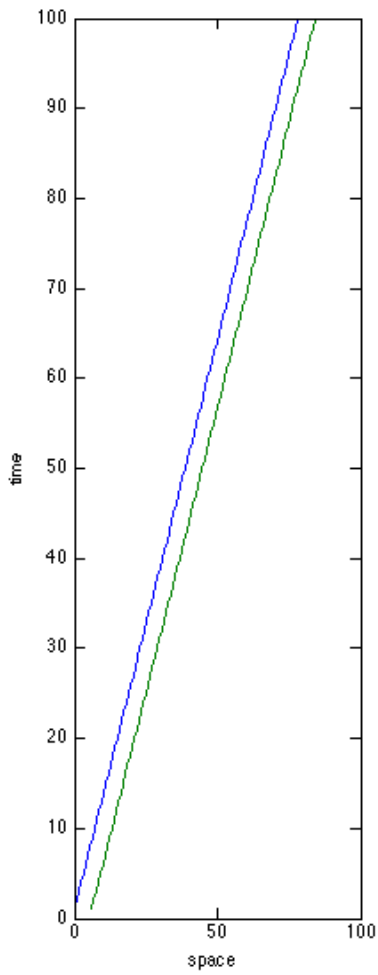
where F is the hopping rate. If the two particles at n and m are in the zone of alignment and are traveling in the same direction, then they will both hop in the direction of travel,

leaving site n and m , hence the $-2FP(n, m, t)$ in (5.15). The remaining terms account for the individuals hopping to sites n and m from $n + 1$ and $m + 1$ if the particles are left moving ($\delta_{v_n, -1} = 1$), or to sites n and m from $n - 1$ and $m - 1$ if the particles are right moving ($\delta_{v_n, 1} = 1$). Writing the master equation reveals the two distinct behaviours of this model: anti-symmetric repulsion and attraction versus directed movement when the individuals are aligned.

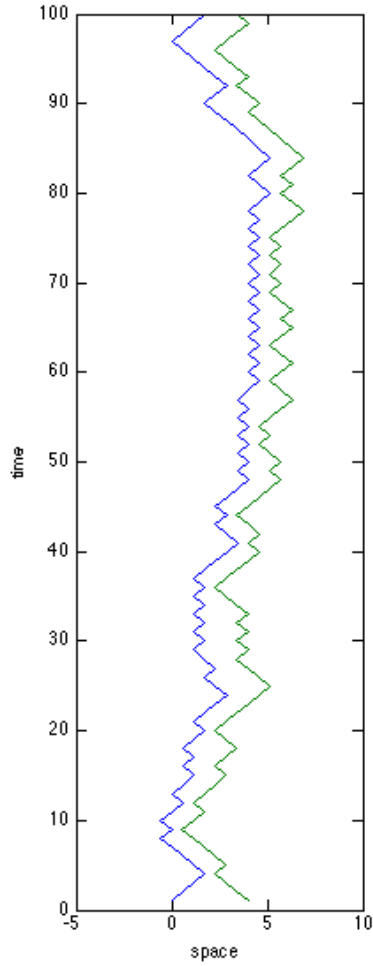
In place of an analysis of the master equation, (5.14), we use stochastic simulations to understand the model behaviour. For our investigation, we will consider the three social interaction functions $p(d)$ from before, a Heaviside function, (5.11), a piecewise linear function, (5.12), and a saturating function, (5.13). The initial conditions for the simulations are that the left-hand particle is at $n = 0$ and the right-hand particle's initial position is randomly chosen from the set $A = \{1, 2, \dots, 10\}$. The initial directions, $v_n(0)$ and $v_m(0)$ are chosen randomly from $\{-1, 1\}$. Not only will the choice of the interaction function, $p(d)$, influence the model behaviour, but also the size of the repulsion and alignment zones will influence behaviour. The master equation for this process, (5.14), contains two distinct behaviours depending on the model's state and the sizes of the interaction zones. Thus, we focus on investigating the mean separation distance and diffusion coefficients for different $p(d)$ and different interaction zone sizes (s_r and s_{al}).

In Figure 5.14, sample particle trajectories are plotted for $s_r = 3$ and $s_{al} = 6$. In (a), $p(d)$ is a Heaviside function, (5.11); in (b), $p(d)$ is piecewise linear, (5.12); and in (c), $p(d)$ is the saturating function, (5.13). In (a) and (c), the two particle ensemble travels to the right, as the particles are in each other's zone of alignment. In (a), the particles are in each other's zone of alignment are both initially traveling to the right. In (c), the particles are initially attracted to each other; however, as the distance between them decreases so that they are in the alignment zone, the right-hand particle changes direction. At this point, the two particles are traveling in the same direction and are in the zone of alignment, hence they travel across the lattice as a group. This behaviour is not observed in the anti-symmetric random walk with social interactions, and may indicate that alignment is required to have traveling groups.

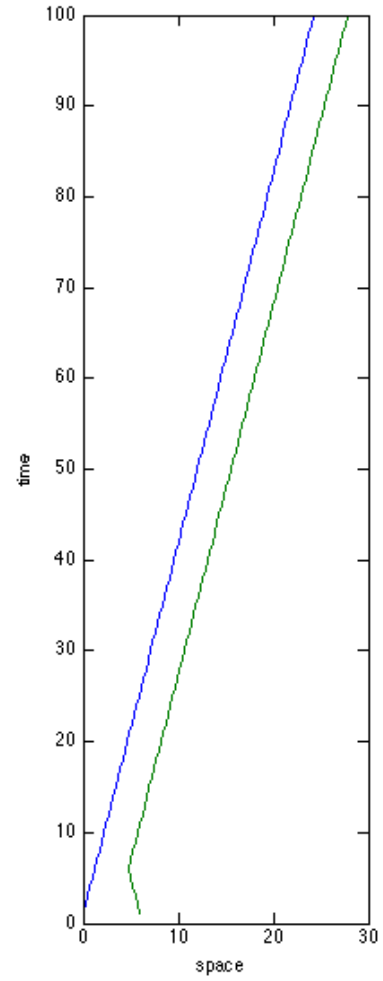
To compare the model behaviour to the anti-symmetric exclusion processes studied in this Chapter, we present statistics from 10000 stochastic simulations. The quantities of interest are again the mean separation distance, $d(t)$, and the mean square displacement (MSD) of the left-hand particle. From the MSD data, we can calculate an average MSD as well as diffusion coefficients to understand how the particles interact and move. In Figures



(a) Heaviside



(b) Piecewise linear



(c) Saturating

Figure 5.14: Example trajectories of the 2-particle model with alignment. In (a), $p(d)$ is chosen to be the Heaviside function, (5.11). In (b), $p(d)$ is chosen to be the piecewise linear function, (5.12). In (c), $p(d)$ is chosen to be the saturating function, (5.13).

$p(d)$	average $d(t)$	D_m	D_M	D_f
(a) Heaviside	3.1812	0.1677	0.8303	2.3937
(b) Piecewise linear	1.9610	0.2692	0.9305	2.5414
(c) Saturating	3.1493	0.7080	4.6118	12.63214

Table 5.3: Mean separation and diffusion coefficients for 10000 samples with different $p(d)$ and alignment. The time-averaged mean separation distance was obtained by averaging $d(t)$ over time after excluding the first 10 steps. Diffusion coefficients calculated by least squares regression.

5.15, 5.16 and 5.17, part (a) shows mean separation distance as a function of time, $\langle d(t) \rangle$, with the average ignoring the first 10 transient time-steps. Part (b) shows the MSD for several simulations as blue curves, with the average MSD, $\langle \Delta x^2(t) \rangle$, as a thick blue line. The slopes of the three lines represent diffusion coefficients. The slope of the green line is D_m , the short-term (or microscopic) diffusion coefficient, calculated by using only the first 4 displacements. The slope of the red line is D_M , the long-term (or macroscopic) diffusion coefficient, calculated by using one-third of the displacements. Lastly, the slope of the black line is D_f , a diffusion coefficient calculated using all of the displacements (f subscript refers to full time).

In Figures 5.15, 5.16, and 5.17, we fixed the length of the interaction zones at $s_r = 3$ and $s_{al} = 6$ and varied $p(d)$. The mean separation distance, $\langle d(t) \rangle$, approaches a constant value in the case of the Heaviside and piecewise linear interaction function; however, appears to increase over time when the interaction function is saturating. This differs from the anti-symmetric random walk with social interactions (without alignment), as the mean separation distance approached a constant with all three interaction functions. More interestingly, the MSD for many trajectories increases very quickly with time, as seen in part (b) of Figures 5.15, 5.16, and 5.17. This rapid increase in MSD is seen in the trend exhibited by the mean MSD, $\langle \Delta x^2(t) \rangle$, thick blue curves. This convex average MSD indicates anomalous diffusion, and in this case, results from the alignment mechanism. Summary statistics are presented in Table 5.3. The piecewise linear choice of $p(d)$ presents the smallest mean separation distance, with the separation distance for the other two choices of functions similar. Comparing these mean separation values with those in Table 5.1 and Table 5.2, we see that the values are of a similar magnitude, indicating that group formation is similar among these models. The diffusion coefficients, on the other hand, are much larger when alignment is included. These large diffusion coefficients, along with convex mean MSD, is indicative of a traveling group.

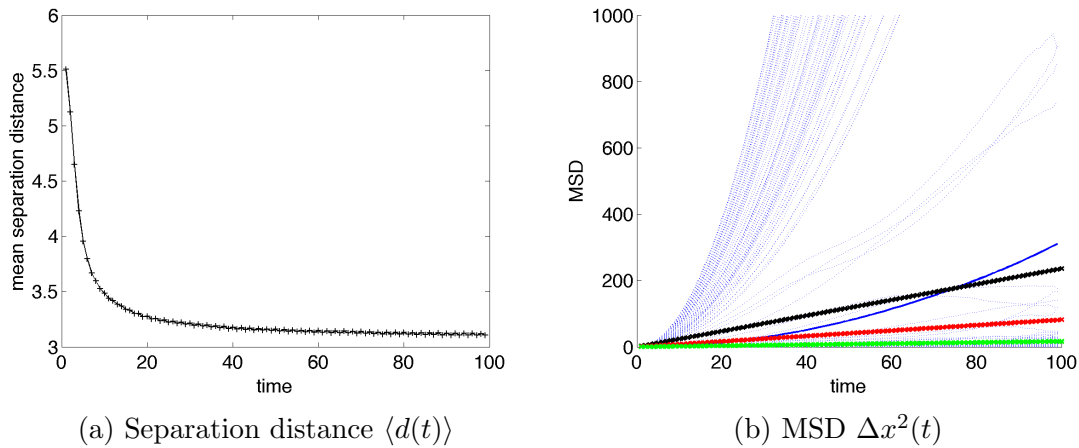


Figure 5.15: Statistics for 10000 samples with the Heaviside $p(d)$ and alignment interactions. In (a), mean separation distance, $d(t)$, is shown as a function of time. In (b), the MSD of the left-hand particle is shown for several trajectories (blue curves), and the average MSD is shown as a thick blue curve. The slope of the green line is D_m , the slope of the red line is D_M , and the slope of the black line is D_f . Here, $s_r = 3$ and $s_{al} = 6$.

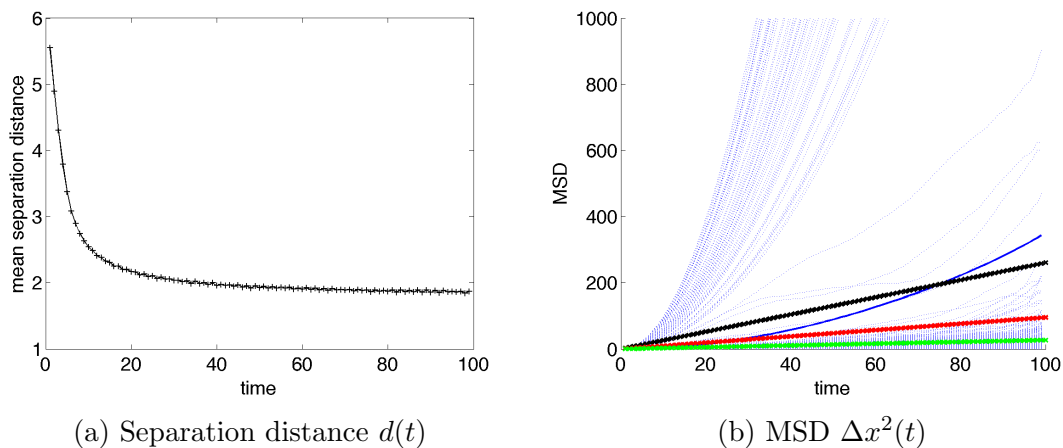


Figure 5.16: Statistics for 10000 samples with the piecewise linear $p(d)$ and alignment interactions. In (a), mean separation distance, $d(t)$, is shown as a function of time. In (b), the MSD of the left-hand particle is shown for several trajectories (blue curves), and the average MSD is shown as a thick blue curve. The slope of the green line is D_m , the slope of the red line is D_M , and the slope of the black line is D_f . Here, $s_r = 3$ and $s_{al} = 6$.

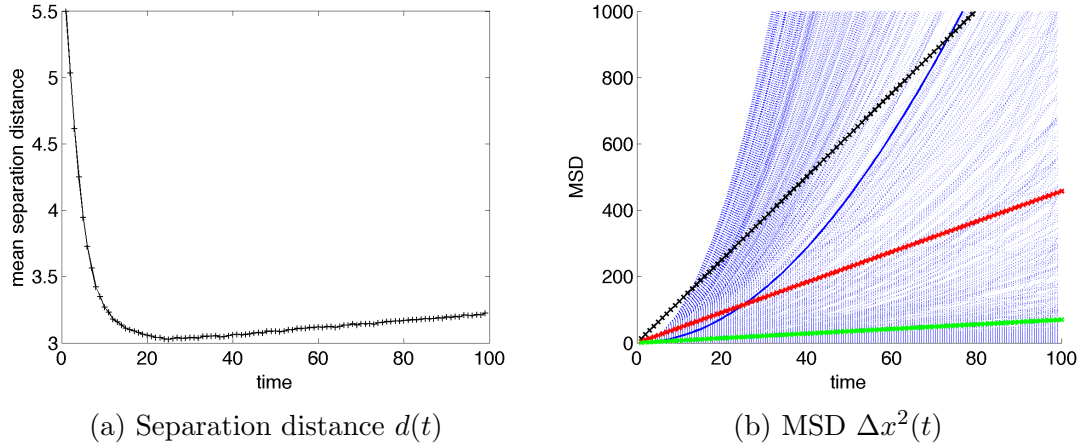


Figure 5.17: Statistics for 10000 samples with the saturating $p(d)$ and alignment interactions. In (a), mean separation distance, $d(t)$, is shown as a function of time. In this case, the mean separation distance appears to be increasing (for $t > 30$). In (b), the MSD of the left-hand particle is shown for several trajectories (blue curves), and the average MSD is shown as a thick blue curve. The slope of the green line is D_m , the slope of the red line is D_M , and the slope of the black line is D_f . Here, $s_r = 3$ and $s_{al} = 6$.

To complete the investigation of the anti-symmetric exclusion process with all three social interactions: repulsion, alignment, and attraction, we will investigate the behaviour of the model with respect to the sizes of the interaction zones. We expect that a larger zone of repulsion will result in a larger mean separation distance. Traveling groups are expected to result from a large zone of alignment, as indicated by a rapidly increasing mean MSD and large diffusion coefficients. For a biologically realistic model, we require $s_r < s_{al}$, and hence we allow s_{al} to take integer values between 4 and 15, and in each of these cases allow s_r to vary between 3 and s_{al} . For this investigation, we consider the piecewise linear interaction function over the Heaviside and saturating functions. We do this because the Heaviside function is slightly slower to evaluate using MATLAB, and because the saturating function reveals a non-constant separation distance and a relatively quickly increasing $\langle \Delta x^2(t) \rangle$. The results of this investigation are shown in Figure 5.18. In Figure 5.18(a), a box plot shows the value of the mean separation distance, $\langle d(t) \rangle$, averaged over 10000 simulations of the alignment model for each pair of interaction zone lengths, (s_r, s_{al}) . In Figure 5.18(b), a box plot shows the value of the diffusion coefficient, D_f , averaged over 10000 simulations of the alignment model for each pair of interaction zone lengths, (s_r, s_{al}) . The full diffusion coefficient, D_f , which is measured using all time steps of the MSD data, qualitatively appears to better estimate the average MSD trend in Figures 5.15, 5.16, and 5.17, and is consequently

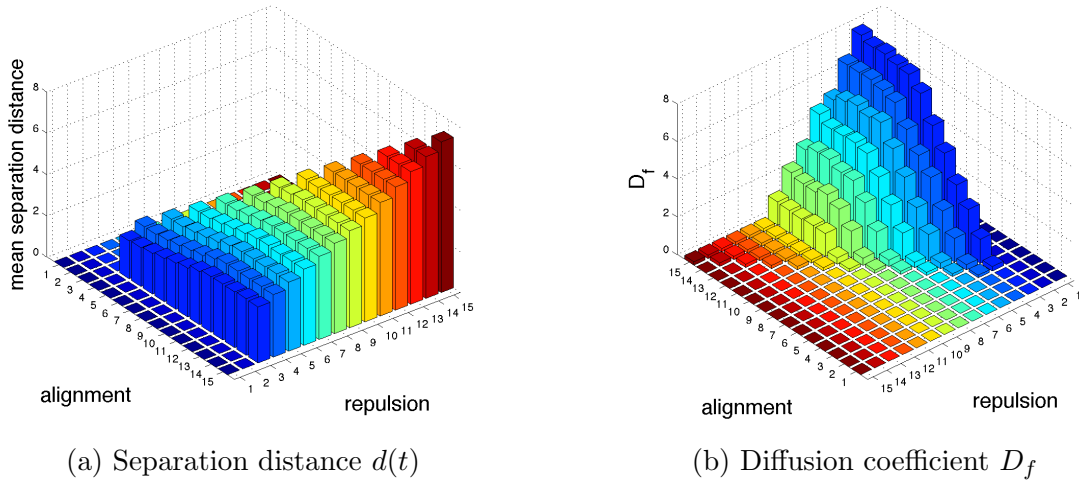


Figure 5.18: Mean separation distance and diffusion coefficient for different interaction zone sizes. In (a), the mean separation distance is measured over 10000 simulations for each pair (s_r, s_{al}) of interaction zone sizes. As the size of the repulsion and alignment zones increase, the mean separation distance increases. In (b), the full diffusion coefficient, D_f , is measured over 10000 simulations for each pair (s_r, s_{al}) of interaction zone sizes. Note the change in axis direction in part (b) to better show the data. For fixed s_r , the diffusion coefficient increases with s_{al} .

shown in Figure 5.18. As the size of the repulsion and alignment zones increases, the mean separation distance, $\langle d(t) \rangle$, increases. This result is biologically consistent: larger inter-individual distances result from repulsive interactions taking place over larger distances. Similarly, a large zone of alignment will allow for a large inter-individual distance to occur while still maintaining group cohesiveness. In Figure 5(b), large alignment zones result in large diffusion coefficients, D_f , especially for small zones of repulsion.

5.5 2-particle Eftimie Model

In this section, we investigate a 2-particle formulation of the IBM with direction-dependent communication mechanisms. We seek to understand how two individuals in a population respond to communication mechanisms, first by proposing a master equation for the 2-particle process with direction-dependent communication mechanisms, and second, by studying mean separation distance and mean square displacement over stochastic simulations.

To begin, we study the interaction of two individuals on an infinite one-dimensional lattice with spacing a . In this section, we relax the condition that the individual cannot

cross, and simply label the individuals 1 and 2. This condition is relaxed as the individuals in the PDE and IBM with direction-dependent communication mechanisms do not exclude each other from space, but instead are allowed to cross. We denote the positions of the two individuals as n and m respectively, and allow the particles to interact according to the direction-dependent communication mechanisms as in the IBM with direction-dependent communication mechanisms (Chapter 3). Recall that the direction-dependent communication mechanisms rely on both the position and direction of the signal emitter and receiver, whence we explicitly track the direction of each individual. Let v_n and v_m be the directions of the two individuals, with $v_n, v_m \in \{-1, 1\}$ indicating either to the left (-1) or to the right (1). The distribution of interest is $P(n, m, v_n, v_m, t)$, the joint occupation probability that individual 1 is at n moving with direction v_n and that individual 2 is at m with direction v_m at time t . To describe the time evolution of $P(n, m, v_n, v_m, t)$, we consider a master equation for each of the marginal distributions, $P(n, m, 1, 1, t)$, $P(n, m, 1, -1, t)$, $P(n, m, -1, 1, t)$, and $P(n, m, -1, -1, t)$. The marginal distributions are considered individually as the movement rules track how a right-moving or left-moving individual arrives at a spatial point. For instance, a right-moving individual arrives at location x at time $t + \Delta t$ if it was either left-moving at $x + \Delta x$ and turns to the right, or if it was right-moving at $x + \Delta x$ and does not turn to the right.

To write the master equation for $P(n, m, 1, 1, t)$, we account for all possible jumps that lead to right-moving individuals arriving at n and m at time $t + \Delta t$ and those right-moving individuals leave n and m , where Δt is the timestep. We find:

$$\begin{aligned}
P(n, m, 1, 1, t + \Delta t) &= P(n, m, 1, 1, t) \\
&+ P(n + 1, m, -1, 1, t)T(n + 1, -1; m, 1, t)\Delta t \\
&+ P(n, m + 1, 1, -1, t)T(m + 1, -1; n, 1, t)\Delta t \\
&+ P(n - 1, m, 1, 1, t)N(n - 1, 1; m, 1, t)\Delta t \\
&+ P(n, m - 1, 1, 1, t)N(m - 1, 1; n, 1, t)\Delta t \\
&- 2P(n, m, 1, 1, t)\Delta t \\
&+ O(\Delta t^2).
\end{aligned} \tag{5.16}$$

In (5.16), $T(n, v_n; m, v_m, t)$ describes the rate that the individual at n heading in direction v_n moves to $n + av_n$ and turns (T) to direction $-v_n$, given that the other individual is located at m with direction v_m at time t . $N(n, v_n; m, v_m, t)$ describes the rate that the individual at n heading in the direction v_n moves to $n + av_n$, but does not (N) change direction, given

that the other individual is located at m with direction v_m at time t .

The master equations for the remaining marginal distributions are written similarly:

$$\begin{aligned}
P(n, m, 1, -1, t + \Delta t) &= P(n, m, 1, -1, t) \\
&+ P(n + 1, m, -1, -1, t)T(n + 1, -1; m, -1, t)\Delta t \\
&+ P(n, m - 1, 1, 1, t)T(m - 1, 1; n, 1, t)\Delta t \\
&+ P(n - 1, m, 1, -1, t)N(n - 1, 1; m, -1, t)\Delta t \\
&+ P(n, m + 1, 1, -1, t)N(m + 1, -1; n, 1, t)\Delta t \\
&- 2P(n, m, 1, -1, t)\Delta t \\
&+ O(\Delta t^2),
\end{aligned} \tag{5.17}$$

$$\begin{aligned}
P(n, m, -1, 1, t + \Delta t) &= P(n, m, -1, 1, t) \\
&+ P(n - 1, 1, m, 1, t)T(n - 1, 1; m, 1, t)\Delta t \\
&+ P(n, m + 1, -1, -1, t)T(m + 1, -1; n, -1, t)\Delta t \\
&+ P(n + 1, m, -1, 1, t)N(n + 1, -1; m, 1, t)\Delta t \\
&+ P(n, m - 1, -1, 1, t)N(m - 1, 1; n, 1, t)\Delta t \\
&- 2P(n, m, -1, 1, t)\Delta t \\
&+ O(\Delta t^2),
\end{aligned} \tag{5.18}$$

and

$$\begin{aligned}
P(n, m, -1, -1, t + \Delta t) &= P(n, m, -1, -1, t) \\
&+ P(n - 1, m, 1, -1, t)T(n - 1, 1; m, -1, t)\Delta t \\
&+ P(n, m - 1, -1, 1, t)T(m - 1, 1; n, -1, t)\Delta t \\
&+ P(n + 1, m, -1, -1, t)N(n + 1, -1; m, -1, t)\Delta t \\
&+ P(n, m + 1, -1, -1, t)N(m + 1, -1; n, -1, t)\Delta t \\
&- 2P(n, m, -1, -1, t)\Delta t \\
&+ O(\Delta t^2).
\end{aligned} \tag{5.19}$$

As in the previous sections, we can form differential equations for the time-evolution for

each of the marginal distribution. These differential equations are not complete without an initial condition, which in the case of a 2-particle system corresponds to the point release of individuals at lattice sites n_0 and m_0 . It remains to describe the functions that prescribe the rates at which individuals turn (T) and do not turn (N).

To describe $T(n, v_n; m, v_m, t)$, recall that, subject to the direction-dependent communication mechanisms as described in Chapter 2 and Chapter 3, a right- or left-moving individual i changes direction with rate

$$\lambda_i^\pm(y_i^\pm) = \lambda_1 + \lambda_2 f(y_i^\pm), \quad (5.20)$$

where

$$y_i^\pm = y_{r,i}^\pm - y_{a,i}^\pm + y_{al,i}^\pm, \quad (5.21)$$

is the integrated interaction force experienced by individual i resulting from interactions from conspecifics. $y_{r,i}^\pm$ is the repulsive force; $y_{al,i}^\pm$ is the alignment force; and $y_{a,i}^\pm$ is the attractive force experience by individual i . These forces depend on the specific direction-dependent communication mechanism considered (submodel), and the magnitudes of the social interaction forces, namely parameters q_r, q_{al} , and q_a . Several example interaction forces are described in Table 3.1. In this case, the interaction with conspecifics only depends on the direction and location of the other individual, hence to calculate the turning rate, (5.20), we need only n, v_n, m and v_m . That is, the turning rate $T(n, v_n; m, v_m, t)$ is simply $\lambda_i^\pm(y_i^\pm)$, where i represents the individual at n , and the sign of v_n prescribes \pm . Thus, in place of $\lambda_i^\pm(y_i^\pm)$, we write $\lambda_n^{v_n}$. Since y_i^\pm depends only on n, v_n, m and v_m , we write n, v_n, m, v_m in place of y_i^\pm . That is,

$$T(n, v_n; m, v_m, t) = \lambda_n^{v_n}(n, v_n, m, v_m), \quad (5.22)$$

is the rate at which individual 1 changes direction as a result of interacting with individual 2 subject to the social interactions prescribed by the direction-dependent communication mechanism. It should be noted that the parameters, $\lambda_1, \lambda_2, q_r, q_{al}$, and q_a enter $T(n, v_n; m, v_m, t)$ via the calculation of y_i^\pm . The rate of not turning, $N(n, v_n; m, v_m, t)$, describes the rate at which individuals move, but not change direction. This quantity should be low when the turning rate is high and vice versa. Given that the turning rate is $T(n, v_n; m, v_m, t)$, the not-turning rate is given by

$$N(n, v_n; m, v_m, t) = \mathcal{T} - T(n, v_n; m, v_m, t), \quad (5.23)$$

where

$$\mathcal{T} = \sup_{x \in \mathbb{R}} (\lambda_1 + \lambda_2 f(x)). \quad (5.24)$$

The supremum exists since we assume that f is a bounded and increasing function of the social interaction forces. That is, the rate of not-turning can be found by calculating the maximal turning rate for the current state of the 2-particle system and subsequently subtracting the turning rate for the current state of the system. The rate of not turning is not given by $1 - T(n, v_n, m, v_m)$, as the turning rate is not a probability, nor is necessarily bounded by 1.

To investigate the behaviour of the 2-particle system with direction-dependent communication mechanisms, we present statistics from 1000 stochastic simulations of the IBM with direction-dependent communication mechanisms. The mean separation distance and the mean square displacement (MSD) are the quantities of interest. The mean separation distance gives the average distance between individuals, and allows for an understanding of how tightly packed the individuals tend to be. The MSD allows for the diffusivity of the aggregation to be understood. From each simulation, the MSD, $\Delta x^2(t)$, of one of the particles is calculated. From this information, the average MSD, $\langle x^2(t) \rangle$, reveals the diffusive trend of the system. We also calculate short-time, long-time, and full diffusion coefficients, D_m , D_M , and D_f , respectively, from the MSD data. These diffusion coefficients are described in Sections 5.3 and 5.4. The initial conditions for these simulations place the individuals one lattice site apart, and are run for 300 timesteps to ensure asymptotic behaviour is visible in the mean separation distance. The parameters and direction-dependent communication mechanisms used are chosen to be those parameters that produced complex spatial patterns in the investigation of the IBM with direction-dependent communication mechanisms (Section 3.3). These parameters and the pattern they produce in the IBM are listed in Table 5.4.

In Figure 5.19, the mean separation distance, $d(t)$, is plotted as a function of time for each set parameter set listed in Table 5.4. Similarly, in Figure 5.20, the MSD of particle 1 is shown for several trajectories (blue curves), and the average MSD, $\langle x^2(t) \rangle$ is shown using a thick blue line. The slope of the green line is D_m ; the slope of the red line is D_M ; and the slope of the black line is D_f . The average mean separation distance, diffusion coefficients, and diffusion type is summarized in Table 5.5.

The statistics presented in Table 5.5 reveal some characteristics of pattern formation. For example, using parameters that produce stationary pulses, traveling groups, and zigzag pulses, the mean separation distance saturates. On the other hand, for ripples, feathers,

Pattern	Submodel	λ_1	λ_2	q_r	q_{al}	q_a
(a) Stationary pulse	M1	0.2	0.9	2.4	0	2
(b) Stationary pulse	M2	0.2	0.9	0.5	0	4
(c) Ripples	M5	0.2	0.9	1.1	2	1.5
(d) Feathers	M3	0.2	0.9	6.4	0	6
(e) Traveling pulse	M1	0.2	0.9	0.5	2	1.6
(f) Traveling train	M3	6.67	30	0	2	6
(g) Zigzag pulse	M2	0.2	0.9	1	2	6
(h) Breathers	M4	0.2	0.9	1	0	2
(i) Traveling breathers	M4	0.2	0.9	4	2	4

Table 5.4: Example parameters and patterns for investigation using the 2-particle Eftimie model. The pattern names will be used to refer to each parameter set.

Pattern	$\langle d(t) \rangle$	D_m	D_M	D_f	Diffusion type
(a) Stationary pulse	4.3853	0.0159	0.1287	0.1511	normal
(b) Stationary pulse	4.1860	0.0159	0.1258	0.1450	normal
(c) Ripples	increasing	0.0162	0.2269	0.3888	super
(d) Feathers	increasing	0.0162	0.2269	0.3522	super
(e) Traveling pulse	5.5860	0.0160	0.1850	0.2693	normal/super
(f) Traveling train	increasing	0.0071	0.0110	0.0169	normal/super
(g) Zigzag pulse	4.6233	0.0160	0.1830	0.2711	normal
(h) Breathers	increasing	0.0162	0.2020	0.2794	super
(i) Traveling breathers	increasing	0.0162	0.2060	0.3074	super

Table 5.5: Mean separation distance and diffusion coefficients for patterns produced by the IBM. The mean separation distance is calculated by averaging the last 50 time steps of $d(t)$, and is said to be increasing if saturating behaviour does not appear within 300 time steps. The type of anomalous diffusion is also stated: super-diffusion, normal diffusion, and sub-diffusion.

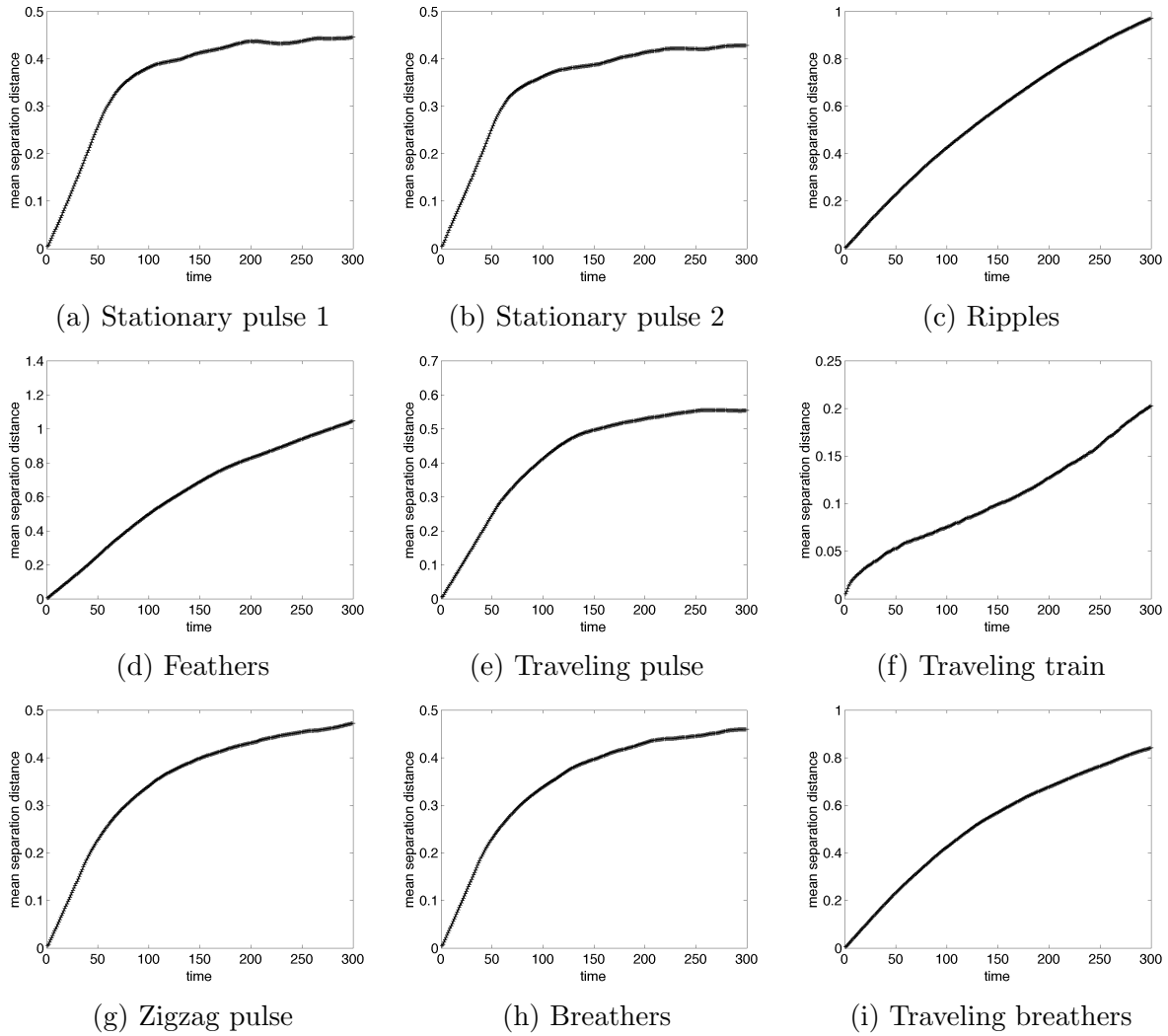


Figure 5.19: Mean separation distance, $d(t)$, for patterns produced by the IBM. Note that the y-axis has been scaled by 0.1. Parameters are listed in Table 5.4.

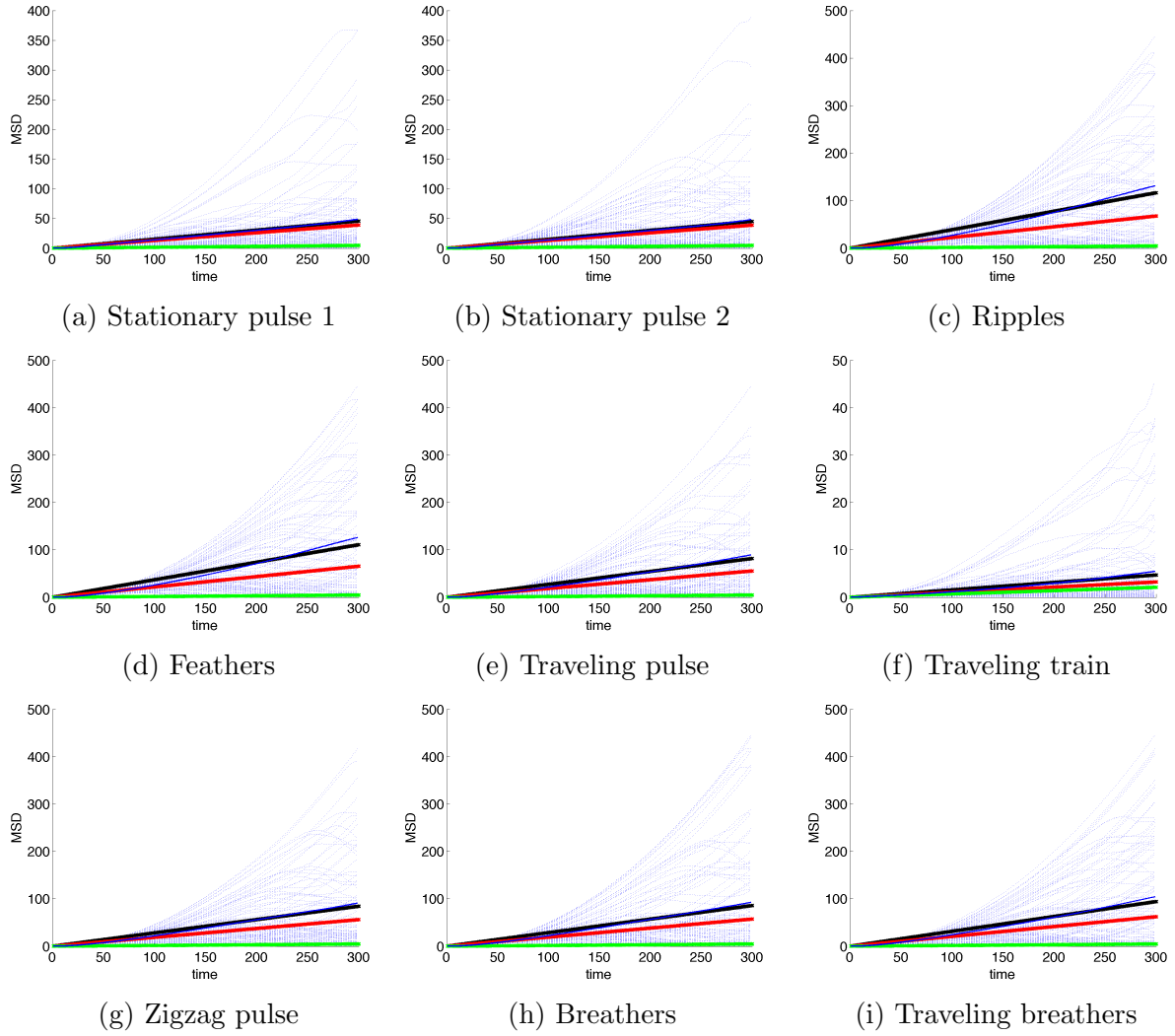


Figure 5.20: MSD for patterns produced by the IBM. The blue curves are MSD curves for individual trajectories and the dark blue curve is the average MSD, $\langle \Delta x^2(t) \rangle$. The slope of the green line is D_m ; the slope of the red line is D_M ; and the slope of the black line is D_f . Parameters are listed in Table 5.4.

traveling trains, breathers, and traveling breathers, individuals tend to move further from neighbours, as indicated by the increasing mean separation distance. The full diffusion coefficient, D_f , qualitatively matches best with the mean MSD for those parameter sets investigated. This diffusion coefficient is much higher for those patterns with very mobile individuals, such as ripples and feathers. In these patterns, individuals travel throughout the entire domain or are shed from a stationary group, respectively. This diffusive behaviour is suggested in large values of D_f . Finally, for those groups that form stationary or traveling groups have normal diffusion properties, as the average MSD is linear (stationary pulse and zigzag pulse) or very close to linear (traveling pulse and traveling train). One expects very small or zero MSD for stationary patterns, and this is likely the case when MSD is measured for stationary patterns produced by the IBM. This results from the fact that those patterns may be stationary at the group level, but the individual particles which form these groups may continue to move within the larger aggregations. For those patterns in which individuals are very mobile, the average MSD is qualitatively convex. This suggests super-diffusion, i.e., a mechanism propelling individuals throughout space. The investigation of the 2-particle model with direction-dependent communication mechanisms reveals a connection between mobile patterns and increasing mean separation distance and high diffusion coefficients. It also reveals a connection between stationary or well-grouped patterns and saturating mean separation distance and relatively small diffusion coefficients.

5.6 Discussion

In this Chapter, we focused on 2-particle models in efforts to understand the response of individuals to social interactions. This modelling approach contrasts with that taken in Chapters 2 and 3, where group-level pattern formation is studied.

In Section 5.2, we reviewed the work of Potts *et al.*, [34], who explicitly solved the anti-symmetric exclusion process for two particles on a one-dimensional lattice. This process involves two particles which randomly hop to the left or to the right. The particles have an intrinsic direction bias: they hop together with probability p , and apart with probability $1-p$. A master equation for this process describes the time evolution of the joint occupation probability distribution, $P(n, m, t)$; analysis reveals that the asymptotic behaviour of the system depends on p . For $0 < p < \frac{1}{2}$, the distance between the particles grows linearly in time; when $p = \frac{1}{2}$, the distance grows with the square root of time; and when $\frac{1}{2} < p < 1$, the distance saturates. Similarly, the asymptotic diffusion coefficient varies with the value of p .

In Section 5.3, social interactions were added to the anti-symmetric exclusion process. The anti-symmetric exclusion process already includes a contact repulsion mechanism, by which individuals would be excluded from the same lattice site. In order to incorporate repulsive and attractive interactions, the probability of hopping toward each other, p , was modified to depend on the separation distance, $d = m - n$, of the two particles. We develop a master equation for the joint occupation probability, and study it using stochastic simulations. The model behaviour depends on the choice of the interaction function, $p(d)$; however, the model exhibits a predictable attraction-repulsion behaviour, with the mean separation distance between the particles approaching a constant. With attraction-repulsion social interactions, the simulations reveal the formation of a group with constant inter-individual separation, that diffuses normally throughout the domain.

In order to incorporate direction-dependent mechanisms, we added alignment interactions to the attraction-repulsion interactions in Section 5.4. To incorporate alignment, we consider the direction of travel of each individual, and we specified the sizes of the social interaction zones. In the zone of repulsion and in the zone of attraction, the 2-particle system was assumed to hop according to the anti-symmetric exclusion process with social interactions, i.e., non-constant $p(d)$; however, if the distance between the two particles places them in the zone of alignment and if the two particles are traveling in the same direction, then they are assumed to continue traveling in this direction. This alignment mechanism describes the tendency of individuals in a group to align their velocity with that of their neighbours over intermediate distances. Again, a master equation for this process was studied through stochastic simulations. In comparison to the anti-symmetric exclusion process with only attraction-repulsion interactions, the inclusion of alignment results in 2-particle groups that move across the lattice. This behaviour does not appear with only attraction-repulsion interactions, and is evident in large diffusion coefficients and convex average MSD. The phenomena that moving groups result from including alignment interactions in this 2-particle system is consistent with results from the PDE model and IBM model from Chapters 2 and 3.

In Section 5.5, we began by writing a master equation for the 2-particle model with direction-dependent communication mechanisms. To understand this process, it was necessary to explicitly track the direction of travel of each individual. To write a master equation for the joint occupation probability, $P(n, m, v_n, v_m, t)$, we considered a master equation for each of the marginal distributions, $P(n, m, 1, 1, t)$, $P(n, m, 1, -1, t)$, $P(n, m, -1, 1, t)$, and $P(n, m, -1, -1, t)$. This leads to a complicated system of master equations, which were sim-

ulated using the IBM from Chapter 3 with $N = 2$ individuals. Parameters were chosen as those parameter sets which produce examples of complex spatial patterns as shown in Figure 3.2. The investigation reveals a relation between mobile patterns and increasing $\langle d(t) \rangle$ and high diffusion coefficients. It also reveals a relation between stationary and well-grouped patterns and saturating $\langle d(t) \rangle$ and small diffusion coefficients. The behaviour of the 2-particle model with direction-dependent communication mechanisms reveals that basic characteristics of group-level pattern formation results from individual-to-individual interactions. In this chapter, a few first steps towards understanding the relationship between group-level pattern formation and individual-level social interactions were taken. Solving the master equations in Sections 5.3, 5.4, and 5.5, following the method of solution in [1, 34] remains as the next step to make this relationship explicit.

Chapter 6

Discussion

In this thesis, we examined direction-dependent communication mechanisms in the context of mathematical models for collective behaviour. Direction-dependent communication mechanisms are motivated biologically, as there are many species which form aggregations and communicate using directional means. The importance of understanding the mechanisms that lead to collective behaviour of groups is twofold: firstly, it is scientifically important to discover those mechanisms that lead to collective behaviour and group patterns; and secondly, understanding these group patterns has application to biological controls, and to robotics and other autonomous systems.

To understand the importance of direction-dependent communication mechanisms, we reviewed an existing one-dimensional partial differential equation model which incorporated direction-dependent communication mechanisms. This PDE model was the first collective behaviour model to incorporate directional communication mechanisms, and pattern formation in this model was consequently enriched. The framework studied in this PDE model allows for a wide variety of communication mechanisms to be studied, and a wide variety of patterns to be linked with particular communication mechanisms. By construction, the PDE model describes the dynamics of the population density, and does not reveal an individual's response to direction-dependent communication. Nonetheless, a wide variety of analytical techniques allow for pattern formation to be studied in great detail, and numerical simulations reveal a rich model behaviour. This led to the question as to whether or not an individual-based model can reproduce the same patterns.

A new one-dimensional IBM with direction-dependent communication mechanisms was developed in this thesis. Following the ideas presented by Wong, [41], we developed an individual-based model to study direction-dependent communication mechanisms. Existing

IBMs are successful in producing spatial patterns, but are unable to produce a wide variety of patterns observed in nature. The new IBM matches the rich behaviour of the PDE model by producing complex spatial patterns using a variety of communication mechanisms. The effects of stochasticity are observed in the IBM, as some individuals escape larger groups. This added detail is significant as it reveals the behaviour of individuals in response to communication mechanisms and conspecifics. Moreover, the IBM formulation allows for changes to be easily made. We have found that revising the social interaction kernels to be more biologically realistic does not highly impact the qualitative model behaviour. Finally, the fact that the stochastic individual-based model reproduces the behaviour of the PDE model across parameter regimes validates the Poisson point assumption, which was necessary to derive the PDE model from a random walk.

The numerical implementation and simulation of the IBM is a relatively straightforward process, and consequently an individual-based approach would be fruitful for the investigation of patterns in two- or three-dimensions. A PDE model with direction-dependent communication mechanisms has been briefly studied in two-dimensions by Fetecau [16]. Extending the new IBM to two- or three-dimensions may allow for not only new patterns to be found, but also for a comparison to biological groups in nature.

Another direction for future work is in investigating scale-free interactions and topological interactions in models of collective behaviour. In [5], Cavagna *et al.* measured the fluctuations of different birds in large flocks of starlings. They found that the range of spatial correlation of behaviour does not have a fixed value; however, the correlation length scales linearly with the size of the flock (hence the name scale-free). It may be enlightening to investigate this correlation length using the IBM, as scale-free interactions indicate that these interactions do not act over a fixed metric distance as in our models, but over a certain number of neighbours. Moreover, there is evidence that those interactions ruling collective behaviour depend on this “topological distance”, i.e. the number of neighbours between individuals [2]. Finally, linking mechanistic models with topological interactions and PDE models via a mean-field limit (individual-based model and PDE model) is a new area of research [15].

Density-dependent speed, which is studied in the Eulerian model literature, is also considered in our IBM with direction-dependent communication mechanisms. This study is motivated by the fact that individuals in a group do not always move at a constant speed. That is, in addition to turning in response to their neighbours, individuals are allowed to adjust their speed in response to neighbours. As a result of including density-dependent

movement speeds, we observe group splitting and merging behaviour. Moreover, the turning rates were found to have an effect on the cohesiveness of aggregations. Large random turning rates lead to compact stationary groups, and small random turning rates in the absence of a biased turning lead to loose or dispersing groups. When individuals do not change direction, but only speed up and slow down in response to neighbours, a compact right- and a compact left-moving group form and travel across the domain. Since splitting and merging behaviour is not observed in the IBM with constant movement speed, we conclude that density-dependent speeds play an important role in group cohesion. It should be noted that the patterns produced by the IBM with density-dependent speed do not match those patterns produced by the PDE model; however, there is a qualitative agreement between the types of behaviours observed. This difference likely results from the differing implementations of density-dependent speed: in the PDE model, the speed appears inside of the spatial derivative in the advection term of the PDE; but in the IBM, we allow each individual to move at the speed prescribed by density-dependent interactions. A full understanding of the correlated random walk that leads to the PDE model with density-dependent speed is needed. A similar PDE model with density-dependent speeds but without direction switching is derived and studied in [6], and may be useful in linking the density-dependent speed with the individual movement mechanics.

The use of the PDE model and IBM to study the effect of direction-dependent communication mechanisms on group level pattern formation allows us to link the complex spatial patterns to animal communication mechanisms. Although the IBM reveals added detail about the behaviour of individuals, the individual response to conspecifics remains unstudied. To describe explicitly how two individuals respond to each other via direction-dependent communication mechanisms, 2-particle models are considered. We began our investigation by reviewing the solution and behaviour of the two particle anti-symmetric exclusion process, which was explicitly solved by Potts *et al.* [34]. In this process, the behaviour of the model depends on the value of p , the probability that the particles will hop toward each other. When $p > \frac{1}{2}$, Potts *et al.* found that the mean separation distance between the particles saturates, suggesting a balance between contact repulsion and the tendency for the particles to hop towards each other. When $p < \frac{1}{2}$ or $p = \frac{1}{2}$, Potts *et al.* found that the mean separation distance grow linearly with time or with the square root of time, respectively. We added non-local attraction and repulsion social interactions to the anti-symmetric exclusion process by assuming that the probability of hopping toward each other, p , depends on the distance between the particles, d . In this case, the behaviour of the 2-particle ensemble

exhibits stationary groups. The formation of stationary groups is evident in the appearance of a constant mean separation distance and small diffusion coefficients. As a next step toward studying direction-dependent communication mechanism with 2-particle models, we added alignment social interactions to the 2-particle model. Incorporating alignment interactions required tracking both the position and direction of travel of the two particles, and this addition complicated the master equation for the process. Stochastic simulations reveal large diffusion coefficients and convex average mean square displacement. This suggests that the alignment interaction forces are critical for obtaining traveling groups. Finally, to understand the fully direction-dependent communication mechanisms, we state a system of master equations. Stochastic simulations reveal that basic characteristics of the complex spatial patterns are evident in the 2-particle ensemble. For example, using parameters that lead to stationary patterns in the IBM and PDE model, the 2-particle ensemble tends to have small diffusion coefficients and has a bounded mean separation distance. On the other hand, using parameters that lead to patterns with very motile groups, such as feathers or ripples, we find an increased mean separation distance and large diffusion coefficients. The use of the 2-particle model framework provides a foundation for further analytical work in studying direction-dependent communication mechanisms. Potts *et al.* presents a lengthy, but straightforward solution to the anti-symmetric exclusion process by introducing a generating function, using a Laplace transform, and solving the resulting Fredholm integral equation [34]. By using similar methods, it is likely that solutions to the master equations described in Chapter 5 can be found. These solutions will likely provide insight into the effect that direction-dependent communication mechanisms have on pattern formation and individual interactions.

In this thesis we studied direction-dependent communication mechanisms from three perspectives: PDE, IBM, and 2-particle model. The work of Eftimie *et al.* demonstrates that complex spatial patterns can be explained by considering a variety of communication mechanisms using only one model. The new IBM developed in this thesis reveals that these complex spatial patterns are not unique to the PDE model, and the added individual-based detail shows how individuals move within these groups. The 2-particle model framework provides further insight into how individuals respond to direction-dependent communication mechanisms, and provides a foundation for further mathematical analysis of communication mechanisms in models of collective behaviour.

Bibliography

- [1] C. Aslangul. Diffusion of two repulsive particles in a one-dimensional lattice. *J. Phys. A: Math. Gen.*, 32:3993–4003, 1999.
- [2] M. Ballerini, N. Cabibbo, R. Candelier, A. Cavagna, E. Cisbani, I. Giardina, V. Lecomte, A. Orlandi, G. Parisi, A. Procaccini, M. Viale, and V. Zdravkovic. Interaction ruling animal collective behavior depends on topological rather than metric distance: Evidence from a field study. *Proc. Natl. Acad. Sci. USA*, (4):1232, 2008.
- [3] A. W. Bowman and A. Azzalini. *Applied Smoothing Techniques for Data Analysis : The Kernel Approach with S-Plus Illustrations*. Oxford Statistical Science Series. Clarendon Press, 1997.
- [4] J. A. Carrillo, M. Fornasier, G. Toscani, and F. Vecil. Particle, kinetic, and hydrodynamic models of swarming. In *Mathematical modeling of collective behavior in socio-economic and life sciences*, Model. Simul. Sci. Eng. Technol., pages 297–336. Birkhäuser Boston Inc., Boston, MA, 2010.
- [5] A. Cavagna, A. Cimorelli, I. Giardina, G. Parisi, R. Santagati, F. Stefanini, and M. Viale. Scale-free correlations in starling flocks. *Proc. Natl. Acad. Sci. USA*, 107(26):11865 – 11870, 2010.
- [6] A. Chertock, A. Kurganov, A. Polizzi, and I. Timofeyev. Pedestrian flow models with slowdown interactions. *Math. Models Methods Appl. Sci.*, 24(02):249–275, 2014.
- [7] I. D. Couzin, J. Krause, R. James, G. D. Ruxton, and N. R. Franks. Collective memory and spatial sorting in animal groups. *J. Theor. Biol.*, 218(1):1 – 11, 2002.
- [8] F. Cucker and E. Mordecki. Flocking in noisy environments. *J. Math. Pures Appl. (9)*, 89(3):278–296, 2008.
- [9] F. Cucker and S. Smale. Emergent behavior in flocks. *IEEE Trans. Automat. Control*, 52(5):852–862, 2007.
- [10] R. Eftimie. *Modeling group formation and activity patterns in self-organizing communities of organisms*. PhD thesis, University of Alberta, 2008.

- [11] R. Eftimie. Hyperbolic and kinetic models for self-organized biological aggregations and movement: a brief review. *J. Math. Biol.*, 65(1):35–75, 2012.
- [12] R. Eftimie, G. de Vries, and M. A. Lewis. Complex spatial group patterns result from different animal communication mechanisms. *Proc. Natl. Acad. Sci. USA*, 104(17):6974–6979 (electronic), 2007.
- [13] R. Eftimie, G. de Vries, and M. A. Lewis. Weakly nonlinear analysis of a hyperbolic model for animal group formation. *J. Math. Biol.*, 59(1):37–74, 2009.
- [14] R. Eftimie, G. de Vries, M. A. Lewis, and F. Lutscher. Modeling group formation and activity patterns in self-organizing collectives of individuals. *Bull. Math. Biol.*, 69(5):1537–1565, 2007.
- [15] R. Erban and J. Haskovec. From individual to collective behaviour of coupled velocity jump processes: A locust example. *Kinet. Relat. Models*, 5(4):817 – 842, n.d.
- [16] R. C. Fetecau. Collective behavior of biological aggregations in two dimensions: A nonlocal kinetic model. *Math. Models Methods Appl. Sci.*, 21(7):1539 – 1569, 2011.
- [17] R. C. Fetecau and R. Eftimie. An investigation of a nonlocal hyperbolic model for self-organization of biological groups. *J. Math. Biol.*, 61(4):545–579, 2010.
- [18] S. Goldstein. On diffusion by discontinuous movements, and on the telegraph equation. *Quart. J. Mech. Appl. Math.*, 4:129–156, 1951.
- [19] D. Grünbaum. Translating stochastic density-dependent individual behavior with sensory constraints to an eulerian model of animal swarming. *J. Math. Biol.*, 33(2):139, 1994.
- [20] S. Gueron, S. A. Levin, and D. I. Rubenstein. The dynamics of herds: From individuals to aggregations. *J. Theor. Biol.*, 182(1):85 – 98, 1996.
- [21] H. Hildenbrandt, C. Carere, and C. Hemelrijk. Self-organized aerial displays of thousands of starlings: a model. *Behav. Ecol.*, 21(6):1349–1359, 2010.
- [22] A. Huth and C. Wissel. The Simulation Of The Movement Of Fish Schools. *J. Theor. Biol.*, 156(3):365–385, Jun 7 1992.
- [23] O. Igoshin, R. Welch, D. Kaiser, and G. Oster. Waves and aggregation patterns in myxobacteria. *Proc. Natl. Acad. Sci. USA*, 101(4256-4261), 2004.
- [24] M. Kac. A stochastic model related to the telegrapher’s equation. *Rocky Mountain J. Math.*, 4:497–509, 1974. Reprinting of an article published in 1956, Papers arising from a Conference on Stochastic Differential Equations (Univ. Alberta, Edmonton, Alta., 1972).

- [25] A. Kolpas, J. Moehlis, T. A. Frewen, and I. G. Kevrekidis. Coarse analysis of collective motion with different communication mechanisms. *Math. Biosci.*, 214(1-2):49–57, 2008.
- [26] A. Kolpas, J. Moehlis, and I. G. Kevrekidis. Coarse-grained analysis of stochasticity-induced switching between collective motion states. *Proc. Natl. Acad. Sci. USA*, 104(14):5931–5935, 2007.
- [27] C. R. Kube and Z. Hong. Collective robotics: From social insects to robots. *Adapt. Behav.*, 2(2):189, 1993.
- [28] F. Lutscher and A. Stevens. Emerging patterns in a hyperbolic model for locally interacting cell systems. *J. Nonlinear Sci.*, 12(6):619–640, NOV-DEC 2002.
- [29] P. Marler. Animal communication signals. *Science*, 157(3790):769–774, 1967.
- [30] A. Mogilner and L. Edelstein-Keshet. A non-local model for a swarm. *J. Math. Biol.*, 38:534–570, 1999.
- [31] J. C. v. Olst and J. R. Hunter. Some aspects of the organization of fish schools. *J. Fish Res. Board Can.*, 27(7):1225–1238, 1970.
- [32] J. K. Parrish. Using behavior and ecology to exploit schooling fishes. *Environ. Biol. Fishes*, 55(1-2):157–181, 1999.
- [33] B. Pfister. Simulation of the dynamics of myxobacteria swarms based on a one-dimensional interaction model. *J. Biol. Sys.*, 3(2):579–588, 1995.
- [34] J. R. Potts, S. Harris, and L. Giuggioli. An anti-symmetric exclusion process for two particles on an infinite 1d lattice. *J. Phys. A: Math. Theor.*, 44(48), 2011.
- [35] V. Rajani. Quantitative analysis of single particle tracking experiments: applying ecological methods in cellular biology. Master’s thesis, University of Alberta, 2010.
- [36] M. J. Saxton. Single-particle tracking: the distribution of diffusion coefficients. *Biophys. J.*, 72(4):1744 – 1753, 1997.
- [37] S. J. Simpson, A. R. McCaffery, and B. F. Hägele. A behavioural analysis of phase change in the desert locust. *Biol. Reviews*, 74(4):461–480, 1999.
- [38] S. J. Simpson, G. A. Sword, P. D. Lorch, and I. D. Couzin. Cannibal crickets on a forced march for protein and salt. *Proc. Natl. Acad. Sci. USA*, 103(11):4152–4156, 2006.
- [39] C. M. Topaz, A. L. Bertozzi, and M. A. Lewis. A nonlocal continuum model for biological aggregation. *Bull. Math. Biol.*, 68:1601–1623, 2006.
- [40] S. R. Witkin. The importance of directional sound radiation in avian vocalization. *The Condor*, 79(4):pp. 490–493, 1977.

- [41] R. Wong. Study of animal movement and group formation with a lagrangian model. Master's thesis, University of Alberta, 2011.
- [42] C. A. Yates, R. E. Baker, R. Erban, and P. K. Maini. Refining self-propelled particle models for collective behaviour. *Can. Appl. Math. Q.*, 18(3):299–350, 2010.